Functional analysis of genetic variants associated with age-related macular degeneration (AMD) - The HtrA serine peptidase 1 (HTRA1)

DISSERTATION

ZUR ERLANGUNG DES DOKTORGRADES

DER NATURWISSENSCHAFTEN (DR. RER. NAT.)

DER FAKULTÄT FÜR BIOLOGIE UND VORKLINISCHE MEDIZIN

DER UNIVERSITÄT REGENSBURG

vorgelegt von
Shyamtanu Datta
aus
INDIA
DECEMBER 2015

Der Promotionsgesuch wurde eingereicht am:

Die Arbeit wurde angeleitet von:
Prof. Dr. Bernhard Weber

Unterschrift:

SHYAMTANU DATTA

To my parents and Gurudev

“The only thing worse than being blind is having sight but no vision.”

Hellen Keller (1880-1968)

DECLARATION

I declare that this thesis is a presentation of my original research work. Wherever contributions of others are involved, every effort is made to indicate this clearly, with due reference to the literature, acknowledgement of collaborative research and discussions. This thesis has not been submitted to any other faculty or university for any kind of examination and a part of the thesis is composed of the following published article:

Friedrich, U.*, Datta, S.*, Schubert, T., Plossl, K., Schneider, M., Grassmann, F., Fuchshofer, R., Tiefenbach, K.J., Langst, G., and Weber, B.H. (2015). Synonymous variants in HTRA1 implicated in AMD susceptibility impair its capacity to regulate TGF-beta signaling. Hum Mol Genet *24*, 6361-6373.

(* indicates shared first authorship)

I have given all information truthfully to the best of my knowledge.

....

Date Signature

Table of Contents

SUMMARY

Background. Age-related macular degeneration (AMD) is a multifactorial retinal neurodegenerative disorder and the leading cause of blindness among the elderly worldwide. Genetics is one of several factors which play role in the pathogenesis. An AMD-risk locus on chromosome 10q26 spans two genes namely age-related maculopathy susceptibility 2 (*ARMS2*) and high temperature requirement factor A1 (*HTRA1*). Controversy exists as to which of the two genes are responsible for increased risk of the disease. HTRA1 is a secreted serine protease reported to play a crucial role in the development of several cancers and neurodegenerative diseases. *ARMS2* is a primate-specific gene and, so far, biological properties attributed to the putative protein remain elusive. Two synonymous single nucleotide polymorphisms (SNPs) in exon 1 of HTRA1 are in complete linkage disequilibrium with several polymorphisms within 10q26 locus which are strongly associated with AMD.

Aim. The aim of the study was to assess an effect of AMD-associated synonymous SNPs on the structure and function of HTRA1. In addition, a putative role of HTRA1 on activation of microglia was investigated.

Methods. Differences in the structures of recombinant non-risk- and risk-associated HTRA1 isoforms were analyzed by MicroScale Thermophoresis (MST) and limited partial proteolysis. The secretion of the different HTRA1 isoforms was analyzed after heterologous expression in Hek293-Ebna cells. By employing MST and *in vitro* digestion assays, the interaction of HTRA1 isoforms with reported interaction partners, transforming growth factor-β1 (TGF-β1) and β-casein, was compared. Luciferase assays were applied to compare the regulation of TGF-β1 signaling by different HTRA1 isoforms in MLEC-PAI/Luc cells (Mink lung epithelial cells stably transfected with an expression construct containing a truncated *PAI-1* promoter fused to the firefly luciferase reporter gene). The influence of HTRA1 non-risk- and risk-associated isoforms was also analyzed on autocrine TGF-β signaling in BV-2 microglial cells addressing protein and transcript levels. Finally, an effect of HTRA1 on classical (M1) and alternative (M2) activation of microglia was assessed by

treating BV-2 cells with known stimulators for both pathways in presence of purified recombinant HTRA1. The gene expression of markers of M1 and M2 activation as well as nitrite production by M1 microglial cells were investigated.

Results. MST and limited partial proteolysis showed that the conformation of the AMD risk-associated HTRA1 protein is different from that of the non-risk-associated HTRA1 isoforms. The risk-associated isoform was also found to have decreased secretion. While there was no difference of the HTRA1 isoforms in casein binding and digestion, the risk-associated isoform exhibited no binding and decreased digestion of TGF-β1. This eventually affected the regulation of TGF-β signaling in MLEC-PAI/Luc cells and microglial cells. In addition, preliminary data indicate that HTRA1 might be a regulator of M2 microglial activation induced by IL4 and TGF-β1. Nevertheless, more experiments are required to support the role of HTRA1 on microglial activation.

Conclusion. Our data show an effect of AMD-associated synonymous polymorphisms on HTRA1 secretion and protein structure, thereby affecting the capacity of HTRA1 to regulate TGF-β signaling. Whether this plays a role in pathogenesis of AMD still remains to be clarified.

1. INTRODUCTION

1.1. Age-related Macular Degeneration (AMD)

Age-related macular degeneration (AMD) is one of the leading causes of irreversible blindness of elderly population worldwide (Resnikoff et al., 2004). First, the condition was described in medical literature as “symmetrical central choroido-retinal disease occurring in senile persons” in 1874 (Hutchinson et al., 1874). AMD is a multifactorial neurodegenerative disease characterized by progressive degeneration of photoreceptors/retinal pigment epithelial (RPE) complex primarily in macular region of the retina, which has the highest concentration of cone photoreceptors and is responsible for visual acuity (Curcio et al., 1990; Smith et al., 2001; Klein et al., 2010). It is a complex disease owing to multiple risk factors such as age, diet, smoking, oxidative stress and genetics (Klein et al., 2010). The disease is associated not only with visual impairment but also with high rates of depression, anxiety and emotional distress (Berman and Brodaty, 2006). A recent meta-analysis has shown that 8.7% of the worldwide population has AMD, and the projected number of people with the disease is around 196 million in 2020, increasing to 288 million in 2040 (Wong et al., 2014).

1.1.1. Anatomy of healthy human retina

The human retina is a light-sensitive layer lining the inside of the posterior segment of the eye (Yanoff et al., 2009). It consists of two distinct layers: 1) the neuroretina consisting of photoreceptor cells, neuronal cells and glial cells; and 2) the RPE separated from the neuroretina by a virtual subretinal space. When light entering the eye is focused on the retina, the neuroretina serves to convert light into neural signals. A complex neural circuitry within the retina relays these signals to visual centres in the brain (Luo et al., 2008). Retinal photoreceptors are metabolically active neurons with oxygen requirements that are among the highest in the human body (Wong-Riley, 2010). The outer segments of photoreceptors comprise stacks of flattened membranous discs containing light-sensitive photopigments (rhodopsin in rods and spectrally tuned red-, green- or blue-sensitive opsins in cones). The macula

(Latin for “spot”) is a distinct feature of human and most non-human primate retina and lies in the central visual axis. The human macula (about 6 mm in diameter) contains a cone-dominated fovea (0.8 mm in diameter) that is associated with high-acuity vision (Curcio et al., 1990) (**Figure 1A and B**).

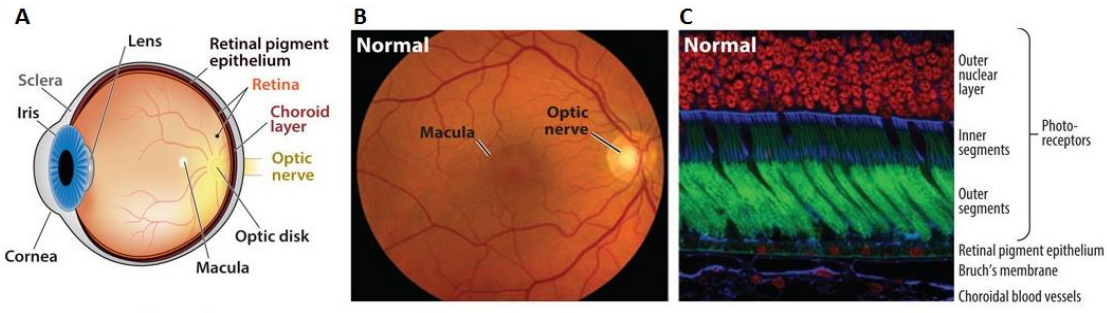

Figure 1: Anatomy of retina. (**A**) Anatomical depiction of the human eye viewed in sagittal section; (**B**) Fundus photograph of the retina of a healthy individual, using an ophthalmoscope; (**C**) Confocal microscopy image of a human retina labeled with fluorescent probes. Cell nuclei in the outer nuclear layer of photoreceptors are indicated by red, photoreceptor outer segments are green and structures containing high concentrations of filamentous actin (cell–cell junctions and vessel walls) are blue. Adapted and modified from Fritsche et al. (2014).

The RPE, which constitutes the outer blood-retinal barrier (BRB) (Bernstein and Hollenberg, 1965), facilitates photoreceptor turnover by phagocytosis and lysosomal degradation of outer segments following shedding (Young, 1969; LaVail, 1983). Moreover, the RPE serves as an excellent support system to the neuroretina, by delivery of oxygen and metabolites to the photoreceptors, preventing extracellular fluid leaking into the subretinal space from the underlying choriocapillaris (a continuous layer of fenestrated capillaries), actively pumping fluid out of the subretinal space and regulating trafficking of immune cells across the BRB (Forrester and Xu, 2012). The inner aspect of the choroid, next to the RPE, is Bruch’s Membrane (BrM), a laminar extracellular matrix (ECM) of collagen and elastin (Curcio et al., 2013). BrM works as a supply chain by transporting oxygen, glucose and other metabolites to RPE and photoreceptors, and returns metabolic wastes to systemic circulation (Booij et al., 2010). Integrity of the BrM appears to be important in suppressing invasion of vessels from the choroidal circulation into the retina (Chong et al., 2005). The choriocapillaris arises from the branches of posterior ciliary arteries and supplies the photoreceptor-RPE complex and outer neuroretina, while the inner parts of the neuroretina are supplied by the central retinal artery (Bernstein

and Hollenberg, 1965). **Figure 1C** shows the order of photoreceptors, RPE, Bruch's membrane and choroidal blood vessels in a confocal microscopy image of a human retinal section.

1.1.2. Pathology and pathogenesis of AMD

A general hallmark of aging retina is the accumulation of lipofuscin in the lysosomal compartments and the cytoplasm of RPE cells. Lipofuscin are autofluorescent granules that are remnants of retinoid metabolites from shed photoreceptor outer-segment membranes. A2E, an abundant component of lipofuscin (Delori et al., 2001; Strauss, 2005) is hypothesized to exacerbate AMD through photo-oxidation and phototoxicity in RPE cells (Sparrow and Boulton, 2005). The photo-oxidation could serve as a trigger for activation of the complement system, a trigger that would thereby predispose the macula to disease and contribute to the chronic inflammatory processes observed in AMD pathogenesis. Furthermore, the excessive accumulation of lipofuscin and the consequent activation of the complement cascade might, over time, also contribute to the formation of drusen (Zhou et al., 2006; Zhou et al., 2009). Drusen are cellular debris at the interface between RPE and BrM (or between RPE and neuroretina). Drusen are classified as small (<63 μm in diameter with discrete margins), medium (63–124 μm) or large (>125 μm with indistinct edges) (Ferris et al., 2005). In a recent study, using a combination of high-resolution analytical techniques, tiny hydroxyapatite (bone mineral) spherules with cholesterol-containing cores are found in all examined drusen, which may be responsible for initiation of drusen formation (Thompson et al., 2015). Drusen components include lipids and an array of proteins, including those involved in complement regulation, Tissue Inhibitor of Matrixmetalloproteases-3 (TIMP3), vitronectin, β-amyloid and apolipoproteins (E, B, A-I, C-I and C-II), plus zinc and iron ions (Arnhold et al., 1998; Mullins et al., 2000; Crabb et al., 2002). AMD patients display a broad spectrum of clinical characteristics based upon drusen size and AMD pigmentary abnormalities, both hypopigmentation and hyperpigmentation. Clinical examination of human retinas can reveal distinct hallmarks of AMD that can be broadly divided into early/intermediate and late (advanced) stages. Age-Related Eye Disease Study (AREDS) has developed a five-step severity scale to define risk categories for development of advanced AMD. Early or intermediate AMD (AREDS grades 2 and 3) is the most common and least severe

form. Late AMD (AREDS grades 4 and 5) is usually subdivided into dry [geographic atrophy (GA)] and wet [choroidal neovascularization (CNV)] (Ferris et al., 2005). These pathological hallmarks of early AMD and late AMD (GA and CNV) are shown in **Figure 2.** The AREDS grades and their characteristics are listed in **Table 1.**

Figure 2: Pathological hallmarks of early AMD and late AMD revealed by fundus photography. (**A**) Eye with drusen: visible as small yellow spots; (**B**) wet AMD: eye with choroidal neovascularization and exudation; (**C**) dry AMD: eye with advanced geographic atrophy. Adapted from Ratnapriya and Chew (2013).

Table 1: Stages of AMD divided into AREDS categories according to characteristics

AREDS Category	**Stages of AMD**	**Characteristics**
Category 1	*No AMD*	A few small or no drusen
Category 2	*Early Stage AMD*	Several small drusen or a few medium-sized drusen in one or both eyes
Category 3	*Intermediate AMD*	Many medium-sized drusen or one or more large drusen in one or both eyes
Category 4 and 5	*Advanced AMD*	In one eye only, either a break-down of light-sensitive cells and supporting tissue in the central retinal area (advanced dry form), or abnormal and fragile blood vessels under the retina (wet form)

To date, although no cure of dry AMD is available, the only available therapy for management of dry AMD is daily intake of antioxidant formulation (Age-Related Eye Disease Study Research, 2001; Age-Related Eye Disease Study 2 Research, 2013).

According to the first AREDS, combination of the following different antioxidants was administered: vitamin C (500 mg), vitamin E (400 international units [IU]), beta-carotene (15 mg), zinc (80 mg) and copper (2 mg). AREDS2 study suggested that lutein/zeaxanthin could be more appropriate than beta carotene in the AREDS-type supplements. Other promising antioxidants for dry AMD therapy include crocetin (Maccarone et al., 2008), curcumin (Mandal et al., 2009; Chang et al., 2014), Resveratrol (King et al., 2005; Nagineni et al., 2014), and vitamins B9, B12 and B6 (Christen et al., 2009). Besides antioxidants, new findings about pathogenesis of AMD have led to several potential therapeutic strategies (Buschini et al., 2015). Both AMD drusen and Alzheimer's disease plaques contain amyloid beta (Aβ) plaques, which are in strong association with activated complement components (Johnson et al., 2002; Ohno-Matsui, 2011). Humanized monoclonal antibodies: RN6G (Pfizer, New York, NY, USA) and GSK933776 (GlaxoSmithKline, Verona, Italy) (Ding et al., 2008; Ding et al., 2011) and a drug named glatiramer acetate (Butovsky et al., 2006a; Landa et al., 2008), directed against Aβ plaques, have been demonstrated to reduce drusen in AMD mice model and are undergoing clinical trials. Another group of drugs (fenretinide, ACU-4429 ALK-001) which showed reduction in accumulation of A2E and lipofuscin also presents an exciting possibility for treating AMD (Mata et al., 2013; Holz et al., 2014). Development of stem cell therapy for treatment of dry AMD is another promising strategy (Brandl et al., 2015). Development of surgical procedures to transplant human embryonic stem cells, which are able to differentiate into RPE cells, is currently under clinical trials (Carr et al., 2013).

The wet form, also known as neovascular or exudative AMD, constitutes only 10–15% of all AMD cases, but accounts for at least 80% of AMD-related blindness (Scholl et al., 2009). In this case, accelerated and profound visual loss typically occurs as a result of CNV, where new vessels grow and invade the retina resulting in sub-RPE or subretinal haemorrhages, or fluid accumulation in or below the layers of the retina (Ferris et al., 1984). In contrast to the typical slow progression of GA, CNV can decrease vision acutely through the abrupt onset of edema and bleeding from new capillaries invading the RPE and neural retina. Vascular endothelial growth factor (VEGF) has been implicated as a key mediator in the pathogenesis of CNV (Kvanta et al., 1996; Barouch and Miller, 2004; Adamis and Shima, 2005). CNV can be treated but not be cured with intraocular anti-VEGF antibodies (Ferris, 2004;

Gragoudas et al., 2004; Rosenfeld et al., 2011). Two most widely used monoclonal antibodies against VEGF are bevacizumab (Avastin™; Genentech, South San Francisco, CA, USA), a full-length, humanized monoclonal antibody against VEGF; and ranibizumab (Lucentis™; Genentech, South San Francisco, CA, USA), a recombinant, humanized, monoclonal antibody fragment directed toward all isoforms of VEGF-A (Presta et al., 1997; Chen et al., 1999; Ferrara et al., 2004). These antibodies bind and neutralize all the biologically active forms of VEGF and thereby inhibit angiogenesis. Aflibercept (VEGF trap-eye), a fusion protein consisting of key domains of the human VEGF1 and VEGF2 receptors coupled to the Fc part of a human IgG molecule, has been approved recently for neovascular AMD (Grisanti et. al, 2013). It is suggested by a theoretical model that Aflibercept may have a longer duration of action compared with other treatments (Ohr and Kaiser, 2012).

1.1.2.1. Role of microglia in AMD pathogenesis

Microglial cells are specialized immune cells that reside in the brain and retina, and are responsible for the initial detection of noxious stimuli arising in the local micro-environment (Kettenmann et al., 2011). Microglia are functionally different from blood-derived macrophages, which originate from bone marrow-derived monocytes and enter the CNS and retina during pathological conditions. Microglia are believed to originate from macrophages produced by primitive haematopoiesis in the yolk sac (Alliot et al., 1999). Morphologically, microglia are very adaptable, changing their phenotype depending on location and role (Gehrmann et al., 1995).

In the healthy retina, microglia are distributed throughout the inner and outer plexiform layers, where they carry out constant and dynamic surveillance of the extracellular microenvironment (Lee et al., 2008). In the resting state, they continuously scan the local environment and phagocytose cell debris (**Figure 3A**). Any detection of signs for challenges in the retina, leading to dysfunctions or degenerations in the RPE, photoreceptor layer and the ganglion cell, rapidly alert the microglia (**Figure 3B**). In the effector phase, microglia migrate to the lesion sites, accumulate in the nuclear layers and the subretinal space and subsequently turn into amoeboid phagocytes (**Figure 3C**).

This complex, multistage activation process converts the “resting microglial cells” into the “activated microglial cell” (Kettenmann et al., 2011). Microglia exhibit different states of activation, termed as proinflammatory M1 activation which includes “classical activation”, and anti-inflammatory M2 activation which includes “alternative activation” and “acquired deactivation”, depending on the milieu in which they become activated and the factors they are stimulated by (Le et al., 2001; Li et al., 2004; Block et al., 2007).

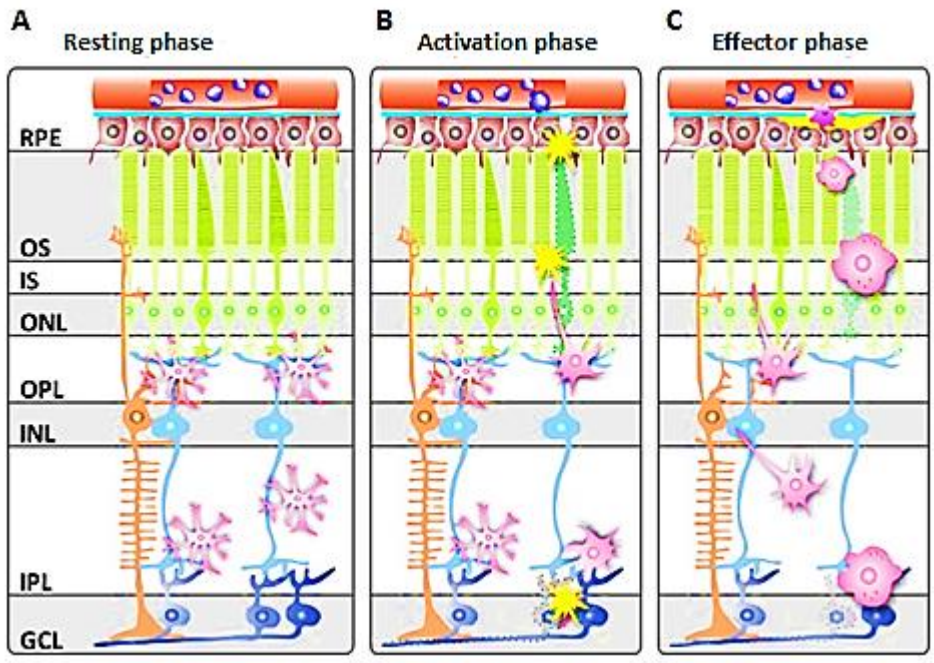

Figure 3*: *Schematic representation of three common phases of microglial activity in the retina. (**A**) Resting phase (**B**) Activation phase (**C**) Effector phase. Pink cell bodies indicate microglia; yellow stars: insults or injury; RPE: retinal pigment epithelium; ONL: outer nuclear layer; OPL: outer plexiform layer; INL: inner nuclear layer; IPL: inner plexiform layer; GCL: ganglion cell layer. Adapted and modified from Karlstetter et al. (2010).

Microglial cell bodies, typically situated in the inner retina in the normal human eye (Combadiere et al., 2007) can migrate to the subretinal space (the potential space between the photoreceptor outer segments and the apical surface of the RPE cells) in response to inflammatory stimuli (Gupta et al., 2003; Xu et al., 2009). Activated microglia have been found in the outer retina and subretinal space in eyes with AMD **(**Gupta et al., 2003**;** Combadiere et al., 2007). Retinal microglia express the chemokine receptor CX3CR1. Genetic polymorphisms in the *CX3CR1* gene have been associated with AMD and reduce the chemotactic ability of monocytes

(Combadiere et al., 2007). In *CX3CR1*-deficient mice, accumulation of microglia and macrophages in the subretinal space has been observed, contributing to drusen formation and photoreceptors degeneration (Combadiere et al., 2007; Sennlaub et al., 2013).

1.1.3. Etiology of AMD

Based on epidemiology and pathobiology, prevalence of AMD phenotypes depends on several risk factors: aging, environmental factors, demographic factors and genetic factors (Leveziel et al., 2011; Ratnapriya and Chew, 2013; Fritsche et al., 2014).

1.1.3.1. Aging

As numerous population-based studies indicate, AMD is particularly prevalent in people who are 60 years and older (Mitchell et al., 1995; Klein et al., 1999a; Klaver et al., 2001; Wong et al., 2008; Wong et al., 2014). Though aging might not be enough to trigger AMD single-handedly, along with genetic and environmental risk factors the pathological changes of AMD become more likely. Aging-associated expression changes in genes associated with mitochondrial function, protein metabolism and immune response have been identified in several tissues (Zahn et al., 2007) and are consistent with some proposed mechanisms for late-onset neurodegenerative diseases (Wright et al., 2004; Lin and Beal, 2006; Rubinsztein, 2006; Morimoto, 2008). A comparison of young and aging human retinas identified differential expression of a small number of genes involved in stress and immune response, protein and energy metabolism, and inflammation (Yoshida et al., 2002). According to another study, advanced age accounts for 30% of rod photoreceptor loss in the central macula (Curcio et al., 2000). Moreover, increasing amounts of A2E in lipofuscin as well as increasing thickness of BrM are also age-related ocular changes (Feeney-Burns and Ellersieck, 1985) that are potential triggers for AMD onset (Spraul et al., 1996). Although association of BrM thickness with AMD is debated (Chong et al., 2005), accumulation of lipoproteins has been found to be a significant age-related change (Curcio et al., 2001).

1.1.3.2. Environmental factors

Like all multifactorial complex diseases, environmental factors play an important role in AMD development. There are increasing number of evidences where smoking has been consistently associated with AMD, leading to a two-fold or greater risk of developing the disease when compared to non-smokers (Vingerling et al., 1996; Age-Related Eye Disease Study Research, 2000; McCarty et al., 2001; Nakayama et al., 2014; Gopinath et al., 2015; Wu et al., 2015). The mechanism by which smoking affects the retina is unknown; it has been proposed that smoking may alter the metabolism of the RPE by interfering with antioxidants and altering choroidal blood flow (Hawkins et al., 1999). Another independent report also supports that smoking causes oxidative insults to the retina (Espinosa-Heidmann et al., 2006).

Total fat intake was positively associated with risk of AMD, which may have been due to intake of individual fatty acids, such as linolenic acid, rather than to total fat intake per se (Cho et al., 2001). High fatty diet, obesity and other risk factors for cardiovascular diseases correlate with higher AMD susceptibility. Although the exact mechanism is not known, it is assumed that the contribution to AMD pathogenesis is related to increased oxidative stress, changes in the lipoprotein profile and increased inflammation resulting in increased cellular damage (Katta et al., 2009). Diet high in antioxidants lutein and zeaxanthin (found mostly in green leafy vegetables) and in omega-3 fatty acids (primarily found in fish) have been linked to a decreased risk of neovascular AMD (Flood et al., 2002; Seddon et al., 2003; Weikel et al., 2012).

Apart from diet and smoking, there are additional environmental factors that may influence AMD pathogenesis, including sunlight exposure (Cruickshanks et al., 2001; Delcourt et al., 2001; Khan et al., 2006), alcohol use (Moss et al., 1998; Cho et al., 2000; Chong et al., 2008) and infection by bacterial pathogens (particularly *Chlamydia pneumoniae*) (Kalayoglu et al., 2003; Baird et al., 2008).

1.1.3.3. Race/ethnicity

In 2006, an analysis of U.S. participants in the Multiethnic Study of Atherosclerosis (MESA) showed prevalence of AMD in persons aged 45 to 85 years to be 2.4% in African-Americans, 4.2% in Hispanics, 4.6% in Chinese-descent individuals and

5.4% in Caucasians (Klein et al., 2006). In a previous study by National Health and Nutritional Examination Survey it was observed that prevalence of AMD was 5.1% in Mexican-Americans, 7.3% in whites, and 2.4% in blacks (Klein et al., 1999b). These differences could be due to either environmental or genetic factors. It has been suggested that melanin may protect against the formation of lipofuscin (Weiter et al., 1986). In 2013, an updated analysis of prevalence of AMD among multiethnic cohort revealed that early AMD was present in 4.0% of the cohort and varied from 2.4% in blacks to 6.0% in whites. However, common factors such as smoking, body mass index, inflammatory factors, diabetes and alcohol were unable to explain the significant difference in risk between whites and blacks (Klein et al., 2013).

1.1.3.4. Genetic factors

The genetic predisposition is a major risk factor for the development of AMD. Evidence for a genetic contribution is undebatable and comes from classical epidemiological and twin studies and gene-mapping studies (Heiba et al., 1994; Klein et al., 1994; Klaver et al., 1998). In the largest twin study published to date, it has been reported that 71% of AMD risk can be attributed to genetic influences (Seddon et al., 2005).

1.1.3.4.1. The 1q31 locus

In 2005, a pioneering genome-wide association study (GWAS) suggested complement factor H (*CFH*) gene on 1q31 as the first major AMD susceptibility gene (Fisher et al., 2005). Simultaneously, several studies have validated this result (Hageman et al., 2005; Haines et al., 2005; Klein et al., 2005; Zareparsi et al., 2005). Among more than 20 variants in and around the *CFH* gene, rs1061170 (c.1204C>T) accounts for an amino acid substitution (Y402H) in the CFH protein (Klein et al., 2005). This synonymous single nucleotide polymorphism (SNP) lies within a haplotype conferring an increased risk for developing AMD by a factor of 2.5 in heterozygous carriers and by a factor of 6.2 in homozygous carriers (Conley et al., 2006). Another common polymorphism in *CFH*, rs1410996 (c.2237-543G>A), was also discovered which, along with rs1061170, has been found to be liable for 17% of AMD susceptibility (Li et al., 2006; Maller et al., 2006; Raychaudhuri et al., 2011). Another rare non-synonymous variant, *CFH* (c.3628C>T), which accounts for an

amino acid substitution (R1210C), increases AMD risk by >20-fold and is virtually absent in the control individuals (1 heterozygous carrier in 2,268 sequenced controls) (Zhan et al., 2013). In addition to simple sequence changes, deletions in two genes near *CFH*, *CFHR1* and *CFHR3*, have been associated with reduced risk of AMD (Hughes et al., 2006; Spencer et al., 2008).

1.1.3.4.2. The 10q26 locus

The second major AMD susceptibility locus is located on chromosome 10q26. The linkage to the genetic region at chromosomal segment 10q26 was first identified by (Weeks et al., 2000). In subsequent fine-mapping efforts designed to narrow the chromosome 10q26 linkage peak, the association signals were refined to three genes, namely, pleckstrin homology domain containing family A member 1 (*PLEKHA1*), age-related maculopathy susceptibility 2 (*ARMS2*, also known as *LOC387715*) and high temperature requirement factor A1 (*HTRA1*) (Jakobsdottir et al., 2005). *PLEKHA1* was later excluded as an AMD susceptibility gene (Rivera et al., 2005; Schmidt et al., 2006). As per the haplotype analysis done by Fritsche et al. (2008), the AMD-associated polymorphisms, that are fine-mapped on 10q26, continue on a 23.3 kb gene region. Overall, 15 AMD-associated polymorphisms were identified in this region (**Figure 4**), which are in a strong linkage disequilibrium (LD) to each other (Fritsche et al., 2008).

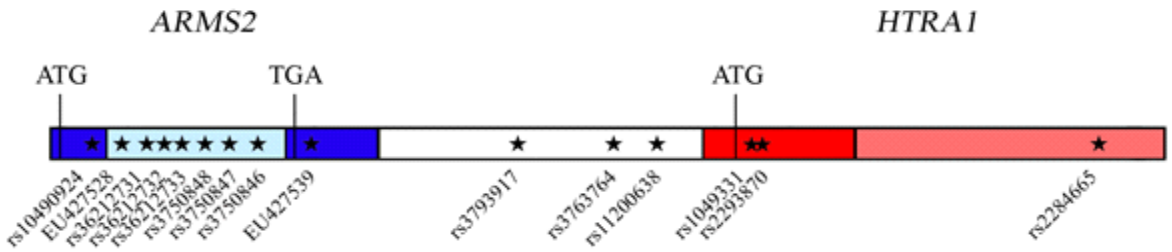

Figure 4: ***Schematic overview of the AMD-associated 23.3 kb region on chromosome 10q26 exhibiting high linkage equilibrium.*** Stars indicate the 15 AMD risk-associated polymorphisms; dark blue: ARMS2 exons 1 and 2; light blue: ARMS2 intron; white: intergenic region; dark red: HTRA1 exon 1; light red: HTRA1 intron 1. Adapted from Friedrich et al. (2011).

Further studies confirmed that all these polymorphisms occur together as an AMD-associated risk haplotype (Yang et al., 2006; Wang et al., 2009; Wang et al., 2010b).

Eleven of these polymorphisms are intronic or intergenic, and two are synonymous SNPs in *HTRA1* exon 1. The remaining two polymorphisms are located in the two exons of *ARMS2*. A non-synonymous SNP rs10490924 (c.205G>T) in the exon 1 of *ARMS2* leads to an amino acid substitution in the ARMS2 protein at position 69 (A69S), while EU427539 refers to a combination of a deletion and an insertion polymorphism within the 3' untranslated region (UTR) of the *ARMS*2 gene (*372_815delins54) (Fritsche et al., 2008).

There are a number of contradictory reports about the effect of these polymorphisms on the functions of ARMS2 or HTRA1. The amino acid substitution caused by rs10490924 could bring a functional change in the ARMS2 protein (Wang et al., 2009). The polymorphism EU427539, was shown to cause a destabilizing effect on the *ARMS2* mRNA (Fritsche et al., 2008; Friedrich et al., 2011). However, other studies suggest that no effect of EU427539 polymorphism on the transcription of *ARMS2* gene could be detected (Kanda et al., 2010; Wang et al., 2010b). Moreover, it has been shown that a common non-risk-associated non-synonymous variant, rs2736911 (c.112C>T), also leads to decreased *ARMS2* transcript levels (Friedrich et al., 2011). Many contradictory reports were also shown either to have or not to have an influence of AMD-associated polymorphisms on expression of HTRA1. Some evidences show a two- to three-fold upregulation in *HTRA1* expression due to the risk-associated polymorphisms (Yang et al., 2006; Chan et al., 2007; An et al., 2010; Yang et al., 2010; Iejima et al., 2015). These results are consistent with a transgenic mouse model that ubiquitously overexpresses HTRA1 and exhibits characteristics similar to those of wet AMD patients (Jones et al., 2011). However, in other publications, no effect of AMD haplotypes was found on the HTRA1 expression level (Kanda et al., 2007; Chowers et al., 2008; Kanda et al., 2010; Wang et al., 2010a; Friedrich et al., 2011; Wang et al., 2013). The effect of two AMD risk-associated synonymous polymorphisms in exon 1 of the *HTRA1*, namely rs1049331 (c.102C>T) and rs2293870 (c.108G>T), have been less studied because of the fact that they do not account for any amino acid change. A recent study by Jacobo et al. (2013) suggests that codon bias due to these synonymous polymorphisms results in difference in translation speed of the HTRA1 protein, which might affect its structure and function (Jacobo et al., 2013).

1.1.3.4.3. Other AMD-associated gene loci

The recent meta-analysis of more than 17,100 AMD cases and more than 60,000 control subjects of European and Asian origin reveals 19 loci from as many as 19 chromosomes to be associated with AMD (Fritsche et al., 2013) (**Figure 5**). After identification of strong association of *CFH* with AMD, subsequent association studies showed additional complement genes to be strongly associated with AMD. These include complement 2 (*C2*) and/or complement factor B (*CFB*) (Gold et al., 2006), complement 3 (*C3*) (Yates et al., 2007) and complement factor I (*CFI*) (Fagerness et al., 2009). In AMD lesions, presence of immunomodulators suggests that local processes driven by complement dysregulation play a vital role in the development and progression of AMD (Johnson et al., 2000; Anderson et al., 2010).

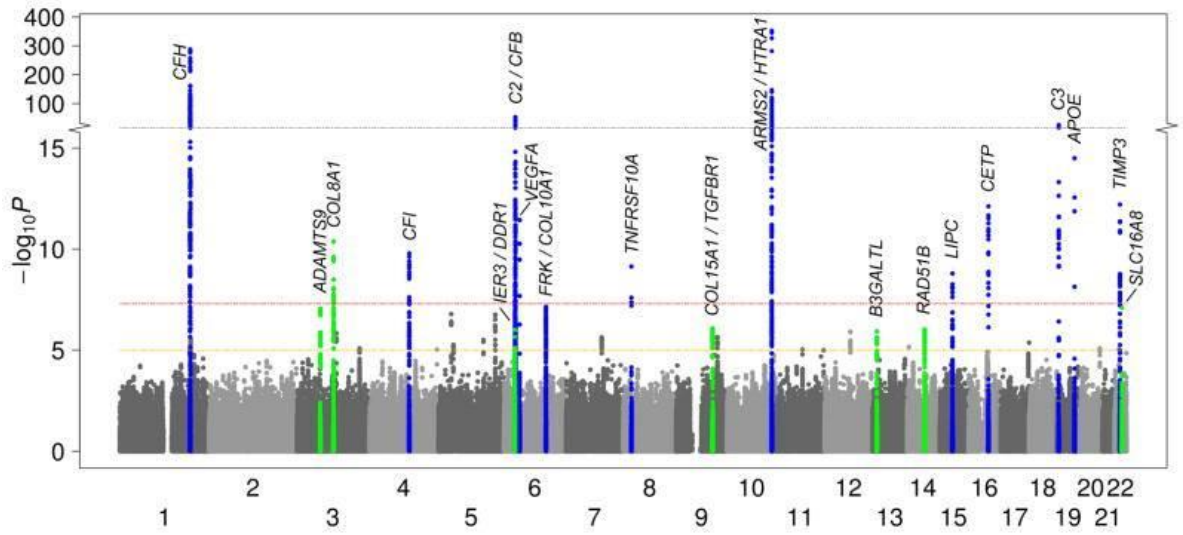

Figure 5*: *Nineteen common AMD risk variants in the discovery study of the AMD Gene Consortium meta-analysis. Summary of genome-wide association scan results in the discovery GWAS sample. Previously described loci before the meta-analysis reaching $p < 5\times10^{-8}$ are labeled in blue; newly found loci in the meta-analysis reaching $p < 5\times10^{-8}$ for the first time after follow-up are labeled in green. Adapted and modified from Fritsche et al. (2013).

Other than genes of complement system and genes on 10q26, functional analysis of a few other genes highly associated with AMD explains the development of AMD lesions. Hepatic lipase (LIPC) and cholesteryl ester transfer protein (CETP), found to be associated with AMD, are expressed in the subretinal space and may participate

in rapid cholesterol transfer from the RPE to the neural retina (Tserentsoodol et al., 2006a; Tserentsoodol et al., 2006b). Apolipoprotein E (ApoE) has also been detected in subretinal lesions where it promotes chronic inflammation in AMD (Levy et al., 2015). Tissue inhibitor of metalloprotienase 3 (TIMP3) has been found to play a pivotal role in ECM maintenance and remodeling in BrM (Fariss et al., 1997; Kamei and Hollyfield, 1999). Apart from this, seven previously unknown loci discovered in the meta-analysis are *COL8A1-FILIP1L, IER3-DDR1, SLC16A8, TGFBR1, RAD51B, ADAMTS9* and *B3GALTL*. Though weakly associated with the disease, functional analysis of these genes might lead to a clear idea of AMD pathogenesis.

1.2. HTRA1 protein

The HTRA family of proteins is broadly characterized by a highly conserved protease domain and one or more C-terminal protein-interaction domains (Singh et al., 2011; Malet et al., 2012). The first described member of HTRA family, the *Escherichia coli* (*E.coli*) HtrA protein (also called DegP or protease Do) is a periplasmic protein (Clausen et al., 2002) that is upregulated under stress conditions such as heat shock (Lipinska et al., 1988; Lipinska et al., 1989). HtrA functions as a chaperone and a protease in a temperature-dependent fashion (Spiess et al., 1999).

1.2.1. Structure of HTRA1

Figure 6: Structure of HTRA1. Boxes represent protein domains; blue box indicates S, signal peptide domain cleaved in mature secreted protein; purple box indicates MAC25/IGFBP(insulin growth factor–binding protein) domain; yellow box indicates Kazal-like domain (KI); green box indicates serine protease domain, which contains Histidine (H), Aspargine (D) and Serine (S) forming a catalytic triad; red box indicates PDZ [postsynaptic density protein (psd95), drosophila disc large tumor suppressor (dlga), and zonula occludens-1 protein (zo-1) domain]. Adapted from An et al. (2010).

HTRA1, a secreted protease was first identified in 1996 as a gene expressed in human fibroblast cells (Zumbrunn and Trueb, 1997). The degree of conservation

between human HTRA1 and its bacterial homologues DegP is very high (Clausen et al., 2002). Human HTRA1 is one of the four members of the human HTRA family and consists of 480 amino acids (about 50 kDa), which are encoded by the nine exons of the *HTRA1* gene. **Figure 6** depicts the structure of HTRA1. It has an N-terminal signal peptide (S) for secretion. After secretion, a 22 amino acid-long signal peptide of the HTRA1 protein is cleaved. The MAC25 domain has a homology to the insulin like growth factor binding protein (IGFBP) and follistatin. Although the MAC25 domain showed homology initially to IGFBP, later it turned out that it has obvious lower affinity for the insulin like growth factor (IGF) than other IGFBPs (Eigenbrot et al., 2012). The homology to follistatin, however, led to the discovery that the MAC25 domain of HTRA1 protein can bind to activin, a member of transforming growth factor-β (TGF-β) superfamily (Oka et al., 2004). Kazal inhibitors, specifically inhibit serine proteases like trypsin and elastase (Rawlings et al., 2004). The largest domain of HTRA1 is the protease domain with the catalytic triad of histidine (His220), asparagine (Asp250) and serine (Ser328), which defines HTRA1 as serine protease (**Figure 6**). By C-terminal protein interaction domain named “postsynaptic density protein (psd95), drosophila disc large tumor suppressor (dlga), and zonula occludens-1 protein (zo-1) domain” (PDZ), HTRA1 binds to its substrates.

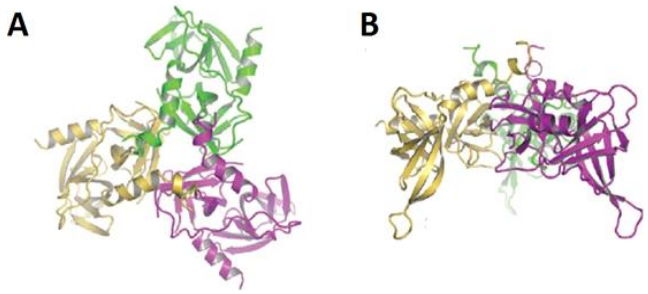

***Figure 7*: Three-dimensional structure of HTRA1 trimer.** Ribbon presentation of HTRA1 (inactive structure) in (**A**) top and (**B**) side views. The individual monomers are shown in different colors. Adapted and modified from Truebestein et al.(2011).

HTRA1 forms a trimeric structure which is mediated by N-terminal amino acid residues of the protease domain (**Figure 7**) (Truebestein et al., 2011). The protein interaction domain (PDZ) binds sequence-specifically to short C-terminal or internal hydrophobic sequences of peptides. In this case, the PDZ domains of the members of HTRA family are different, when it comes to ligand specificity. Previously, it was

assumed that the PDZ domain of HTRA1 negatively regulates the proteolytic activity. Thus, the protease activity is to be activated only when the PDZ domain binds to the ligands (Murwantoko et al., 2004). However, based on the latest study of the crystal structure of HTRA1 trimers, the research groups of Tim Clausen and Michael Ehrmann showed that PDZ domain is not indespensible for the protease activity. Instead substrate binding to the active site is sufficient to stimulate protease activity (Truebestein et al., 2011). Accordingly, no allosteric ligands would be necessary for the activation of HTRA1 as opposed to activation of bacterial HtrA.

1.2.2. Function of HTRA1

HTRA1 was reported to influence cell signaling (Oka et al., 2004; Zhang et al., 2012; Graham et al., 2013; Supanji et al., 2013), organization of the ECM (Mauney et al., 2010; Vierkotten et al., 2011), embryogenesis (De Luca et al., 2004) and skeletal development and osteogenesis (Tsuchiya et al., 2005; Hadfield et al., 2008). Various publications have identified an array of interaction partners of HTRA1 such as members of TGF-β family (BMP3, GDF5, activin, TGF-βs) (Oka et al., 2004); aggrecan, biglycan, decorin, fibromodulin, fibronectin, soluble type II collagen and elastin (Tsuchiya et al., 2005); mature TGF-β1 (Launay et al., 2008); tubulin (Chien et al., 2009); tuberous sclerosic complex 2 (Campioni et al., 2010); clusterin, vitronectin, fibromodulin, alpha-2 macroglobulin and ADAM9 (An et al., 2010); fibronectin, fibulin 5 and nidogen 1 (Vierkotten et al., 2011); pro-TGF-β1 (Shiga et al., 2011); IGF-1(Jacobo et al., 2013); and TGF-β receptors II and III (Graham et al., 2013). In addition, HTRA1 was suggested to influence the pathogenic processes of several diseases including CARASIL (cerebral autosomal recessive arteriopathy with subcortical infarcts and leukoencephalopathy) (Hara et al., 2009; Shiga et al., 2011), osteoarthritic cartilage (Grau et al., 2006; Chamberland et al., 2009; Polur et al., 2010), preeclampsia (Ajayi et al., 2008) and AMD (Vierkotten et al., 2011; Zhang et al., 2012; Nakayama et al., 2014). HTRA1 may also exhibit tumor suppressor activities (Baldi et al., 2002; De Luca et al., 2003; Chien et al., 2004), as downregulation of the protein was observed in a variety of cancers, e.g., endometrial, ovarian or breast cancers, and melanomas (Baldi et al., 2002; Shridhar et al., 2002; Chien et al., 2004; Bowden et al., 2006; Mullany et al., 2011; Wang et al., 2012). Despite its suspected role in the various disease processes, the exact mechanisms of HTRA1 are largely unknown.

2. AIM OF THE STUDY

Several polymorphisms in *HTRA1* located in chromosomes 10q26 have been reported to be associated with AMD by various independent studies (Dewan et al., 2006; Fritsche et al., 2013). Recently, two synonymous polymorphisms have been found to have effect on the translational efficiency of HTRA1 and its binding capacity of IGF-1 (Jacobo et al., 2013). The focus of our study was set on unraveling the effect of AMD-associated synonymous SNPs rs1049331 (c.102C>T) and rs2293870 (c.108G>T) within exon 1 of *HTRA1* on the conformation, secretion and substrate affinity of HTRA1 protein. In several studies, HTRA1 has been shown to inhibit TGF-β signaling (Oka et al., 2004; Launay et al., 2008; Shiga et al., 2011; Zhang et al., 2012; Graham et al., 2013; Karring et al., 2013). So, the aim also included the influence of synonymous polymorphisms on regulation of intracellular TGF-β signaling. The final aim was to investigate the effect of HTRA1 on activation of microglial cells.

3. MATERIALS AND METHODS

3.1. Materials

3.1.1. Chemicals and reagents

Table 2: Chemicals and reagents

Chemical/reagent	Supplier
2-Nitrophenyl β-D-galactopyranoside (ONPG)	Sigma-Aldrich, St. Louis, MO, USA
2-Propanol	Merck Chemicals GmbH, Schwalbach, Germany
4',6-diamidino-2-phenylindole (DAPI)	Merck Chemicals GmbH, Schwalbach, Germany
5-Bromo-4-chloro-3-indolyl β-D-galactopyranoside (X-Gal)	AppliChem GmbH, Darmstadt, Germany
β-casein from bovine milk	Sigma-Aldrich, St. Louis, MO, USA
β-Mercaptoethanol	Sigma-Aldrich, St. Louis, MO, USA
Acetic Acid (100%)	Merck Chemicals GmbH, Schwalbach, Germany
Albumin fraction V (BSA)	AppliChem GmbH, Darmstadt, Germany
Ammonium persulfate (APS)	AppliChem GmbH, Darmstadt, Germany
Agarose (Byozyme LE)	Biozym Scientific GmbH, Hessisch Oldendorf, Germany
Ampicillin	Carl Roth GmbH, Karlsruhe, Germany
Bacto™ Agar	Becton, Dickinson and Company, Franklin Lakes, USA
Bacto™ Yeast Extract	Becton, Dickinson and Company, Franklin Lakes, USA
Boric acid (H_3BO_3)	Merck Chemicals GmbH, Schwalbach, Germany
Bromphenol blue	Sigma-Aldrich, St. Louis, MO, USA
Casein from Bovine Milk	Merck Chemicals GmbH, Schwalbach, Germany
Coomassie Billiant Blue	(Thermo Scientific) VWR International, Germany

Chemical/reagent	Supplier
Developer solution	AGFA, Mortsel, Belgium
Dimethyl sulfoxide (DMSO)	Merck Chemicals GmbH, Schwalbach, Germany
Ethanol	J.T. Baker, Phillipsburg, USA
Ethanol ≥99,8 p.a	Carl Roth GmbH, Karlsruhe, Deutschland
Ethidium bromide	AppliChem GmbH, Darmstadt, Germany
Ethylenediaminetetraacetic acid (EDTA)	(Titriplex) Merck Chemicals GmbH, Schwalbach, Germany
FlAsH-EDT_2	Invitrogen, Carlsbad, CA, USA
Fixer solution	AGFA, Mortsel, Belgium
Glycerol	AppliChem GmbH, Darmstadt, Germany
Hi-Di™ Formamide	Applied Biosystems Inc., Foster City, USA
HTRA1(His-tagged)	ProteaImmun GmbH, Berlin, Germany
Hydrogen chloride (HCl)	Merck Chemicals GmbH, Schwalbach, Germany
Hydrogen peroxide	Merck Chemicals GmbH, Schwalbach, Germany
Isopropyl β-D-1-thiogalactopyranoside (IPTG)	AppliChem GmbH, Darmstadt, Germany
Luminol	Sigma-Aldrich, St. Louis, MO, USA
Methanol	Merck Chemicals GmbH, Schwalbach, Germany
Milk powder	Carl Roth GmbH, Karlsruhe, Germany
p-Coumarin acid	Sigma-Aldrich, St. Louis, MO, USA
Paraformaldehyde (PFA)	Merck Chemicals GmbH, Schwalbach, Germany
Phenylmethanesulfonylfluoride (PMSF)	Merck Chemicals GmbH, Schwalbach, Germany
Roti® Quant	Carl Roth GmbH, Karlsruhe, Germany
Rotiphorese Gel 40 (29:1) acrylamide/bisacrylamide	Carl Roth GmbH, Karlsruhe, Germany
Sodium acetate, trihydrate	AppliChem GmbH, Darmstadt, Germany
Sodium carbonate (Na_2CO_3)	Merck Chemicals GmbH, Schwalbach, Germany

Chemical/reagent	Supplier
Sodium chloride (NaCl)	VWR International, LLC, West Chester, USA
Sodium hydroxide (NaOH)	Merck Chemicals GmbH, Schwalbach, Germany
Sodium dodecyl sulfate (SDS)	Carl Roth GmbH, Karlsruhe, Germany
Sodium hydrogen carbonate ($NaHCO_3$)	AppliChem GmbH, Darmstadt, Germany
TCEP HCl	Thermo Fisher Scientific, Hudson, USA
Tetramethylethylenediamine (TEMED)	AppliChem GmbH, Darmstadt, Germany
Tris(hydroxymethyl)aminomethane (Tris)	Merck Chemicals GmbH, Schwalbach, Germany
Trypsin EDTA in 10X Buffer	PAA Laboratories GmbH, Parsching, Austria
TPCK-trypsin	Sigma-Aldrich, St. Louis, MO, USA
Tryptone/Peptone from casein	Carl Roth GmbH, Karlsruhe, Germany
Xylene cyanol	Sigma-Aldrich, St. Louis, MO, USA
X-gal (5-bromo-4-chloro-3-indolyl-β-D-galactopyranoside)	AppliChem GmbH, Darmstadt, Germany
Recombinant TGF-β1	PeproTech, Hamburg, Germany
Recombinant interleukin 4 (IL4)	PeproTech, Hamburg, Germany
Lipopolysaccharide (LPS) from *E.coli*	Sigma-Aldrich, St. Louis, MO, USA

3.1.2. Kits and ready-made solutions

Table 3: Kits and ready-made solutions

Kit/solution	Supplier	Application
10X ThermoPol Reaction Buffer	New England BioLabs® Inc., Ipswich, USA	A-tailing of PCR products
5X GoTaq® Reaction Buffer Kit	Promega Corporation, Madison, USA	PCR
Griess Reagent System	Promega Corporation, Madison, USA	Nitrite measurement
AccuPrime™ Taq Polymerase PCR	Life Technologies, Carlsbad, CA, USA	PCR

Kit/solution	Supplier	Application
BigDye® Terminator v1.1 Cycle Sequencing Kit	Applied Biosystems Inc., Foster City, USA	Cycle sequencing
dNTP-Set	Genaxxon BioScience GmbH, Ulm, Germany	PCR, cDNA synthesis
Luciferase Assay Reagent	Promega Corporation, Madison, USA	Luciferase assay
NEBuffer CutSmart®	New England BioLabs® Inc., Ipswich, USA	Restriction digestion
NucleoBond® Xtra Midi	MACHEREY-NAGEL GmbH & Co. KG, Düren, Germany	Plasmid isolation
NucleoSpin® Extract II	MACHEREY-NAGEL GmbH & Co. KG, Düren, Germany	Gel extraction of DNA fragments
NucleoSpin® Plasmid	MACHEREY-NAGEL GmbH & Co. KG, Düren, Germany	Plasmid isolation
GeneRuler™ DNA Ladder Mix	Fermentas International Inc., Burlington, Canada	Marker for DNA electrophoresis
PageRuler™ Prestained Protein Ladder	Fermentas International Inc., Burlington, Canada	Marker for protein electrophoresis
pGEM®-T Vector System	Promega Corporation, Madison, USA	Subcloning
Reporter Lysis 5X Buffer	Promega Corporation, Madison, USA	Luciferase assay
RevertAid™ 5X Reaction Buffer	Fermentas International Inc., Burlington, Canada	cDNA synthesis
RNA*later*®	Applied Biosystems/Ambion, Austin, USA	RNA purification
RNase-Free DNase Set	Qiagen N.V., Hilden, Germany	RNA purification
RNeasy® Mini Kit	Qiagen N.V., Hilden, Germany	RNA purification
SuperSignal West Femto Maximum Sensitivity Substrate	Thermo Fisher Scientific, Hudson, USA	Immunoblot: protein detection by chemiluminescence
T4 DNA Ligase Reaction Buffer (10X)	New England BioLabs® Inc., Ipswich, USA	Ligation
Taq buffer 15 mM $MgCl_2$ (10X)	New England BioLabs® Inc., Ipswich, USA	PCR
TaqMan® Gene Expression Master Mix	Applied Biosystems Inc., Foster City, USA	qRT-PCR

Kit/solution	Supplier	Application
TC-FlAsH™ II In-Cell Tetracysteine Tag Detection (Green Fluorescence)	Invitrogen, Carlsbad, CA, USA	MicroScale Thermophoresis
*Trans*IT®-LT1 Transfection Reagent	Mirus Bio LLC, Madison, USA	Transfection
SuperSignal West Femto Maximum Sensitivity Substrate	VWR International Germany GmbH, Darmstadt, Germany	Western blot
Twin-Strep® Kit	IBA GmbH, Göttingen, Germany	Recombinant protein purification

3.1.3. Buffers and solutions

Table 4: Buffers and solutions

Buffer	Chemical Composition	Percentage Composition
Blocking solution	Milk powder 1X PBS or 1XPBST	3% (w/v)
Coomassie stainer	Methanol Acetic acid Coomassie Brilliant Blue	30% 10% 0.10% w/v
Coomassie destainer	Methanol Acetic acid	30% 10%
DNA-loading buffer (10X)	Tris-HCl pH 7.5, Sodium acetate, EDTA, Glycine, Bromphenol blue Xylene cyanol	10 mM 5 mM 2 mM 10% v/v 0.001% v/v 0.001% v/v
ECL solution 1	Luminol 0.1 M Tris-HCl	50 mg 200 ml
ECL solution 2	p-Coumarin acid DMSO	0.0011%
Laemmli buffer	Tris-HCl pH 6.8, Glycerine β-mercaptoethanol SDS Bromphenol blue	195 mM 30% 10% 6% 0.75%

Buffer	Chemical Composition	Percentage Composition
PBS (10X)	NaCl Na_2HPO_4 KCl KH_2PO_4, pH 7.4	1.37 M 100 mM 27 mM 18 mM
SDS-running buffer (10X)	Tris-HCl Glycine SDS, pH 8.6	25 M 2 M 10% (w/v)
Digestion buffer pH 7.5	Tris-HCl NaCl $CaCl_2$	50 mM 150 mM 5 mM
Casein solution	Casein from bovine milk Digestion buffer pH 7.5	0.02%
TBE (5X)	Tris-HCl, H_3BO_3, EDTA, pH 7.4	0.5 M 0.5 M 10 mM
TE buffer	Tris-HCl EDTA, pH 7.5 or pH 8.0	10 mM 1 mM
TRIS buffer saline	Tris-HCl [pH 8.0], NaCl	150 mM 100 mM
Towbin transfer buffer	Tris-HCl Glycine Methanol	0.025 M 0.192 M 20%
Twin-Strep® Elution Buffer (Buffer E)	Tris-HCl pH 8 NaCl EDTA Desthiobiotin	100 mM 150 mM 1 mM 2.5 mM
Twin-Strep® Regeneration Buffer (Buffer R)	Tris-HCl pH 8 NaCl EDTA HABA	100 mM 150 mM 1 mM 1 mM
Twin-Strep® Wash Buffer (Buffer W)	NaCl EDTA Tris-HCl pH 8	150 mM 1 mM 100 mM
X-Gal solution	X-Gal DMSO	0.04% w/v
Xylene cyanol	Xylene cyanol Glycerin (87%) H_2O dest.	0.1% v/v 40% v/v Ad. 50 ml

3.1.4. Cell lines

3.1.4.1. Bacterial cells

Table 5: E.coli strains

Strain	Genotype	Reference/Origin
E.coli strain DH5α	*fhuA2 Δ(argF-lacZ)U169 phoA glnV44 Φ80 Δ(lacZ)M15 gyrA96 recA1 relA1 endA1 thi-1 hsdR17*	Life Technologies, Carlsbad, CA, USA
E.coli strain JM110	*rpsL (Strr) thr leu thi-1 lacY galK galT ara tonA tsx dam dcm supE44 ∆(lac-proAB) [F´ traD36 proAB laclq Z∆M15].*	Life Technologies, Carlsbad, CA, USA

3.1.4.2 Mammalian cell lines

Table 6: Mammalian cell lines

Cell line	Origin	Culture
Hek293-Ebna cells	Human embryonic kidney cells	Invitrogen, Carlsbad, CA, USA
MLEC-PAI/Luc cells	Mouse lung epithelial cells (MLEC) stably transfected with an expression construct containing a truncated PAI-1 promoter fused to the firefly luciferase reporter gene	ATCC, Manassas, VA, USA
BV-2	Mouse microglia cells	Kindly provided by Prof. Thomas Langmann, Department of Ophthalmology, University of Cologne, Germany

3.1.4.3. Media and supplements

Table 7: Cell culture media and supplements

Cell culture medium	Suppliers
DMEM High Glucose (4.5 g/l) with L-Glutamine	(Gibco) Life Technologies GmbH, Darmstadt, Germany
Fetal Bovine Serum Gold (FBS)	(Gibco) Life Technologies GmbH, Darmstadt, Germany
Opti-MEM® I Reduced Serum Media	(Gibco) Life Technologies GmbH, Darmstadt, Germany
Genticin Sulphate (G418) Solution	(PAA) GE Healthcare, Galfont St Giles, United Kingdom
Penicillin/Streptomycin/L-Glutamine	(PAA) GE Healthcare, Galfont St Giles, United Kingdom
RPMI 1640 without L-Glutamine	(PAA) GE Healthcare, Galfont St Giles, United Kingdom
Dulbecco's 10X PBS	(Gibco) Life Technologies GmbH, Darmstadt, Germany

Table 8: Medium for cultivation of E.coli

Medium	Composition
LB medium	1% NaCl, 1% Tryptone/Peptone from casein, 0.5% Bacto™ Yeast Extract

LB medium for cultivation of *E.coli* was sterilized by autoclaving and stored at 4°C. For casting of plates, 1.5% Bacto™ Agar were added to the medium prior to autoclaving. If needed, autoclaved medium was supplemented with 100 µg/ml ampicillin (LB_{Amp}).

3.1.5. Enzymes

Table 9: Enzymes

Enzyme	Supplier	Application
AccuPrime™ Taq Polymerase	Life Technologies, Carlsbad, CA, USA	PCR
XhoI	New England BioLabs® Inc., Ipswich, USA	Restriction digestion

Enzyme	Supplier	Application
BseRI	New England BioLabs® Inc., Ipswich, USA	Restriction digestion
FseI	New England BioLabs® Inc., Ipswich, USA	Restriction digestion
NotI-HF™	New England BioLabs® Inc., Ipswich, USA	Restriction digestion
DpnI	New England BioLabs® Inc., Ipswich, USA	Methylated sequence cutter
PfuUltra HF DNA polymerase	Agilent Technologies, CA, USA	PCR
Proteinase K	Merck KGaA, Darmstadt, Germany	DNA isolation
RevertAid™ M-MuLV Reverse Transcriptase	Fermentas International Inc., Burlington, Canada	cDNA synthesis
T4 DNA Ligase	New England BioLabs® Inc., Ipswich, USA	Ligation
Taq DNA Polymerase	New England BioLabs® Inc., Ipswich, USA	A-tailing of PCR products

3.1.6. Antibodies

Table 10: Primary antibodies (mAB: monoclonal antibody; pAB: polyclonal antibody; WB: Western blot)

Antibody	Type	Species	Dilution	Use	Reference
HTRA-1 (AB 65902)	pAB	Rabbit	1:2000	WB	abcam, Cambridge, United Kingdom
β-actin(ACTB)	mAB	Mouse	1:10,000	WB	Sigma-Aldrich, St. Louis, MO, USA
TGF-β1(SC-146)	pAB	Rabbit	1:10,000	WB	Santa CruzBiotechnology, Inc., Dallas, TX, USA
SMAD-2	pAB	Rabbit	1:1000	WB	Cell Signaling Technology, Beverly, MA, USA
pSMAD-2	pAB	Rabbit	1:1000	WB	Cell Signaling Technology, Beverly, MA, USA

Table 11: Secondary antibodies

Antibody	Supplier	Application
Goat anti-mouse IgG, peroxidase conjugate	(Calbiochem) Merck Chemicals GmbH, Schwalbach, Germany	WB
Goat anti-rabbit IgG, peroxidase conjugate	(Calbiochem) Merck Chemicals GmbH, Schwalbach, Germany	WB

3.1.7. Vectors and plasmids

Table 12: Starting vectors

Vector	Supplier
pCEP4	Invitrogen™, Carlsbad, USA
pGEM®-T Vector	Promega Corporation, Madison, USA
pEXPR-IBA103	IBA GMBH, Göttingen, Germany

Table 13: Control plasmids and plasmids with insert already available

Plasmid	Supplier
"pGEM®-T + HTRA1 mRNA non-risk" (pGEM®-T construct for *HTRA1:CG* variant)	Institute of Human Genetics, University Hospital Regensburg, Regensburg, Germany
"pCEP4 + HTRA1 mRNA non-risk" (pCEP4 construct for *HTRA1:CG* variant)	Institute of Human Genetics, University Hospital Regensburg, Regensburg, Germany
"pCEP4 + HTRA1 mRNA risk" (pCEP4 construct for *HTRA1:TT* variant)	Institute of Human Genetics, University Hospital Regensburg, Regensburg, Germany
"pEXPR-IBA103 + HTRA1 mRNA non-risk" (pEXPR-IBA103 construct for *HTRA1:CG* variant)	Institute of Human Genetics, University Hospital Regensburg, Regensburg, Germany
"pEXPR-IBA103 + HTRA1 mRNA risk" (pEXPR-IBA103 construct for *HTRA1:CG* variant)	Institute of Human Genetics, University Hospital Regensburg, Regensburg, Germany

3.1.8. Oligonucleotides

The following oligonucleotides were used as primers and were supplied by Metabion International AG (Martinsried, Germany).

Table 14: Sequence and use of oligonucleotides for PCR in the study

Primer Name	Sequence 5'-3'	Use
Htra1- endoBseRI-F	CAAAATTGACCACCAGGGCAAGC	Cloning TC-tagged *HTRA1:CG* or *HTRA1:TT* in pCEP4 vector
Htra1-TCtag-R	GCAACAGCCAGGACAACATGGGTCAATTTCTTCGGGAATCACTGTGAT	Cloning TC-tagged *HTRA1:CG* in pCEP4 vector
Htra1-TCtag-R2	AAGAAATTGACCCATGTTGTCCTGGCTGTTGCTAGCTCGAG	Cloning TC-tagged *HTRA1:CG* or *HTRA1:TT* in pCEP4 vector
Htra1-TCtag-R2 (rev. comp.)	CTCGAGCTAGCAACAGCCAGGACAACATGGGTCAATTTCTT	Cloning TC-tagged *HTRA1:CG* or *HTRA1:TT* in pCEP4 vector
Htra1-mRNA-NotI-F	GCGGCCGCGCGCACTCGCACCCGCT	Cloning TC-tagged *HTRA1:TT* in pCEP4 vector
Htra1-RT-R2	GATGGCGACCACGAACTC	Cloning TC-tagged *HTRA1:TT* in pCEP4 vector
HTRA1_SN_MUT_F	GCAGCGGTCTGGGCACCCGGCGGCCAAAGGC	Cloning TC-tagged *HTRA1:CC* in pCEP4 vector
HTRA1_SN_MUT_R	GCCTTTGGCCGCCGGGTGCCCAGACCGCTGC	Cloning TC-tagged *HTRA1:CC* in pCEP4 vector
HTRA1-RT-F2	AGCAGACATCGCACTCATCA	Sequencing of HTRA1 constructs
HTRA-Ex1-F0	AGGCCCTCCTGCACTCT	Sequencing of HTRA1 constructs
HTRA1-Ex1-R2	CGCCGCACGGGCCCTCC	Sequencing of HTRA1 constructs
HTRA1-Ex2-R	GCCATCTTCCCACCACGT	Sequencing of HTRA1 constructs

Primer Name	Sequence 5'-3'	Use
HTRA1-Ex1-F	AGAGCGCCATGCAGATCC	Sequencing of HTRA1 constructs
pEXPR-IBA103-F	GAGAACCCACTGCTTACTGGC	Sequencing of Strep-tagged constructs
pEXPR-IBA103-R	TAGAAGGCACAGTCGAGG	Sequencing of Strep-tagged constructs
M13-F	CACGACGTTGTAAAACGAC	Sequencing of pGEM®-T constructs
M13-R	GGATAACAATTTCACACAGG	Sequencing of pGEM®-T constructs

Table 15: Primers for first strand cDNA synthesis

Name	**Supplier**
Random hexamer primer	Fermentas International Inc., Burlington, Canada

Table 16: Probes and oligonucleotides used for qRT-PCR

Gene	Primer Name	Sequence	Roche Probe #
Arg1	mARG1_RT_F1	GAATCTGCATGGGCAACC	2
	mARG1_RT_R1	GAATCCTGGTACATCTGGGAAC	
Ym1	mYM1-RT-F3	AAGACACTGAGCTAAAAACTCTCC	88
	mYM1-RT-R3	GAGACCATGGCACTGAACG	
IL6	mIL6-RT-F	CCAGGTAGCTATGGTACTCCAGA	6
	mIL6-RT-R	GATGGATGCTACCAAACTGGAT	
iNOS	mINOS-RT-F	CTTTGCCACGGACGAGAC	3
	mINOS-RT-R	TCATTGTACTCTGAGGGCTGA	
Mouse *ATPase*	mATPase-RT-F	CAGCAGATTTTAGCAGGTGAA	77
	mATPase-RT-R	CTGCCAGCTTATCAGCCTTT	

3.1.9. Consumables

Table 17: Consumables

Consumable	Supplier
96-well Plate	Applied Biosystems Inc., Foster City, USA
Amicon Ultra 10,000 Kw 4 ml columns	Merck, Millipore, Billercia, MA, USA
Cell culture dishes: 100 mm x 20 mm style	Sarstedt AG & Co., Nümbrecht, Germany
Cell culture plates: 12-well	Corning Incorporated, Corning, USA
Cell culture plates: Costar 6-well	Corning Incorporated, Corning, USA
Cell scraper 30 cm	Orange Scientific, Braine-l'Alleud, Belgium
Disposable gloves: Blue	VWR International Germany GmbH, Darmstadt, Germany
Disposable gloves: Green	Kimberly-Clark Professional, Roswell, GA, USA
Disposable scalpels	Feather Safety Razor Co., Ltd., Osaka, Japan
Falcon tubes (15, 50 ml)	Sarstedt AG, Nürnbrecht, Germany
Forceps: Dumont #5	Fine Science Tools GmbH, Heidelberg, Germany
Insulin syringes: BD Micro-Fine™+ 0.5 ml 0.33 mm (29G) x 12.7 mm U-100	Becton, Dickinson and Company, Franklin Lakes, USA
Magnetic stir bars	Carl Roth GmbH + Co. KG, Karlsruhe, Germany
Micro tubes: SafeSeal Micro Tubes	Sarstedt AG, Nürnbrecht, Germany
Microplate: LUMITRAC™ 200	Greiner Bio-One GmbH, Frickenhausen, Germany
PCR stripes: PCR SoftStrips	Biozym Scientific GmbH, Oldendorf, Germany
Pipette filter tips: SafeSeal-Tips Professional	Biozym Scientific GmbH, Oldendorf, Germany
Pipette tips (10,100, 1000 µl)	VWR International Germany GmbH, Darmstadt, Germany
Pipette tips (qRT-PCR): 30 µl (384 tips)	Thermo Fisher Scientific, Hudson, USA
Plastic weighing trays	VWR International Germany GmbH, Germany
PVDF transfer membrane: Immobilon-P	Millipore Corporation, Billerica, USA

Consumable	Supplier
qRT-PCR plates: MicroAmp Optical 384-Well Reaction Plate	Applied Biosystems Inc., Foster City, USA
Scissors: HB 7459	HEBUmedical GmbH, Tuttlingen, Germany
Scissors: Vannas-Tübingen Spring Scissors - 5mm Blades	Fine Science Tools GmbH, Heidelberg, Germany
Standard Capillaries	NanoTemper Technologies, Munich, Germany
Standard Cuvettes	Sarstedt AG, Nürnbrecht, Germany
Syringe needles: Microlance 3 20G	Becton, Dickinson and Company, Franklin Lakes, USA
Syringes: Plastipak 1 ml	Becton, Dickinson and Company, Franklin Lakes, USA
Tissue culture flasks: 175 cm^2 (vented cap)	Becton, Dickinson and Company, Franklin Lakes, USA
Tissue culture flasks: 25 cm^2 (filter cap)	TPP AG, Trasadingen, Switzerland
Tissue culture flasks: 75 cm^2 (PE vented cap)	Sarstedt AG, Nürnbrecht, Germany
Whatman Paper: 3M Chr	Whatman plc, Maidstone, UK
X-ray film: CRONEX™ 5 (13x18)	Agfa-Gevaert N.V., Mortsel, Belgium

3.1.10. Instruments

Table 18: Instruments

Instrument	Name	Supplier
Automated sample disruption	TissueLyser	Qiagen N.V., Hilden, Germany
Balance	SBC52	Scaltec Instruments GmbH, Göttingen, Germany
Capillary sequencer	3130*xl* Genetic Analyzer	Applied Biosystems Inc., Foster City, USA
Centrifuge (for cell culture)	5810	Eppendorf AG, Hamburg, Germany
Tabletop centrifuge	Biofuge fresco	Heraeus Holding GmbH, Hanau, Germany

Instrument	Name	Supplier
Cold Falcon centrifuge	Megafuge 1.0R	Heraeus Holding GmbH, Hanau, Germany
Falcon centrifuge	Megafuge 3L	Heraeus Holding GmbH, Hanau, Germany
Clean bench (for bacteria)	Hera guard HPA 12/65	Thermo Fisher Scientific, Hudson, USA
Dark Hood	DH-40	biostep GmbH, Jahnsdorf, Germany
Dark Hood (printer)	P93D	Mitsubishi Electric Corporation, Tokyo, Japan
DNA electrophoresis system	BlueMarine 200	Serva Electrophoresis GmbH, Heidelberg, Germany
Flake-ice machine	AF100	Scotsman Ice Systems, Vernon Hills, USA
Fluorescence microscope	Axioskop 2 mot plus	Carl Zeiss GmbH, Jena, Germany
Fluorescence microscope (camera)	AxioCam MRc	Carl Zeiss GmbH, Jena, Germany
Fluorescence microscope (light-source)	FluoArc	Carl Zeiss GmbH, Jena, Germany
Image scanner	Fujifilm FLA-5000	Fujifilm, Düsseldorf, Germany
Incubation hood	Certomat® HK	B. Braun Biotech International GmbH, Melsungen, Germany
Incubator (for bacteria)	INB 400	Memmert GmbH + Co. KG, Schwabach, Germany
Incubator (for cell culture)	CB 210	Binder GmbH, Tuttlingen, Germany
Laminar flow (for cell culture)	SK1200	BDK Luft- und Reinraumtechnik GmbH, Sonnenbühl-Genkingen, Germany
Microscope (for cell culture)	DM IL	Leica Microsystems GmbH, Wetzlar, Germany
MicroScale Thermophoresis	Monolith NT.115	NanoTemper Technologies, Munich, Germany
Microwave	Kor-6D07	Daewoo Electronics Europe GmbH, Butzbach, Germany
MilliQ water system	MilliQ synthesis	Millipore Corporation, Billerica, USA

Instrument	Name	Supplier
Minicentrifuge	Spectrafuge Mini	Labnet International Inc., Edison, USA
Multichannel pipette (10µl)	Discovery Eight-Channel Pipette	Labnet International Inc., Edison, USA
Multichannel pipette (100µl)	Research (multi-channel)	Eppendorf AG, Hamburg, Germany
Multichannel pipette (30µl)	Matrix Equalizer Pipette	Thermo Fisher Scientific, Hudson, USA
Pipette controller	Accu-jet	Brand GmbH + Co. KG, Wertheim, Germany
Pipettes (10, 100 and 1000 µl)	Research	Eppendorf AG, Hamburg, Germany
Plate reader	FLUOstar OPTIMA	BMG LABTECH GmbH, Offenburg, Germany
Plate reader	Magellan™ Plate Reader	TECAN US, Durham, NC, USA) (available at Institute of Clinical Chemistry, University Hospital Regensburg, Regensburg, Germany)
Power supply (DNA electrophoresis)	Blue PowerPlus	Serva Electrophoresis GmbH, Heidelberg, Germany
Power supply (protein electrophoresis)	Blue Power 500	Serva Electrophoresis GmbH, Heidelberg, Germany
Protein electrophoresis system	Mini Protean 3 System	Bio-Rad Laboratories Inc., Hercules, USA
Semi-dry electrophoretic transfer cell	Trans-Blot SD	Bio-Rad Laboratories Inc., Hercules, USA
Shaker	Rocking Platform	VWR International, LLC, West Chester, USA
Shaker (for bacteria)	Certomat® R	B. Braun Biotech International GmbH, Melsungen, Germany
Spectrophotometer	Amersham Biosciences Ultrospec 2100	GE Healthcare Bio-Sciences AB, Uppsala, Sweden
Spectrophotometer	Nanodrop ND-1000	Thermo Fisher Scientific, Hudson, USA

Instrument	Name	Supplier
Thermocycler	T1/T300 Thermocycler	Biometra biomedizinische Analytik GmbH, Göttingen, Germany
Thermocycler qRT-PCR	ViiA™ 7 System Taqman	Life Technologies, Carlsbad, CA, USA
Thermomixer	Thermomixer compact	Eppendorf AG, Hamburg, Germany
Transilluminator	UST-30_M-8R	BioView Ltd., Billerica, MA, USA
Ultrasonic processor	Vibra Cell™ VCX400	Sonics & Materials, Inc., Newtown, USA
Vortexer	Vortexer Genie 2	Scientific Industries, Bohemia, USA
Water bath	Medingen WBT 12	P-D Industriegesellschaft mbH Prüfgerätewerk Dresden, Dresden, Germany
Water still (for buffers)	2012	GFL Gesellschaft für Labortechnik GmbH, Burgwedel, Germany

3.1.11. Software tools

Table 19: Software tools

Software	Application	Supplier
Ape Plasmid Editor	Sequence Analysis	M.Wayne Davis, Department of Biology, University of Utah, USA
ArgusX1 V4.0.81	Agarose gel documentation	biostep GmbH, Jahnsdorf, Germany
BioEdit Sequence Alignment Editor v7.0.9.0	Sequence alignment	Tom Hall, Ibis Therapeutics, Carlsbad, USA
KaleidaGraph 4.1	MicroScale Thermophoresis	NanoTemper Technologies, Munich, Germany
Magellan™ Plate Reader	NO assay	TECAN US, Durham, NC, USA (available at the Institute of Clinical Chemistry, University Hospital, Regensburg, Germany)

Software	Application	Supplier
Nanodrop ND-1000 v.3.5.2	Measurement of DNA/RNA concentration	Thermo Fisher Scientific, Hudson, USA
ViiA™ 7 System software	qRT-PCR data analysis	Applied Biosystems Inc., Foster City, USA
Total lab TL100 software	Densitometry of immunoblots	Nonlinear Dynamics, Durham, NC, USA

3.2. Methods

3.2.1. Cultivation of mammalian cell lines

Cells were grown in a humidified incubator at 37°C (atmosphere 95% air, 5% CO_2). The medium, cultivation volume and growth supply are described in **Table 20**.

Table 20: Cultivation of mammalian cells

Cell line	Growth medium	Growth supply	Cultivation volume
Hek293-Ebna	DMEM High Glucose (4,5 g/l) with L-Glutamine	100 mm dish	10 ml
BV-2	RPMI 1640 without L-Glutamine	75 cm^2 flask	10 ml
MLEC-PAI/Luc	DMEM High Glucose (4,5 g/l) with L-Glutamine	100 mm dish	10 ml

DMEM High Glucose (4.5 g/l) with L-Glutamine was supplemented with 10% FBS, 100 U/ml penicillin and 0.1 mg/ml streptomycin. RPMI 1640 without L-Glutamine is supplemented with 5% FBS, 1% of L-Glutamine, 195 nM β -Mercaptoethanol, 100 U/ml penicillin and 0.1 mg/ml streptomycin. For Hek293-Ebna cells, 1% G418 was also supplemented with the DMEM High Glucose medium.

Human Embryonic Kidney 293 (Hek293)-Ebna cells and MLEC-PAI/Luc (Mink lung epithelial cells stably transfected with an expression construct containing a truncated PAI-1 promoter fused to the firefly luciferase reporter gene) cells were split for propagation at an estimated confluence of 90%. To this end, the medium was aspirated and both the cells were washed once with 5 ml of PBS.

For Hek293-Ebna cells, no trypsinization was required for the detachment of cells. After washing with 1X PBS, corresponding media was pipetted gently onto the cells. Cells with media were collected in sterile 15 ml Falcon tubes. The cells were pelleted by centrifuging at a speed of 1000 rpm in centrifuge for Falcon tubes in cell culture (5810 Eppendorf Centrifuge) at RT. After equally redistributing the cells in the total amount of solution, they were split 1:6 to a final volume of 10 ml on a new cell culture dish.

On the other hand, 2 ml of trypsin-EDTA solution was pipetted directly onto the MLEC-PAI/Luc cells. The dishes of MLEC-PAI/Luc cells were then incubated for 3-5 min at 37°C, allowing the cells to detach from the plastic surface. As soon as most cells were floating, the trypsinization process was stopped by adding 10 ml of the corresponding medium. Cells with media were collected in sterile 15 ml Falcon tubes. The cells were pelleted by centrifuging at a speed of 1000 rpm in centrifuge for Falcon tubes (in cell culture) at RT. After equally redistributing the cells in the total amount of solution, they were split 1:6 to a final volume of 10 ml on a new cell culture dish.

BV-2 microglial cells were split according to a different procedure: first the medium was aspirated and replaced with 10 ml of fresh medium. Cells were then scraped and 3 ml of the suspension were transferred to a fresh flask containing 10 ml of medium.

3.2.2. Cultivation of *E.coli*

E.coli cells were cultivated either on LB_{Amp} dishes or in liquid LB_{Amp} medium (for the medium's composition, see **Table 8**). Plates were incubated ON at 37°C; liquid cultures were shaken ON at 37°C to ensure oxygen circulation.

3.2.3. Cloning strategy

3.2.3.1. Amplification of DNA fragments

Three variants of the *HTRA1* gene [the most frequent *HTRA1* haplotype (*HTRA1:CG*), as well as two less common *HTRA1* haplotypes (*HTRA1:TT* and *HTRA1:CC*)] were tagged with a six-amino acid-long Tetracysteine (TC) tag at the C-terminal end and were cloned into the pCEP4 vector (Invitrogen, Carlsbad, CA, USA).

The expression constructs for *HTRA1:CG*, *HTRA1:CC* and *HTRA1:TT* variants tagged with TC-tag were constructed by the following procedure.

To obtain the TC-tagged *HTRA1:CG* and *HTRA1:TT* expression constructs, two steps of amplification were performed. In the first step, coding sequence of *HTRA1:CG* and *HTRA1:TT* without the stop codon were amplified from expression construct for untagged *HTRA1:CG* variant (an already existing construct available at the Institute of Human Genetics, University Hospital Regensburg, Regensburg, Germany) and from cDNA of ARPE-19 (human retinal pigment epithelium) cells respectively. It is to be noted that ARPE-19 cells are heterozygous for the synonymous polymorphisms rs1049331 and rs2293870 (TT/CG). Thus amplified coding sequences were subcloned into the pGEM®-T vector for sequencing (see the procedure below). In the second step, after sequencing, the correct cDNAs were amplified with two reverse complimentary oligonucleotides to introduce a six-amino acid-long (Cysteine-Cysteine-Proline-Glycine-Cysteine-Cysteine), peptide sequence at the C-terminal end, the "TC-tag. Thus obtained TC-tagged coding sequence of *HTRA1:CG* and *HTRA1:TT* in pGEM®-T was then restriction digested and ligated into the pCEP4 vector (see the procedure below).

The PCR reaction mixture for amplification of *HTRA1:CG* and *HTRA1:TT* fragments was prepared according to the following protocol:

AccuPrime™ PCR Buffer B (5X)	2.5 µl
5'-Primer (5 µM)	1 µl
3'-Primer (5 µM)	1 µl
AccuPrime™ Taq Polymerase	0.25 µl
Template (cDNA/plasmid)	100-200 ng
H_2O	upto 25 µl

PCRs were performed with the following cycling conditions:

Initial denaturation	95°C	5 min	
Denaturation	95°C	30 s	30x
Annealing	59°C	30 s	
Extension	72°C	45 s	
Final extension	72°C	5 min	

The expression construct for TC-tagged *HTRA1:CC* was obtained by first introducing site-directed mutagenesis in pGEM®-T construct for *HTRA1:CG* variant (available at the Institute of Human Genetics, University Hospital Regensburg, Regensburg, Germany). The correct sequences were detected by sequencing. Then the amplified product was digested by *DpnI* to get rid of methylated parent plasmid. The amplified product was then restriction digested from pGEM®-T vector and ligated into the pCEP4 vector (see the procedure below). The PCR reaction mixture for amplification of *HTRA1:CC* fragments was prepared according to the following protocol:

Pfu Ultra HF buffer(10X)	5 µl
dNTPs (2.5 mM each)	2 µl
5'-Primer (5 µM)	2 µl
3'-Primer (5 µM)	2 µl
DMSO	2 µl
PfuUltra HF DNA polymerase	1 µl
Template (plasmid DNA)	100-200 ng
H_2O	upto 25 µl

PCRs were performed with the following cycling conditions:

Initial denaturation	95°C	5 min	
Denaturation	95°C	30 s	18x
Annealing	55°C	30 s	
Extension	72°C	45 s	
Final extension	72°C	5 min	

Primers used for cloning the expression constructs for *HTRA1* variants for protein expression in cell cultures are listed in **Table 14**.

3.2.3.2. Agarose gel electrophoresis

The PCR products were resolved by agarose gel electrophoresis. 1-1.5% agarose was dissolved in TBE buffer by heating the solution in the microwave. After cooling

the liquid on ice it was mixed with two drops of ethidium bromide solution (AppliChem GmbH, Darmstadt, Germany) and poured in a casting tray. The GeneRuler™ DNA Ladder Mix (Fermentas International Inc., Burlington, Canada) served as a marker. Samples were mixed before loading the gel with a drop of 5X DNA-loading buffer. Electrophoresis was performed at 100-200 V in a chamber filled with TBE buffer. Amplification products were visualized using the dark hood DH-40 (biostep GmbH, Jahnsdorf, Germany). Gel runs were documented with the software ArgusX1 V4.0.81 (biostep GmbH, Jahnsdorf, Germany) and bands with the correct size were excised from the gel.

3.2.3.3. DNA extraction from agarose gels

DNA extraction from agarose gels was performed with the NucleoSpin® Extract II Kit (MACHEREY-NAGEL GmbH & Co. KG, Düren, Germany) according to the manufacturer's instructions. DNA was eluted in 20 µl of H_2O.

3.2.3.4. Determination of DNA concentrations

DNA concentrations were determined in 2 µl of samples with the Nanodrop ND-1000 spectrophotometer using the Nanodrop ND-1000 v.3.5.2 software (Thermo Fisher Scientific, Hudson, USA).

3.2.3.5. *DpnI* digestion

DpnI (New England BioLabs® Inc., Ipswich, USA) digestion of the amplified product of *HTRA1:CC* variant (**Section 3.2.3.1**) was done. *DpnI* cut only the methylated (adenine) recognition sequence 5'-GATC-3' from the purified plasmid of "pGEM®-T+HTRA1:CC". Thus to get rid of the parent plasmid and proceed the further work with only the unmethylated amplified product, *DpnI* digestion was carried out. For digestion, the following components were mixed together in a cup and incubated for 2 h at 37°C.

Gel excised PCR product (50 ng/µl)	20 µl
DpnI	3 µl
NEBuffer CutSmart®	1 µl
H_2O	6 µl

3.2.3.6. A-tailing of blunt-ended PCR fragments

The polymerases used for the amplifications (**Section 3.2.3.1**) generated blunt-ended fragments because of their 3'-5'-exonuclease proofreading activity. However, for subcloning PCR products into the pGEM®-T vector, they needed 3'-A-overhangs. The purified PCR fragments were modified with the following A-tailing procedure: 7 µl of the purified PCR products was mixed with 1 µl of 2 mM dATP, 1 µl of ThermoPol Reaction Buffer (10X) and 0.5 µl of *Taq* DNA Polymerase (New England BioLabs® Inc., Ipswich, USA) in a total reaction volume of 10 µl. The mixture was incubated at 72°C for 30 min.

3.2.3.7. Ligation into pGEM®-T vector

Next, subcloning of the PCR products with the pGEM®-T Vector System (Promega Corporation, Madison, USA) occurred. Vector and A-tailed PCR products were added in a molar ratio between 1:1 and 1:3 to the following ligation reaction.

2X Rapid Ligation Buffer	5 µl
T4 DNA Ligase	1 µl
pGEM®-T Vector	0.5 µl
Insert	1-3 µl
H_2O	upto 10 µl

The ligation was performed either for 1 h at RT or ON at 4°C.

3.2.3.8. Heat shock transformation of competent *E.coli* cells

For transformation of competent *E.coli* DH5α and JM110 cells, the heat shock method was applied. 50 µl of DH5α cell suspension was thawed on ice and mixed with 5 µl of the ligation reaction. After 30 min incubation on ice, the cells were heat shocked for 1 min at 42°C. 5 min incubation on ice followed, before 800 µl of LB medium (without antibiotics) was added to the suspension. During the recovery phase, cells were incubated for 45 min at 37°C on a shaker. The bacteria were then centrifuged at 4500 rpm in tabletop centrifuge for microfuge tubes (Heraeus Biofuge Fresco centrifuge) for 3 min at RT and resuspended in 100 µl of LB medium. Finally, cells were plated on LB_{Amp} plates and incubated ON at 37°C.

For transformation with pGEM®-T vector, 40 µl of X-Gal (40 mg/ml dissolved in DMSO) and 20 µl of 0.1M IPTG were additionally plated on LB_{Amp} plates before applying the *E.coli* cells.

3.2.3.9. Selection of positive clones

A helpful feature of the pGEM®-T vector is the ability to perform a so-called "blue/white screening" of recombinant cells on LB_{Amp} plates supplemented with X-Gal and IPTG. The uptake site of the insert lies within the coding region of the α-peptide of β-galactosidase, an enzyme that catalyzes the hydrolysis of β-galactosides into monosaccharides. The organic compound X-Gal is also cleaved by β-galactosidase, leading to the accumulation of an insoluble blue product. Bacteria harboring the pGEM®-T vector without an insert express β-galactosidase after IPTG induction. The colonies will appear blue. However, if an insert is ligated into the vector, the transformed cells do not express a functional β-galactosidase protein. They are unable to cleave X-Gal and the colonies will remain white. It should be mentioned that the *E.coli* strain DH5α used for transformation does not express a functional copy of this gene. Sixteen white clones were picked and inoculated ON into 5 ml LB_{Amp} medium for subsequent plasmid preparation and sequencing.

3.2.3.10. Plasmid isolation

For sequencing and restriction digestion, plasmids were isolated with the NucleoSpin® Plasmid Kit (MACHEREY-NAGEL GmbH & Co. KG, Düren, Germany) from 4 ml of ON cultures. Isolation was performed according to the manufacturer's instructions. DNA was eluted in 50 µl of H_2O and the concentration was determined with the Nanodrop ND-1000 spectrophotometer (Thermo Fisher Scientific, Hudson, USA).

For transfection of mammalian cell lines, plasmids were isolated with the NucleoBond® Xtra Midi Kit (MACHEREY-NAGEL GmbH & Co. KG, Düren, Germany) from 100 ml of ON cultures. DNA pellets were reconstituted in 100 µl of H_2O and diluted to a final concentration of approximately 1 µg/µl.

3.2.3.11. Cycle sequencing of inserts

The correctness of the insert's sequence was determined by cycle sequencing with the BigDye® Terminator v1.1 Cycle Sequencing Kit (Applied Biosystems Inc., Foster City, USA). Sequencing reactions were performed with the primers mentioned in **Table 14**. The following components were pipetted on ice:

BigDye® Terminator Sequencing Buffer (5X)	2 µl
Primer (10 µM)	1 µl
BigDye® Terminator v1.1	0.8 µl
Plasmid DNA	50-100 ng
H_2O	upto 10 µl

The cycling conditions were set as follows:

Initial denaturation	95°C	2 min	
Denaturation	95°C	30 s	27 x
Annealing	58°C	30 s	
Extension	60°C	3 min	
Final extension	60°C	5 min	

The DNA was then precipitated with 2 µl of 3M sodium acetate and 25 µl of 100% ethanol at 2800 rpm for 20 min at RT in centrifuge for Falcon tubes (Heraeus Megafuge 1.0R centrifuge). After washing with 50 µl of 70% ethanol and subsequent centrifugation, the DNA was briefly air-dried, resuspended in 15 µl of Hi-Di™ Formamide (Applied Biosystems Inc., Foster City, USA) and transferred to a 96-well sample plate. Sequencing was performed with the 3130*xl* Genetic Analyzer capillary sequencer (Applied Biosystems Inc., Foster City, USA). The outputs were aligned to the expected sequences with BioEdit Sequence Alignment Editor v7.0.9.0 (Tom Hall, Ibis Therapeutics, Carlsbad, USA).

3.2.3.12. Restriction digestion of correct inserts and ligation into target vectors

Restriction sites compatible with the multiple cloning sites of the pCEP4 vectors containing "TC-tagged *HTRA1:CG*" and "TC-tagged *HTRA1:TT*" were already

introduced in the primers used for amplifying the fragments, which were first subcloned into the pGEM®-T vector. The enzymes *NotI* and *XhoI* were used for the restriction digestion of the TC-tagged *HTRA1* variants cloned for protein expression in cell culture. To obtain pCEP4 containing TC-tagged *HTRA1:CC* variant from its subclone of pGEM®-T vector, *FseI* enzyme was used to digest. It is to be noted that, for restriction digestion by *FseI* (a *dcm* methylation sensitive enzyme), pGEM®-T vector containing TC-tagged *HTRA1:CC* variant were transformed into *dam-/dcm-* competent *E.coli* JM110 cells. After ligation and obtaining pCEP4 vector containing TC-tagged *HTRA1:CC* variant, the plasmids were transformed into DH5α cells. To obtain expression constructs for Strep-tagged *HTRA1:CC* variant, pCEP4 construct for TC-tagged *HTRA1:CC* (construct obtained as described in **Section 3.2.3.1**) was digested by *FseI.* The digested fragment was inserted into pEXPR-IBA103 (consisting of Twin Strep tag) construct for *HTRA1:CG* variant (already available in Institute of Human Genetics, University Hospital Regensburg, Regensburg, Germany). The pEXPR-IBA103 construct for *HTRA1:CC* variant was transformed into DH5α cells.

pGEM®-T plasmids (2-3 µg) carrying a correct insert and the target vectors (2-3 µg) were digested at least for 1 h at 37°C. 1 µl of each restriction enzyme from New England BioLabs® Inc. (Ipswich, USA) was used. The NEBuffer CutSmart® was chosen according to the supplier's recommendations. After restriction digestion fragments were resolved on agarose gels and the fragment of interest was excised from the gel. DNA purification was performed according to **Section 3.2.3.3.**

Next, ligation into the target vectors was performed. Similar to ligations into pGEM®-T, vector and insert were added in a molar ratio between 1:1 and 1:3 in the following ligation assay:

T4 DNA Ligase Reaction Buffer (10X)	5 µl
T4 DNA Ligase	1 µl
Vector	50-100 ng
Insert (molar ratio vector:insert)	1:1 to 1:3
H_2O	ad 10 µl

The ligation was performed either for 1 h at RT or ON at 16°C.

Transformation, selection of positive clones, plasmid isolation and cycle sequencing were accomplished as described in the previous sections.

3.2.3.13. Long-term storage of positive clones

Positive clones were maintained as glycerol stocks for long-term storage. To this end, bacteria from 4 ml of fresh overnight culture were pelleted at 4000 rpm in centrifuge for Falcon tubes for 3 min at RT. Cells were then resuspended in 500 µl of LB medium (without antibiotics) and mixed with 600 µl of sterile 80% glycerol. The stocks were immediately frozen at 80°C.

3.2.4. Transfection of Hek293-Ebna cell lines

For introducing TC-tagged and Strep-tagged *HTRA1* expression constructs in Hek293-Ebna cells, transfection was performed with the *Trans*IT®-LT1 Transfection Reagent (Mirus Bio LLC, Madison, USA), a broad spectrum protein/polyamine-based reagent that contains histones and lipids. According to manufacturer's indications, optimal transfection efficiency is reached at a cell confluence of approximately 50-70%. Transfection of cells grown in a 100 mm dish was performed after 24 h as follows: 10 µg of plasmid DNA was diluted and vortexed in 1 ml of the respective growth medium without supplements (**Table 20**). Subsequently 30 µl of *Trans*IT®-LT1 transfection reagent was added to the tube, which was gently vortexed again. During the incubation time of 15-20 min at RT, transfection reagent-DNA complexes were formed. The mixture was finally added dropwise to the cells and the culture plate was gently shaken and incubated under standard conditions for 48 h.

3.2.5. Secretion assay

To analyze HTRA1 secretion from Hek293-Ebna cells, cells were seeded ON into 6-well plates using 3 ml of Opti-MEM® I Reduced Serum Media (Gibco Life Technologies). At 70% confluence, the cells were transfected with 2.5 µg of the expression constructs for untagged *HTRA1* (*HTRA1:CG*, *HTRA1:TT* or empty vector) and 7.5 µl TransIT-LT1 transfection reagent (Mirus Bio LLC) following the

manufacturer's instructions. Supernatants and cells were harvested 0, 10, 16, 20 and 24 h after transfection (see **Section 3.2.6**). Proteins isolated were subjected to Western blot analyses against α-HTRA1 and α-ACTB antibodies as described in **Section 3.2.9**.

3.2.6. Preparation of protein samples for gel loading

Supernatants were collected in 15 ml Falcon tubes (Sarstedt AG, Nürnbrecht, Germany) from the top of cells. Supernatants were centrifuged at 1000 rpm in centrifuge for Falcon tubes for 3 min at RT to get rid of the debris. Clear supernatants were collected and the total protein concentration was measured by Bradford assay (see **Section 3.2.7**). Cells from 100 mm dishes were washed twice with 1X PBS and were then resuspended in 1X PBS. The cells in PBS were then transferred into a 15 ml Falcon tube and centrifuged for 10 min at 4000 rpm in the centrifuge for Falcon tubes. The cell pellet was resuspended in 1 ml 1X PBS, transferred into a 1.5 ml Eppendorf cup and centrifuged for at 4000 rpm in tabletop centrifuge (for microfuge tubes) for 10 min at RT and resuspended in 750 µl of 1X PBS. Total protein concentration of the cells was then measured.

3.2.7. Bradford assay for measurement of protein concentration

To find out the total protein concentration of cells or supernatants, according to Bradford assay principle, Roti® Quant solution was used. 10-50 µl of resuspended cells or supernatant was added to a mixture of 200 µl of Roti® Quant solution and 800 µl H_2O (Millipore). To calibrate the photometer, a sample was prepared from 800 µl H_2O and 200 µl Roti® Quant (without protein), which is termed as "Blank". The samples were incubated for 20 min at RT and then the optical density (OD) was measured at 595 nm in a photometer. The determination of each protein concentration was always done in triplets. The total protein concentration of cells or supernatants was then analyzed by comparing with the OD of the titration series of known concentration of a protein such as bovine serum albumin (BSA). The total protein concentration of each protein in each experiment was equalized before subjecting to SDS-PAGE.

3.2.8. SDS PAGE (Sodium Dodecyl Sulfate-Polyacrylamide Gel Electrophoresis)

12.5 µl of 5X Laemmli buffer was added to 50 µl of each protein sample and heated for 10 min at 95°C before loading onto SDS PAGE.

15% SDS-polyacrylamide gels were poured into the Mini Protean 3 setup (Bio-Rad Laboratories Inc., Hercules, USA) using the following mixtures:

Resolving gel (15%)	3.75	ml	Rotiphorese Gel 40 (29:1) acrylamide/bisacrylamide
	3.38	ml	1 M Tris-HCl pH 8.8
	2.42	ml	H_2O
	100	µl	20% SDS
	100	µl	10% APS
	10	µl	TEMED
Stacking gel (3%)	0.55	ml	Rotiphorese Gel 40 (29:1) acrylamide/bisacrylamide
	2.76	ml	1 M Tris-HCl pH 6.8
	1.69	ml	H_2O
	50	µl	20% SDS
	50	µl	10% APS
	5	µl	TEMED

The gels were transferred to a chamber containing SDS-running buffer and were loaded with 25 µl of sample per lane. 4 µl of the PageRuler™ Prestained Protein Ladder (Fermentas International Inc., Burlington, Canada) was used as marker. The running program was first set at 50 V for approximately 1 h until the samples entered the resolving gel and then at 150 V until the bromophenol blue front (contained in Laemmli buffer) reached the lower end of the gel.

3.2.9. Western blot (WB)/Immunoblot (IB)

For Western blot analyses proteins were blotted after SDS-PAGE in the semi-dry procedure onto a PVDF membrane. The membrane was activated for 30 s in methanol, and then equilibrated for at least 15 min in 1X Towbin transfer buffer. Likewise, two 3 mm Whatman Paper and the SDS gel were equilibrated in 1X Towbin transfer buffer. The transfer of the proteins from the gel to the membrane was

performed for 40 min at 24 V. After transfer, the membrane was pivoted in block solution for 1 h at 4°C, before it was incubated ON in the primary antibody. Before incubation in secondary antibody (1 h, 4°C), the membrane was washed three times for 10 min in 1X PBS. The secondary antibody (Horseradish Peroxidase conjugated) was added and the membranes were incubated for at least 1 h at 4°C. The membranes were washed again three times with 1X PBS for 10 min.

The protein-antibody complexes were visualized by chemiluminescence using the SuperSignal West Femto Maximum Sensitivity Substrate (Thermo Fisher Scientific, Hudson, USA) according to the manufacturer's instructions. The blot was exposed to CRONEX™ 5 X-ray film (Agfa-Gevaert N.V., Mortsel, Belgium). The films were finally developed with the G153 developer and G354 fixer (Agfa-Gevaert N.V., Mortsel, Belgium). All antibodies used are enlisted in **Table 10**.

3.2.10. MicroScale Thermophoresis (MST) to study conformation of HTRA1 isoforms

3.2.10.1. In-Gel TC-tagged HTRA1 detection

In-Gel detection of the TC-tagged HTRA1 was carried out to identify the optimal concentration of FlAsH EDT_2 fluorescence labeling reagent (Invitrogen, Carlsbad, CA, USA) needed for the TC-tagged HTRA1 to exhibit fluorescence without background.

Hek293-Ebna cells were transfected as described in**Section 3.2.4**. After 48 h of transfection, the supernatant of Hek293-Ebna cells transfected with empty pCEP4 vector, expression vectors for TC-tagged *HTRA1:CG* or *HTRA1:TT* variants were harvested as described in **Section 3.2.6** and concentrated with Amicon Ultra 10,000 Kw 4 ml columns (Merck, Millipore, Billercia, MA). 30 µl of concentrated protein was mixed with 10 µl of 4x loading dye (Laemmli buffer) without β-Mercaptoethanol and 1 µl of 80 mM TCEP. The mixture was heated at 70°C for 10 min. The mixture was cooled down to RT. 1 µl of 200 µM FlAsH EDT_2 in DMSO was added to the mixture. This mixture was incubated for another 10 min at RT. 40 µl of respective protein in 15% SDS Polyacrylamide Gel was run at 150 V for 1 h 20 min. The fluorescent

protein bands were visualized in Fujifilm FLA-5000 image scanner (Fujifilm, Dusseldorf, Germany).

3.2.10.2. The temperature-dependent structural assays by MST

MST analyses were performed by Dr. Thomas Schubert, 2bind GmbH, Regensburg, Germany. Total protein concentration of the concentrated supernatant of the cells transfected with expression vectors containing TC-tagged *HTRA1 CC, CG, or TT* variants was measured by Bradford assay as described in **Section 3.2.7**. 4 µl of the concentrated supernatants (2 µg/µl) were incubated with 1 µl of 20 µM of FlAsH-EDT_2. Samples were incubated for 10 min and sucked into the standard capillaries. The capillaries were plugged with paraffin to avoid evaporation. The temperature-dependent structural assays were performed as biological triplicates at 15% LED (light-emitting diode) power and 50% MST power in a Monolith NT.115 (NanoTemper Technologies, Munich, Germany) with varied temperatures (32-52 °C). The recorded fluorescence of each protein was normalized to the same baseline fluorescence and plotted against the temperature into one graph using KaleidaGraph 4.1.

3.2.11. Purification of Strep-tagged variants of the HTRA1

For purification of the secreted HTRA1 isoforms, 10 ml supernatants of Hek293-Ebna cells transfected with expressions constructs for Strep-tagged HTRA1: *CG, CC or TT* variants were collected in Falcon tubes. To get rid of cellular debris, supernatants were centrifuged at a speed of 1000 rpm in centrifuge for Falcon tubes for 3 min at RT. The purification of heterologously expressed HTRA1 was carried out with the Twin Strep Purification Kit from IBA Life Sciences, Göttingen, Germany. 1 ml Gravity flow Strep Tactin Superflow® columns were used. W buffer, pH 8.0 (wash buffer) was prepared in accordance with **Table 4**. The buffer E (elution buffer) and R (regeneration buffer) were purchased from IBA Life Sciences.

The purification of the proteins was carried out at 4°C with pre-cooled solutions and buffers according to the Short Purification Protocol of IBA Life Sciences. Elution of

the proteins was carried out in five steps with 500 µl buffer E. The eluate fractions were stored in aliquots of 100 µl at -20°C.

3.2.12. Coomassie staining

The Coomassie staining of SDS gels was carried out directly following the SDS-PAGE. SDS-gels were stained in Comassie Stainer for 1 h and then destained in Coomassie destainer till the distinct protein bands were visible. The composition of the solutions was mentioned in **Table 4**.

3.2.13. Casein digest to test bio-activity of HTRA1 protein

Bioactivity of HTRA1 protein from supernatant or purified HTRA1 was tested by *in vitro* β-casein digestions. The casein solution used herein contains a casein mixture of α-S1 (22 kDa), α-S2 (25 kDa), β (24 kDa), γ (70 kDa) and κ (19 kDa). HTRA1 is capable of digesting β-casein. 20 µg of casein from bovine milk (Merck Chemicals GmbH, Schwalbach, Germany) was mixed with 2 µg purified HTRA1 isoforms in 100 µl of digestion buffer pH 7.5 (see **Table 4** for composition). After 0 and 3 h, 50 µl aliquots were taken and the reaction was stopped by adding 5X Laemmli buffer and boiling the sample for 10 min at 90 °C. Samples were resolved by SDS PAGE and stained with Coomassie.

3.2.14. Limited partial proteolysis

25 µl of 40 ng/µl of Strep-purified HTRA1 in 1X elution buffer along with 50 µl of TRIS buffer saline (see **Table 4** for composition) was preincubated at 37, 42 and 46°C for 10 min. 25 µl of 480 µg/ml of TPCK-Trypsin (Sigma-Aldrich, St. Louis, MO, USA) in TRIS buffer saline was added to denatured HTRA1 at 37°C for another 5 min. 25 µl of 5X Laemmli buffer was added to the reaction mixture and boiled. Subsequently, samples were subjected to Western blot analyses with α-HTRA1 antibody.

3.2.15. MST interaction analysis

MST binding experiments were carried out with 100 nM labeled HTRA1 in supernatant with varied concentrations of recombinant TGF-β1 (PeproTech,

Hamburg, Germany) and β-casein from bovine milk (Sigma-Aldrich, St. Louis, MO, USA) at 80% MST power, 20% LED power in standard capillaries on a Monolith NT.115 at 25°C. The recorded fluorescence was normalized to the fraction of the protein bound (0 = unbound, 1 = bound) and processed with KaleidaGraph 4.1 software. The data were fitted with the help of the quadratic fitting formula (Kd formula) derived from the law of mass action. Each binding experiment was done with biological triplicates. MST interaction analyses were performed by Dr. Thomas Schubert.

3.2.16. TGF-β1/β-casein *in vitro* digestion

TGF-β1 (PeproTech) was dissolved in 10mM citric acid pH 3.0 to make a stock concentration of 100 ng/µl. 10 µl from stock, i.e., 1 µg of TGF-β1 was added to 90 µl of digestion buffer pH 7.5 (see **Table 4** for composition). 1 µg of TGF-β1 was incubated with 300 µl serum-free medium of Hek293-Ebna cells transfected with expression constructs for *HTRA1:CG*, *HTRA1:TT* or control (empty pCEP4 vector) for 24 h. After 0, 4, 8, 16 and 24 h, 50 µl aliquots were taken from respective supernatants. To 50 µl of aliquots, 12.5 µl of 5X Laemmli buffer was added and boiled to stop the reaction.

In vitro digestion of β-casein by HTRA1 was analyzed by Karolina Ploessl, Institute of Human Genetics, University Hospital Regensburg, Regensburg, Germany. To compare β-casein cleavage catalyzed by HTRA1:CG and HTRA1:TT, 20 µg of β-casein was incubated with 300 µl serum-free medium of Hek293-Ebna cells transfected with expression constructs for *HTRA1:CG*, *HTRA1:TT* or control (empty pCEP4 vector). After 0.5, 1, 2 and 3 h, 50 µl aliquots were taken and the reaction was stopped by adding 5X Laemmli buffer and by boiling the sample for 10 min at 90°C. Samples were resolved by SDS PAGE and stained with Coomassie.

3.2.17. MLEC luciferase assay

MLEC-PAI/Luc cells were seeded into 96-well plates at a density of 1.5×10^4 cells per well with 100 µl of appropriate medium with growth supplements (**Table 20**). Cells

were allowed to attach for 3 h at 37°C in 5% CO_2 incubator. The cells were treated with 2 ng/ml of recombinant TGF-β1 (PeproTech) in combination with 40 ng/ml of purified HTRA1 (Strep-tagged HTRA1:CG or HTRA1:TT) or eluate of empty vector. After 16 h, cultures were centrifuged at a speed of 2500 rpm centrifuge for Falcon tubes for 6 min at RT. After washing with 1 ml of PBS, cells were resuspended in 500 µl of Reporter Lysis Buffer and incubated for 15 min at RT. Cellular debris was then pelleted at a speed of 8000 rpm in tabletop centrifuge (for microfuge tubes) for 3 min at RT, and 350 µl of the supernatant was transferred to a fresh tube. 10 µl of cell lysate was assayed for luciferase activity with 100 µl of Luciferase Assay Reagent (Promega Corporation, Madison, USA), which contains the luciferase's substrate. Luminescence was measured in the FLUOstar OPTIMA plate reader (BMG LABTECH GmbH, Offenburg, Germany) for 15 s upon injection of the reagent.

3.2.18. Treatment of BV-2 cells with BV-2-conditioned medium and HTRA1

The procedure for inducing endogenous TGF-β signaling in BV-2 cells was followed in concordance with Spittau et al. (2013). For this treatment, two sets of BV-2 cells were seeded.

The first set of BV-2 cells were seeded at a density of 1.5×10^5 in 12-well cell culture plates with 1.5 ml of appropriate medium with serum and growth supplements (for immunocytochemistry) and at a density of 3×10^5 in 6-well cell culture plates with 3 ml of appropriate medium with serum and growth supplements (for Western Blot analyses and *Pai-1* gene expression). Cells were allowed to attach and reach the subconfluence for 6 h at 37°C in 5% CO_2 incubator. After 6 h, medium with serum and growth supplements was replaced by equal volume of serum-free medium. Cells were serum-starved for 24 h. After 24 h microglia-conditioned medium from this set of BV-2 cells was collected, cellular debris was removed by centrifuging in centrifuge for Falcon tubes in (cell culture) at 1000 rpm for 3 min at RT.

The second set of BV-2 cells was seeded similarly and was allowed to attach and grow to subconfluence for similar time and similar condition as for the first set. Instead of 24 h, these cells were kept serum-starved for 2 h. After 2 h, the serum-free medium was removed. The harvested microglia-conditioned medium of the first set of

BV-2 cells was transferred into the second set of BV-2 cells as shown in **Figure 8**. The treatment was continued with the second set of BV-2 cells in the conditioned medium.

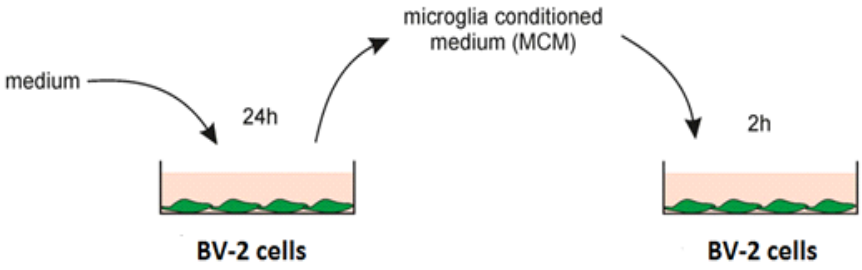

Figure 8: ***Schematic overview of inducing autocrine TGF-β/SMAD signaling in BV-2 cells.*** Adapted and modified from Spittau et al. (2013).

For, SMAD signaling analysis, 40 ng/ml of Strep-tagged HTRA1:CG and HTRA1:TT eluates (3 µl of 40ng/µl HTRA1 eluates and equal volume of Strep-tagged empty eluate was added to 3 ml of media in six-well plates and 1.5 µl of 40ng/µl HTRA1 eluates and equal volume of Strep-tagged empty eluate was added to 1.5 ml of media in 12-well plates) was added to the BV-2 cells in the conditioned media for 2 h. After 2 h, BV-2 cells in 6-well plates were harvested for protein isolation. Subsequently, the proteins were subjected to Western blot analyses (**Section 3.2.9**) with SMAD and pSMAD2 antibodies (**Table 10**). Immunocytochemistry for pSMAD2 antibody was performed by Magdalena Schneider, Institute of Human Anatomy and Embryology, Faculty of Biology and Preclinical Medicine, University of Regensburg, Regensburg, Germany, as described in (Friedrich et al., 2015)

For relative *Pai-1* gene expression, BV-2 cells (in conditioned medium) in 6-well plates were harvested after 3 h and 24 h of treatment with Strep-tagged HTRA1 eluates (same concentration as above). The cells were harvested for RNA isolation and cDNA treatment (see below). The relative gene expression analysis via Quantitative Real-Time PCR (qRT-PCR) was done by Magdalena Schneider as described in (Friedrich et al., 2015).

3.2.19. BV-2 cells treatment with lipopolysaccharide (LPS) and HTRA1

BV-2 cells were seeded at a density of 3×10^5 in 6-well plates with 3 ml of media. BV-2 cells were serum-starved for 24 h before any treatment. To identify an effect of HTRA1 on classical activation of microglia, cells were first seeded and serum-starved as described before. BV-2 cells were treated with 50 ng/ml LPS for 24 h, (as described in Dirscherl et al., 2010; Karlstetter et al., 2014; Aslanidis et al., 2015) in presence of increasing HTRA1 concentrations (30 ng/ml, 60 ng/ml and 90 ng/ml). After 24 h, cells were harvested for RNA isolation followed by relative gene expression analysis and the supernatant was collected for NO assay.

3.2.20. BV-2 cells treatment with interleukin 4 (IL4), TGF-β1 and HTRA1

BV-2 cells were seeded at a density of 3×10^5 in 6-well plates in 3 ml of appropriate medium. The cells were serum-starved for 24 h before any treatment, as described before. BV-2 cells were treated separately or in combination with 1 ng/ml of TGF-β1 and 10 ng/ml of IL4 for 24 h (as described in Zhou et al., 2012) in presence of increasing HTRA1 concentrations (30 ng/ml, 60 ng/ml and 90 ng/ml). Cells were harvested after 24 h for RNA isolation and relative gene expression analysis.

3.2.21. Nitrite measurement by nitric oxide (NO) assay

After 24 h, supernatant of LPS- and HTRA1-treated BV-2 cells were harvested. Supernatant was centrifuged at a speed of 8000 rpm in tabletop centrifuge (for microfuge tubes) for 5 min to get rid of cellular debris. Nitrite measurement was carried out with the clear supernatant as per manufacturer's instruction (Griess Reagent System, Promega Corporation, Madison, USA). The colorimetric assay was measured in Magellan™ Plate Reader (TECAN US, Durham, NC, USA) (available at Institute of Clinical Chemistry, University Hospital Regensburg, Regensburg, Germany) according to manufacturer's instructions. This assay is also known as NO assay.

3.2.22. RNA analysis

3.2.22.1. RNA isolation from cell cultures

Total RNA was isolated from cell cultures with the RNeasy® Mini Kit (Qiagen N.V., Hilden, Germany). Before isolating RNA from BV-2 cell lines, they were washed twice in PBS. Cells were harvested with a sterile scraper in 600 µl of RLT buffer with 1% β-mercaptoethanol, freshly added before use. Complete cell wall disruption and homogenization was achieved by passing the suspension 20 times through a blunt 20-gauge needle fitted to a 1 ml syringe. Subsequently, 600 µl of RNase-free 70% ethanol was added to the lysate. Further steps were performed according to the manufacturer's protocol including the on-column DNase digestion with the RNase-Free DNase Set (Qiagen N.V., Hilden, Germany). RNA concentrations were determined in 2 µl of samples with the Nanodrop ND-1000 spectrophotometer using the Nanodrop ND-1000 v.3.5.2 software (Thermo Fisher Scientific, Hudson, USA). After RNA elution in 50 µl of H_2O, samples were permanently kept on ice and fast processed or stored at -80 °C.

3.2.22.2. First strand cDNA synthesis from RNA

For first strand cDNA synthesis from RNA the RevertAid™ M-MuLV Reverse Transcriptase enzyme (Fermentas International Inc., Burlington, Canada) was used. cDNA synthesis was performed with 500-1000 ng of RNA template and random primers. As a first step, pre-incubation of RNA for 5 min at 65°C with 1 µl of primers (100 pmol) was carried out in 12.5 µl reaction volume, adjusted with RNase-free H_2O. Afterwards the following components were added on ice:

RevertAid™ 5X Reaction Buffer (5X)	4 µl
dNTPs(10 mM each)	2 µl
RevertAid™ M-MuLV Reverse Transcriptase	1 µl
H_2O(Millipore)	0.5 µl

The reaction mixture was then incubated for 10 min at 25°C, followed incubation at 42°C for 60 min. The reaction was stopped by heating the mixture to 70°C for 10 mins.

3.2.22.3. qRT-PCR

qRT-PCR was performed for each sample in triplicates. The cDNA was diluted for the qRT-PCR to a concentration of 20 ng/µl. The primer and probe design of all primers was carried out via the "Universal Probe Libary" (Hoffmann-La Roche). The PCR reactions as shown below were pipetted in a 384-well plate. The PCR was performed according to the PCR program shown below using the ViiA™ system 7(Life Technologies) machine. The analysis was performed according to the ΔΔCt method. Relative gene expressions of classical (M1) microglial activation markers namely *interleukin 6* (*IL6*) and *inducible nitric oxide synthase* (*iNOS*) or alternative (M2) microglial activation markers namely *arginase 1* (*Arg1)* and *chitinase 3-like 3* (*Ym1*) were analyzed by normalizing the expression to mouse *ATPase*, a housekeeper gene. All primers and probes used for these experiments are enlisted in **Table 16**. The statistical significance of the test results was determined in Microsoft Excel with a Student's t-test. Reaction mixture for qRT-PCR for *Arg1*, *iNOS*, *IL6*, *YM1* and mouse *ATPase* are as follows:

TaqMan Gene Expression Master Mix(MM)(2X)	5 µl
5'-Primer (50 µM)	1 µl
3'-Primer (50 µM)	1 µl
Roche Probe	2 µl
cDNA	5 µl
H_2O(Millipore)	0.375 µl

Following cycling conditions were set for qRT-PCR:

Denaturation	95°C	40 s	1X
Annealing	60°C	60 s	1X
Extension	60°C	2 min	40X

4. RESULTS

4.1. Cloning and expression of *HTRA1* variants

4.1.1. *HTRA1* haplotypes applied in subsequent studies

Three expression constructs for *HTRA1* were generated including *HTRA1* exon 1 variants rs1049331:C and rs2293870:G, the reference haplotype (Fritsche et al., 2008) (referred to as *HTRA1:CG*), the AMD-associated variants rs1049331:T and rs2293870:T (*HTRA1:TT*), and the non-disease associated variants rs1049331:C and rs2293870:C (*HTRA1:CC*) (**Figure 9**).

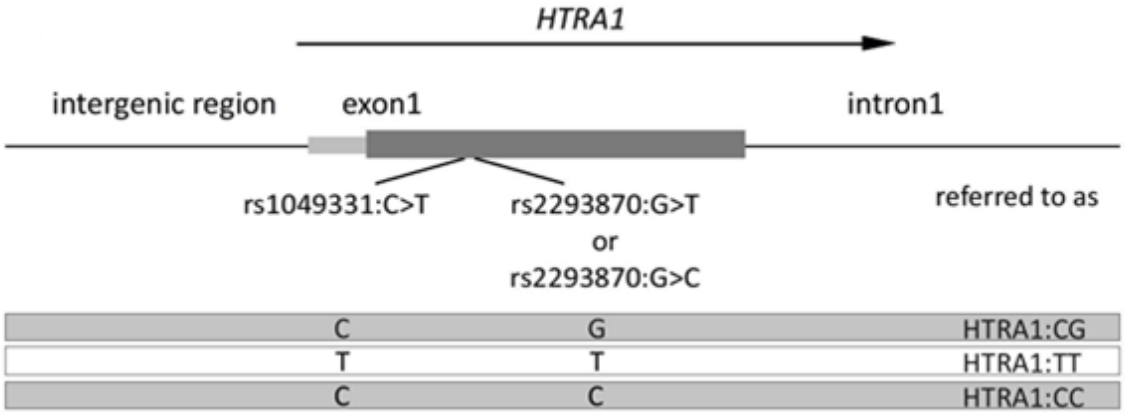

Figure 9: ***Schematic diagram of relative positions of synonymous polymorphisms in exon 1 of HTRA1.*** This scheme is used to illustrate HTRA1 haplotypes chosen for generating expression constructs for *HTRA1* variants; *HTRA1:CG* and *HTRA1 CC* are not associated with AMD risk, *HTRA1:TT* is associated with increased AMD risk. Figure adapted from Friedrich et al. (2011).

4.1.2. *HTRA1* expression constructs

Expression constructs for untagged *HTRA1* variants in pCEP4 vector (already available at Institute of Human Genetics, University Hospital Regensburg, Germany) were used for analyzing secretion and intracellular accumulation of HTRA1 isoforms (**Figure 10A**). Expression constructs for Strep-tagged *HTRA1* variants were used for purifying HTRA1. *HTRA1:CG* and *HTRA1:TT* variants (in pEXPR-IBA103) were already available at Institute of Human Genetics, University Hospital Regensburg, Germany. Strep-tagged *HTRA1:CC* variant was generated within this study (**Figure**

10B). For MST analyses, the three *HTRA1* variants were C-terminally fused to a Tetracystein (TC)-motif (Cys-Cys-Pro-Gly-Cys-Cys), allowing labeling with FlAsH-EDT_2 to show fluorescence. (**Figure 10C**).

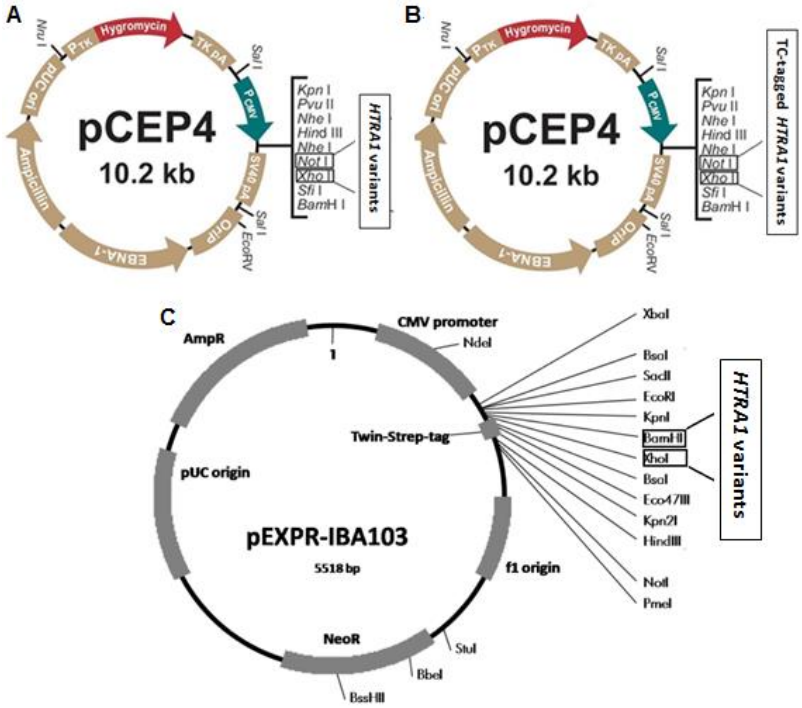

Figure 10: ***Schematic representation of expression constructs for (A) untagged, (B)TC-tagged and (C)Strep-tagged HTRA1 variants*.** Vector backbones used for heterologous expression of *HTRA1* variants are depicted: pCEP4 (Figure modified and adapted from www.invitrogen.com) was used for heterologous expression of (**A**) untagged *HTRA1*, as well as (**B**) TC-tagged *HTRA1* variants. pEXPR-IBA103 (Figure modified and adapted from www.iba-lifesciences.com) was used for generating (**C**) Strep-tagged *HTRA1* variants. Restriction sites used for inserting *HTRA1* variants are labeled within the figures.

4.1.3. Characterization of *HTRA1* expression constructs

Before performing experiment with heterologously expressed *HTRA1* variants, the expressed proteins were subjected to quality control by Bradford Assay, Western Blot and casein *in vitro* digest (**Figure 11**). Cells transfected with expression constructs for *HTRA1* variants were harvested. The total protein concentration was measured by using Bradford assay and equal amount of respectively tagged or untagged proteins were subjected to Western blot to compare the expression of both AMD non-risk- and risk-associated HTRA1 isoforms (exemplarily shown for HTRA1:CG and HTRA1:TT in **Figure 11**). 300 µl of the supernatants were incubated with casein for 3 h to test for

HTRA1 bioactivity (exemplarily shown for HTRA1:CG and HTRA1:TT in **Figure 11**), as described in (Murwantoko et al., 2004; Vierkotten et al., 2011; Eigenbrot et al., 2012).

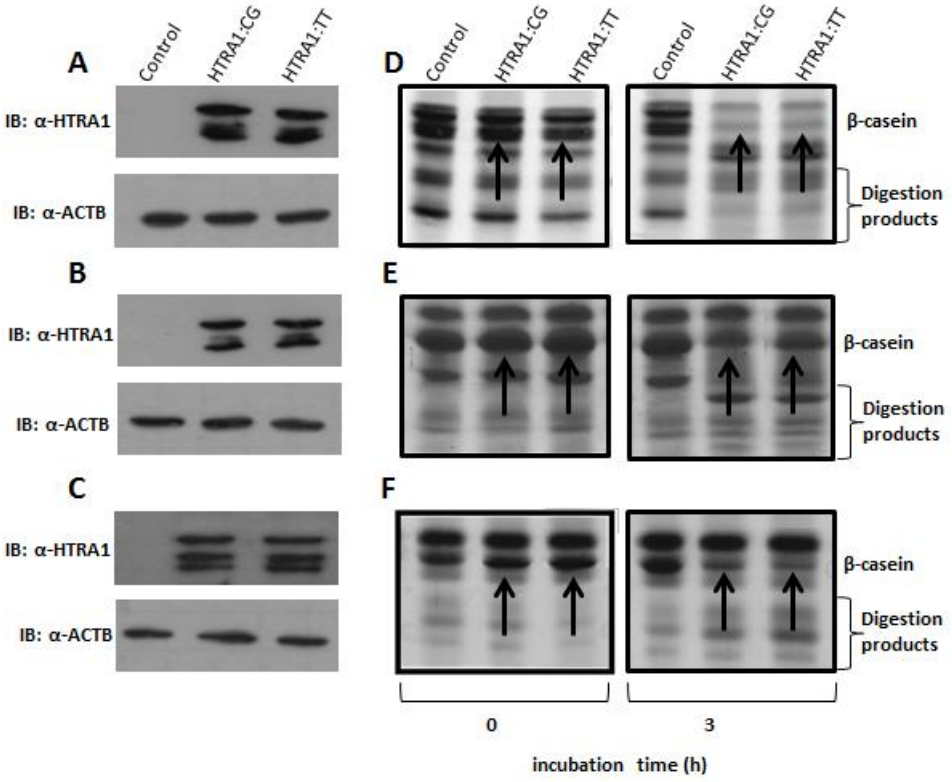

Figure 11: ***Characterization of HTRA1 expression and bioactivity*.** Hek293 cells were transfected with expression constructs for *HTRA1:CG* and *HTRA1:TT* variants. These *HTRA1* variants were either untagged (**A** and **D**) or TC-tagged (**B** and **E**) or Strep-tagged (**C** and **F**). Immunoblots were performed with cell lysates using α-HTRA1 antibodies. The β-actin (ACTB) immunoblot served as loading control. For analyzing bio-activity of untagged and TC-tagged HTRA1 isoforms (**D** and **E)** respectively, 300 µl of serum-free supernatants were mixed with 20 µg of β-casein and incubated at 37°C over a period of 3 h. Samples were taken after 0 h and 3 h and subjected to SDS-PAGE with subsequent Coomassie staining. For analyzing bio-activity of Strep-tagged HTRA1 (**F**), first 10 ml of serum-free supernatants of Hek293 cells transfected with expression constructs of Strep-tagged *HTRA1* variants were used to purify the HTRA1 isoforms in Strep Tactin Superflow® columns according to manufacturer's instructions. After purification 5 µg of each purified Strep-tagged HTRA1 isoform was mixed with 20 µg of β-casein and incubated at 37°C over a period of 3 h. Samples taken after 0 h and 3 h were subjected to Coomassie staining and analyzed as described above.

The bio-activity of HTRA1:CG and HTRA1:TT isoforms did not show any significant difference. This result was consistent whether the isoforms were untagged, TC-tagged or Strep-tagged.

4.2 Influence of synonymous SNPs within *HTRA1* exon 1 on protein structure

To assess protein folding properties of the different *HTRA1* haplotypes, MST, a method which determines the movement of molecules along a temperature gradient, was applied (Duhr and Braun, 2006; Baaske et al., 2010). The thermophoretic movement is sensitive to changes in the molecular structure or conformation, thus allowing detection of minimal alterations of protein variants or complexes.

For monitoring purposes, a C-terminal tetracysteine (TC)-tag motif was fused to each of the haplotype constructs providing a specific fluorescent labeling of the translated protein (Adams et al., 2002; Madani et al., 2009). The TC-tagged haplotype constructs were then fused into pCEP4 expression vector (Invitrogen, Carlsbad, USA). Therefore, TC-tagged *HTRA1* variants were heterologously expressed in Hek293 cells. After 72 h, supernatants were harvested, TC-tagged HTRA1 isoforms within the supernatants were labeled by a fluorescent dye and MST analyses were performed with the labeled HTRA1 isoforms.

4.2.1. Preparation and adjustment of TC-tagged HTRA1 isoforms

After harvesting the supernatant from Hek293 cells transfected with expression vectors containing the different TC-tagged *HTRA1* variants, the supernatants were concentrated by Amicon Ultra 10,000 Kw 4 ml columns and the total protein concentrations were measured by Bradford assay. The protein concentration of all supernatants containing TC-tagged HTRA1 isoforms were adjusted to 2 µg/µl and subjected to Western blot.

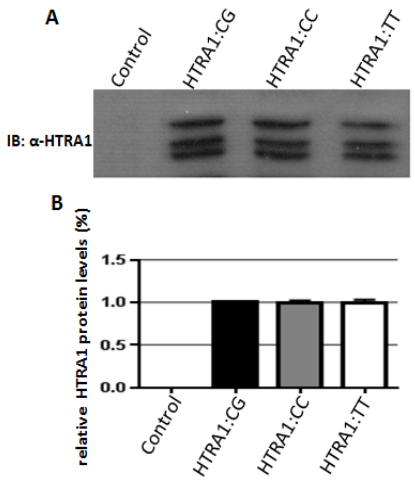

Figure 12: Adjustment of HTRA1 concentrations in supernatant of Hek293 cells transfected with expression vectors containing TC-tagged HTRA1 variants. (**A**) Supernatants of transfected Hek293 cells with expression vectors for TC-tagged variants or control (empty expression vector) were adjusted to a protein concentration of 2 µg/µl and subjected to Western blot analyses using α-HTRA1 antibodies. (**B**) Densitometry analysis of relative HTRA1 protein levels from (**A**), calibrated against measurements for HTRA1:CG. Data represent the mean +/- SD of three independent immunoblots before each independent MST analyses.

Each supernatant of Hek293 cells transfected with expression constructs for either TC-tagged *HTRA1:CG, HTRA1:CC* or *HTRA1:TT* variants showed similar HTRA1 protein level (**Figure 12**).

4.2.2. Labeling TC-tagged HTRA1 with FlAsH-EDT$_2$ for MST analyses

The biarsenical labeling reagent FlAsH-EDT$_2$, used in bioanalytical research, becomes fluorescent upon binding to TC-tagged recombinant proteins containing the tetracysteine (TC) motif (Adams et al., 2002; Adams and Tsien, 2008). In order to label TC-tagged HTRA1, the supernatants were incubated with 5 µM concentration of FlAsH-EDT$_2$ according to manufacturer's instructions. The labeled samples were subjected to SDS-PAGE and the image was captured by Fujifilm FLA-5000 image scanner (available at the Institute of Microbiology, Faculty of Biology and Preclinical Medicine, University of Regensburg, Germany).

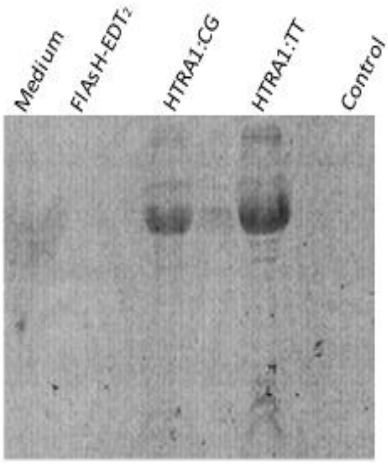

Figure 13: ***Labeling TC-tagged HTRA1 with FlAsH-EDT2 for MST analyses.*** The following samples were loaded (from left to right): Medium: Serum-free medium for Hek293 cells; FlAsH-EDT$_2$: 5 µM FlAsH-EDT$_2$ labeling reagent; HTRA1:CG: TC-tagged HTRA1:CG labeled with 5 µM FlAsH-EDT$_2$ in supernatant of Hek293 cells transfected with expression construct for TC-tagged *HTRA1:CG* variant; HTRA1:TT: TC-tagged HTRA1:TT labeled with 5 µM FlAsH-EDT$_2$ in supernatant of Hek293 cells transfected with expression construct for TC-tagged *HTRA1:TT* variant; and control: supernatant of Hek293 cells transfected with empty vector, labeled with 5 µM FlAsH-EDT$_2$.

Figure 13 illustrates that 5 µM concentration of FlAsH-EDT$_2$ specifically binds to TC-tagged HTRA1:TT and CG isoforms but did not give any signal in the control (supernatant of cells transfected with empty pCEP4 vector). The free dye also does not show any fluorescence.

4.2.3. HTRA1:CG, HTRA1:TT and HTRA1:CC protein conformation comparison by MST

Adjusted and labeled HTRA1 variants in supernatants were subjected to MST analyses by increasing the temperature gradually from 32°C to 52°C, with an interval of 2°C. The thermophoretic mobility of each HTRA1 isoform at the given temperature was recorded in Monolith NT.115 (NanoTemper Technologies, Munich, Germany). MST analyses were carried out by Dr. Thomas Schubert, 2bind GmbH, Regensburg,Germany.

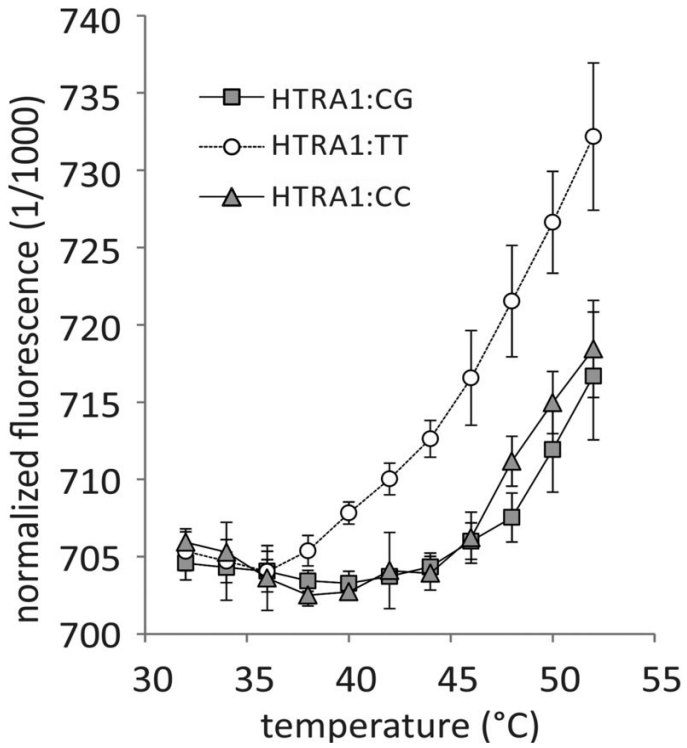

Figure 14: MST analysis of HTRA1:CG, HTRA1:TT and HTRA1:CC. TC-tagged HTRA1 isoforms were heterologously expressed in Hek293 cells. TC-tagged HTRA1 was labeled with a FlAsH-EDT_2, and subjected to MST analyses. Electrophoretic mobility of the fluorescent protein was assessed at increasing temperatures (from 32°C to 52°C). Supernatant of cells transfected with an empty vector were used for normalization. Data represent the mean +/- standard deviation (SD) of three independent experiments. The MST analyses were done by Dr. Thomas Schubert, 2bind GmbH, Regensburg, Germany.

MST analyses revealed a similar thermal migration behavior of the HTRA1 isoforms HTRA1:CG and HTRA1:CC. In contrast, HTRA1:TT exhibited a significantly different thermophoretic mobility suggesting an influence of AMD-associated polymorphisms rs1049331:T and rs2293870:T on the tertiary structure of the protein (**Figure 14**).

4.3. HTRA1:CG, HTRA1:TT and HTRA1:CC protein conformation comparison by limited partial proteolysis

In an independent approach, structural differences of the three protein isoforms were assessed by partial proteolysis. This assay is sensitive to detect minor alterations in protein structure by measuring the susceptibility of the protein substrate for proteases

such as Trypsin (Park and Marqusee, 2005; Kimchi-Sarfaty et al., 2007; Kim et al., 2009; Na and Park, 2009).

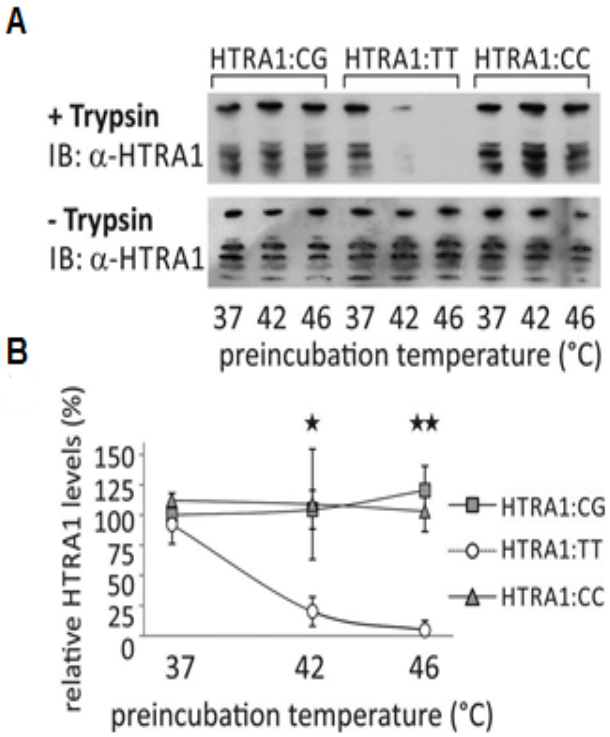

Figure 15: Partial proteolysis of recombinant HTRA1:CG, HTRA1:TT and HTRA1:CC with Trypsin. Strep-tagged HTRA1 isoforms were purified after heterologous expression in Hek293 cells. 1 µg of purified HTRA1 was incubated for 10 min at 37, 42 and 46 °C, respectively. Proteolysis was performed at 37°C for 5 min with 120 µg/ml Trypsin. Samples were subjected to Western blot analysis with α-HTRA1 antibodies. (**A**) shows a representative immunoblot. (**B**) shows densitometric analysis of immunoblots of three independent experiments from (**A**). HTRA1 signals were calibrated with measurements for HTRA1:CG after preincubation at 37°C. Data represent the mean +/- SD. Asterisks mark significant (*P < 0.05) and highly significant differences (**P < 0.01) between relative amounts of protein for HTRA1:CG or HTRA1:CC and HTRA1:TT.

Figure 15A shows that HTRA1:TT was more susceptible to trypsin digestion than HTRA1:CG or HTRA1:CC under partial denaturing conditions. A strong decrease of HTRA1:TT was observed after preincubation at 42°C, and after preincubation at 46°C, HTRA1:TT was completely digested. In contrast, no significant reduction of HTRA1:CG and HTRA1:CC, subjected to these conditions, was observed. **Figure 15B** shows that the differences in protein levels between HTRA1:CG or HTRA1:CC and HTRA1:TT were statistically significant after preincubation at 42°C ($P<0.05$), and highly significant after preincubation at 46°C ($P<0.01$). Autoproteolysis of HTRA1 was negligible. Together, the results from MST analyses and from partial proteolysis suggest that HTRA1:CG and HTRA1:CC exhibit a similar tertiary structure that is different from HTRA1:TT. With a further focus on the functional relevance of the altered structure of HTRA1:TT, its properties were compared with that of the HTRA1 isoform translated from the reference haplotype, namely *HTRA1:CG*.

4.4. Influence of synonymous SNPs within *HTRA1* exon 1 on protein secretion

Secreted proteins are subjected to ER quality control which retains and eventually degrades misfolded protein species with a high sensitivity towards minor structural alterations (Ruggiano et al., 2014). Secretion of HTRA1:CG and HTRA1:TT in Hek293 cells was therefore monitored. Supernatant and cells were collected at various time points between 0 h and 24 h after transfection with expression constructs for *HTRA1:CG* and *HTRA1:TT* (**Figure 16**).

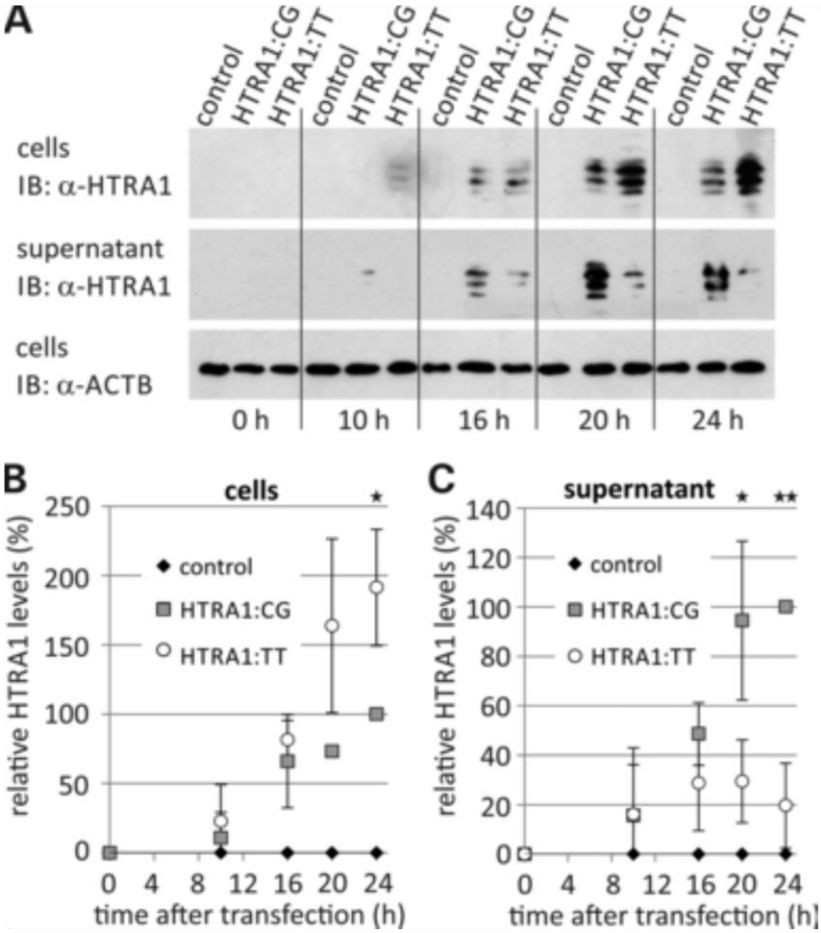

Figure 16*: *Influence of synonymous polymophisms on secretion of HTRA1 analyzed by immunoblot. After transfection of Hek293 cells with expression constructs for *HTRA1:CG*, *HTRA1:TT* or control, cells and cell culture medium (supernatant) were harvested at the indicated time points (0 to 24 h) and subjected to Western blot analyses with α-HTRA1 antibodies. The ACTB immunoblot served as loading control (**A**). Densitometric quantification of immunoblots of three independent repetitions of experiments from focusing on (**B**) intracellular or (**C**) extracellular HTRA1 protein shows HTRA1 signals were normalized against ACTB and calibrated

against measurements for HTRA1:CG at 24 h. Data represent the mean +/- SD. Asterisks indicate statistically significant (*P < 0.05) and highly significant differences (**P < 0.01) between relative amount of protein for HTRA1:CG and HTRA1:TT.

Western blot analyses were performed with α-HTRA1 antibody. At 0 h, no HTRA1 is detected. There is a strong increase in HTRA1 expression from 16 to 24 h. However, relative to HTRA1:CG, intracellular amounts of HTRA1:TT were increased with a statistically significant difference at 24 h (P < 0.05) (**Figure 16A and B**). Contrary to this, a statistically significant reduction of HTRA1:TT protein relative to HTRA1:CG was detected in the supernatant at 20 h and 24 h (**Figure 16A and C**). At time points 20 h and 24 h, the differences in amounts of extracellular protein of HTRA1:CG and HTRA1:TT were statistically significant (P < 0.05) (**Figure 16C**).

Cumulatively, these data suggest a delayed secretion of HTRA1:TT relative to HTRA1:CG.

4.5. Influence of synonymous SNPs within *HTRA1* exon 1 on its substrate affinity

4.5.1. Interaction of HTRA1 isoforms with TGF-β and β-casein analyzed by MST

Several studies demonstrated a inhibiting influence of HTRA1 on TGF-β signaling, although the type of interaction between the two molecules remained debatable (Oka et al., 2004; Shiga et al., 2011; Zhang et al., 2012; Graham et al., 2013; Karring et al., 2013). To investigate the interplay between HTRA1 and TGF-β, thermophoretic mobility of TC-tagged HTRA1 dependent on increasing TGF-β1 concentrations was measured using MST analyses. In order to label TC-tagged HTRA1 isoforms with FlAsH-EDT_2 dye, supernatants of Hek293 cells transfected with expression constructs for TC-tagged *HTRA1:CG* and *HTRA1 TT* were incubated with 5 µM FlAsH-EDT_2. 100 nM of each labeled HTRA1 isoform was incubated with increasing concentration of purified TGF-β1 ranging from 0.122 nM to 4000 nM or with β-casein (from 1,22 nM to 40 µM). At a constant temperature of 25°C, at 80% MST power and 20% LED power, the binding affinity of fluorescently labeled HTRA1:CG and HTRA1:TT with TGF-β1 was recorded on a Monolith NT.115.

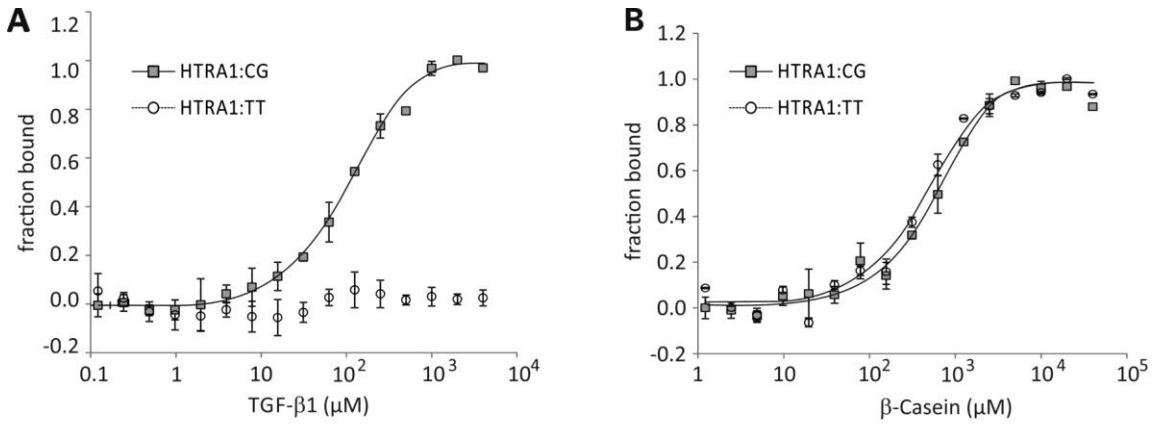

Figure 17: HTRA1 and its interaction with TGF-β1 and β-casein as measured by MST. Fluorescence-labeled HTRA1 (100 nM) was incubated with increasing concentrations of (A) TGF-β1 (0.122 nM to 4000 nM) or (B) β-casein (1.22 nM to 40,000 nM). Protein-protein interactions for HTRA1 and TGF-β1 were quantified by MST and binding data were plotted applying the Hill equation. The recorded fluorescence was normalized to the fraction bound (0 = unbound, 1 = bound). Data represent the mean +/- SD of three independent experiments. MST analyses were performed by Dr. Thomas Schubert, 2bind GmbH, Regensburg, Germany.

The analyses of the MST interaction of HTRA1 isoforms and TGF-β1 were performed by Dr. Thomas Schubert, 2bind GmbH, Regensburg, Germany. For HTRA1:CG in the presence of mature TGF-β1, a typical sigmoidal binding curve with a binding affinity of 63.2 +/- 8.8 nM was observed (**Figure 17A**). These results support a direct interaction between HTRA1 and mature TGF-β. In comparison, HTRA1:TT isoform failed to interact with TGF-β1 (**Figure 17A**). In contrast, titration of HTRA1 with its substrate β-casein revealed a similar sigmoidal binding curve for both HTRA1 isoforms, HTRA1:CG and HTRA1:TT. The binding affinities were 527.9 +/- 96.4 nM for HTRA1:CG, and 410.3 +/- 77.4 nM for HTRA1:TT, with the differences in binding affinities not being statistically significant (**Figure 17B**).

4.5.2. Proteolytic cleavage of TGF-β and β-casein by different HTRA1 isoforms

Next, the proteolytic capacity of HTRA1:CG and HTRA1:TT for TGF-β and β-casein, was analyzed respectively. Supernatants of Hek293 cells transfected with expression vectors for *HTRA1:CG*, *HTRA1:TT* and control (empty expression vector) were harvested. HTRA1 protein concentration in supernatant containing each HTRA1 isoform was 15 ng/µl. 4.5 µg of HTRA1 (in 300 µl supernatant) was incubated with 1 µg of TGF-β1 for 24 h and 20 µg of β-casein for 3 h. Same volume of supernatants

transfected with empty expression vector were incubated with TGF-β1 and β-casein similarly. This served as control. After 0, 4, 8, 16 and 24 h, samples were collected from each mixture of TGF-β1 incubated with HTRA1:CG, HTRA1:TT and control. Samples for casein-containing mixtures were collected at 0, 0.5, 1 and 3 h. The casein *in vitro* digestion and the densitometry analysis of three independent experiments was performed by Karolina Ploessl, Institute of Human Genetics, University Hospital Regensburg, Regensburg, Germany.

Co-incubation of HTRA1:CG with mature TGF-β1 resulted in a gradual digestion of TGF-β1. However, TGF-β1 cleavage by HTRA1:TT was strongly reduced compared to HTRA1:CG (**Figure 18A**). Densitometry of three independent experiments revealed that approximately 85% of TGF-β1 was cleaved by HTRA1:CG after 4 h, whereas only 10% of TGF-β1 cleavage was observed in the presence of HTRA1:TT. After 16 h, TGF-β1 was completely cleaved by HTRA1:CG, while at this time point almost 60% of mature TGF-β1 was still present when incubated with HTRA1:TT (**Figure 18B**). The observed differences for TGF-β1 cleavage by HTRA1:CG and HTRA1:TT were statistically highly significant ($P < 0.01$).

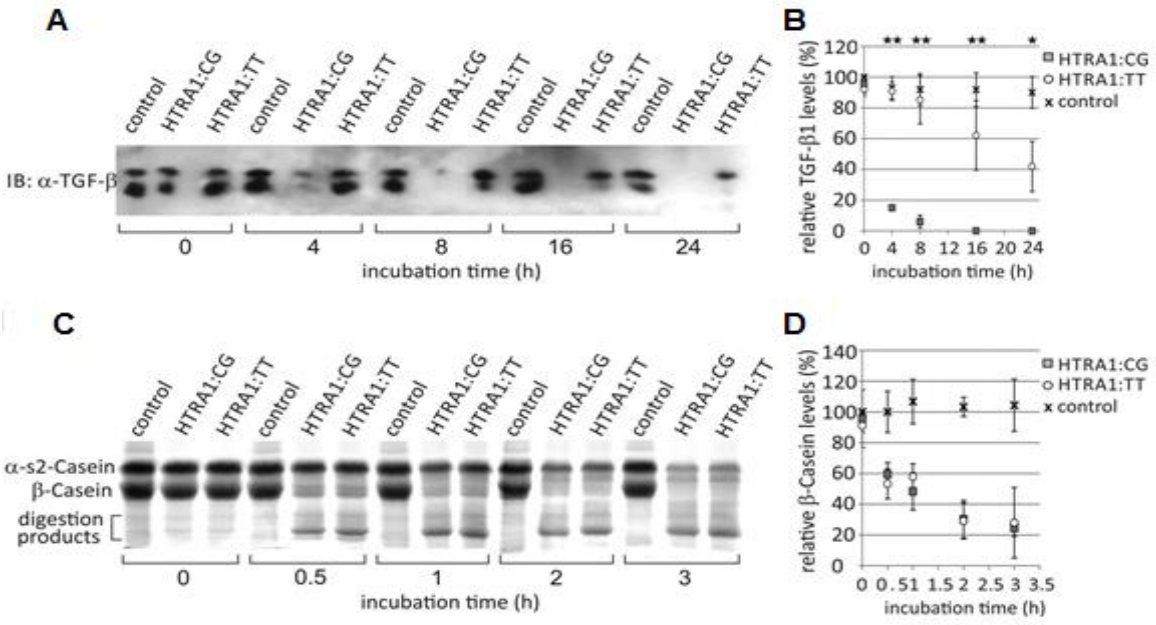

Figure 18: Proteolysis of TGF-β1 and β-casein by HTRA1:CG, HTRA1:TT or control. (**A**) 1 µg of TGF-β1 or (**C**) 20 µg of casein were mixed with 300 µl serum-free medium of transfected Hek293 cells, containing 15 ng/µl of each HTRA1 isoform and incubated at 37°C. As a control, supernatant of Hek293 cells transfected with the empty expression vector was used. Samples were taken at the indicated time points.

TGF-β1 proteolysis was captured via Western blot analyses with α-TGF-β antibody; casein digest was followed by Coomassie staining. Casein digest was conducted by Karolina Ploessl, Institute of Human Genetics, University Hospital Regensburg, Regensburg, Germany. Three independent experiments as described in (**A**) and (**B**) were performed and subjected to densitometric analysis for TGF-β1 (**B**) or β-casein (**D**). TGF-β1 or β-casein signals were calibrated against measurements for HTRA1:CG at 0 h. Data represent the mean +/- SD. Asterisks indicate statistically highly significant differences (**P<0.01) between TGF-β1 cleavage by HTRA1:CG and HTRA1:TT, respectively. Densitometry analysis for casein digest was performed by Karolina Ploessl, Institute of Human Genetics, University Hospital Regensburg, Regensburg, Germany.

In contrast to the effect of synonymous polymorphisms on TGF-β1 cleavage, both HTRA1 isoforms exhibited similar proteolytic activities for the β-casein substrate (**Figure 18C and D**).

4.6. Effect of HTRA1:CG and HTRA1:TT on TGF-β signaling

The different affinities of HTRA1:CG and HTRA1:TT for TGF-β indicate that the two variants might also exhibit different effects on TGF-β-induced signal pathways. Therefore, the effect of HTRA1:CG and HTRA1:TT on TGF-β signaling was investigated.

4.6.1. Effect of HTRA1:CG and HTRA1:TT on TGF-β1-induced *PAI-1* promoter activity in MLEC-PAI/Luc cells.

A reporter assay based on MLEC-PAI/Luc cells was used to analyze the effect of HTRA1 on TGF-β1 signaling. These cells are stably transfected with a luciferase-coding sequence under the control of the TGF-β-responsive element of the *PAI-1* promoter, and thus, respond to stimulation by TGF-β family members (e.g. TGF-β1) with heterologous luciferase expression (Abe et al., 1994). MLEC-PAI/Luc cells were treated with 2 ng/ml of TGF-β1 in presence of Strep-tagged HTRA1:CG and HTRA1:TT, or control protein (purified from supernatant of empty Strep-vector transfected cells) for 16 h.

Addition of HTRA1:CG to MLEC-PAI/Luc cells resulted in a strong reduction of TGF-β1-activated luciferase expression (15.6 +/- 2.8% luciferase activity compared to control cells). HTRA1:TT was also capable of inhibiting TGF-β1-activated luciferase expression, but only at 64.6 +/- 21.1% (**Figure 19**). The difference in luciferase expression between cells treated with HTRA1:CG and HTRA1:TT was statistically highly significant ($P < 0.01$).

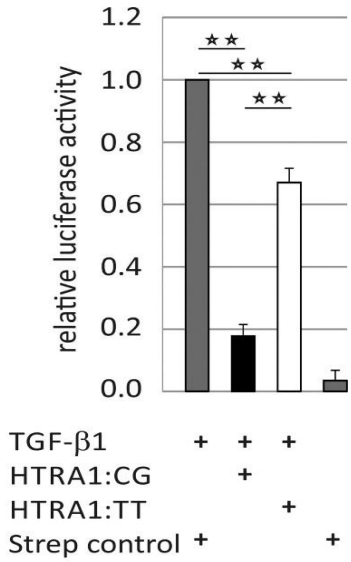

Figure 19: Effect of HTRA1:CG and HTRA1:TT on TGF-β1-induced PAI-1 promoter activity in MLEC-PAI/Luc cells. MLEC-PAI/Luc cells were stimulated with 2 ng/ml TGF-β1 in the presence of 40 ng/ml HTRA1:CG, or HTRA1:TT purified from supernatants of Hek293 cells transfected with expression constructs for Strep-tagged *HTRA1* variants, or control protein (purified from supernatant of empty Strep-vector-transfected cells). After 16 h, luciferase activity was measured in triplicate wells each in three independent experiments. Measurements for each experiment were calibrated against the control (TGF-β1 + control protein). The mean +/- SD for the three independent experiments is given for each treatment. Asterisks indicate statistically highly significant differences (**P < 0.01).

4.6.2. Effect of HTRA1:CG and HTRA1:TT on SMAD phosphorylation

TGF-β signaling has been reported to be an important regulator of microglial development and activation (Suzumura et al., 1993; Paglinawan et al., 2003; Li et al., 2008; Butovsky et al., 2014). Specifically, extracellular binding of TGF-β family members by TGF-β receptors lead to phosphorylation of SMAD proteins (Javelaud and Mauviel, 2004a, b, 2005), important mediators of TGF-β-induced signaling cascades. Therefore, the influence of HTRA1:CG and HTRA1:TT on the phosphorylation of SMAD2 in BV-2 micoglial cells was analyzed. Autocrine SMAD phosphorylation was triggered in BV-2 cells by adding BV-2-conditioned medium to serum-starved BV-2 cells as described in Spittau et. al (2013). BV-2 cells (in conditioned medium) were treated for 2 h with 40 ng/ml of Strep-tagged HTRA1:CG, HTRA1:TT or control protein. The control protein was purified from supernatant of cells transfected with empty Strep-vector (pEXPR-IBA103). Immunocytochemistry of the treated cells with antibody against pSMAD2 was carried out by Magdalena Schneider, Institute of Human Anatomy and Embryology, Faculty of Biology and Preclinical Medicine, University of Regensburg, Germany **(Figure 20A).**

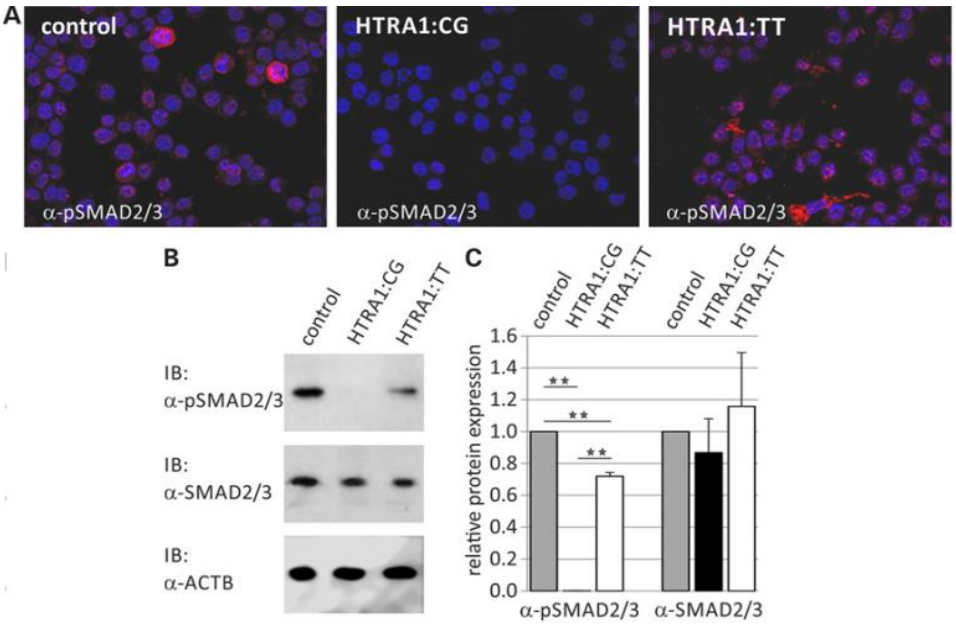

Figure 20: Effect of HTRA1 variants on SMAD-phosphorylation analyzed via immunocytochemistry. BV-2 cells (in conditioned medium) were treated for 2 h with protein purified from supernatant of cells transfected with empty Strep-vector (control) (**Left**); *HTRA1:CG* (**Centre**) and *HTRA1:TT* (**Right**). Subsequently, the cells were subjected to immunocytochemistry with antibodies against pSMAD2 (performed by Ms. Magdalena Schneider, Institute of Human Anatomy and Embryology, Faculty of Biology and Preclinical Medicine, University of Regensburg, Germany) (**A**) or to immunoblot analyses using antibodies against pSMAD2, SMAD2 and ACTB (**B**). (**C**) Densitometry quantification of immunoblots was analyzed from (**B**) with three independent experiments. Signals for pSMAD2 and SMAD2 were normalized against ACTB and calibrated against the control. Data represent the mean +/- SD. Asterisks indicate statistically highly significant differences (**P < 0.01).

Immunocytochemistry with control cells showed a strong immunoreactivity for phosphorylated SMAD2 (pSMAD2) within BV-2 cells, indicating an activated TGF-β signaling pathway by endogenously synthesized and secreted TGF-β proteins derived from BV-2-conditioned medium (**Figure 20A Left**). This result is in full agreement with data on autocrine TGF-β expression and signaling in microglial cells (Spittau et al., 2013). BV-2 cells treated with HTRA1:CG exhibited a significantly reduced signal intensity of pSMAD2 indicating an inhibiting effect of HTRA1:CG upon TGF-β signaling (**Figure 20A Centre**). In contrast, staining for pSMAD2 in BV-2 cells treated with HTRA1:TT had a similar intensity as in the control experiment (**Figure 20A Right**).

To quantify the effects of HTRA1 isoforms on SMAD phosphorylation, Western blot analyses were performed with protein isolated from BV-2 cells treated as described above.

The data of immunoblot analyses show that SMAD2 phosphorylation is almost completely absent in BV-2 cells treated with HTRA1:CG, while HTRA1:TT reduced measurable pSMAD2 levels to 71.9 +/- 2.5% compared to control (**20B and C**). While the amounts in SMAD2 protein were comparable, the observed differences in phosphorylated pSMAD2 were statistically highly significant ($P < 0.01$) (**Figure 20C**).

4.6.3. Effect of HTRA1:CG and HTRA1:TT on relative *Pai-1* gene expression

PAI-1 is a prominent target gene of TGF-β signaling (Cao et al., 1995; Kutz et al., 2001; Dong et al., 2002). Upon TGF-β stimulation, phosphorylated SMAD2 and SMAD3 form a complex with SMAD4, which is then translocated into the nucleus. This complex stimulates expression of TGF-β response genes (Javelaud and Mauviel, 2004b, a, 2005). Autocrine TGF-β signaling was triggered in BV-2 cells by adding BV-2-conditioned medium to serum-starved BV-2 cells as described in Spittau et. al (2013). BV-2 cells in conditioned medium were treated with 40 ng/ml Strep-tagged HTRA1:CG and HTRA1:TT for 3 h and 24 h.

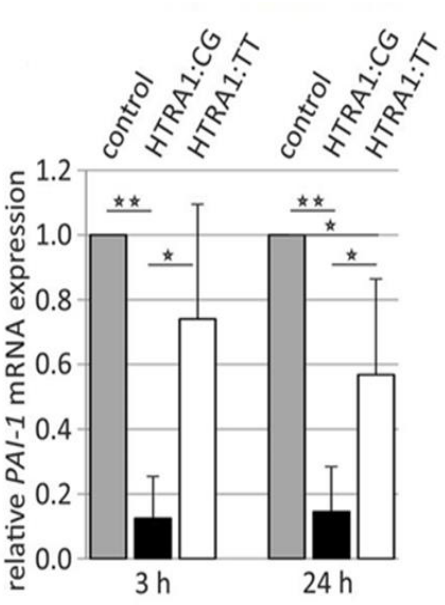

Figure 21: Effect of HTRA1:CG and HTRA1:TT on relative Pai-1 gene expression in BV-2 cells. BV-2 cells were treated for 3 and 24 h with recombinant HTRA1:CG, HTRA1:TT or control protein. PAI-1 mRNA expression was determined via qRT-PCR by Ms. Magdalena Schneider and Dr. Rudolf Fuchshofer, Institute of Human Anatomy and Embryology, Faculty of Biology and Preclinical Medicine, University of Regensburg, Germany. Experiments were performed in triplicates in four independent experiments. Results were normalized to the transcript levels of a mouse housekeeper gene, *GNB2L* and calibrated with the control at 3 h and 24 h, respectively. The mean +/- SD for the four independent experiments are

given. Asterisks indicate statistically significant (*P < 0.05) and highly significant differences (**P < 0.01).

After 3h and 24 h respectively, RNA was isolated from the treated cells and cDNA was synthesized. The relative *Pai-1* gene expression was analyzed *via* qRT PCR by Magdalena Schneider and Dr. Rudolf Fuchshofer, Institute of Human Anatomy and Embryology, Faculty of Biology and Preclinical Medicine, University of Regensburg, Germany (**Figure 21**). A strong downregulation of *Pai-1* mRNA expression was noted in BV-2 cells treated with HTRA1:CG when compared to control cells (12.5 +/- 12.9% after 3 h; 14.5 +/- 13.9% after 24 h). In contrast, a less prominent decrease of *Pai-1* transcripts was found after treatment with HTRA1:TT (74.0 +/- 35.5% after 3 h; 56.8 +/- 29.6% after 24 h, compared to control cells). The difference in *Pai-1* expression following treatment with HTRA1:CG or HTRA1:TT was statistically significant (P < 0.05) (**Figure 21**).

4.7. Effect of HTRA1 on microglial activation

Microglial activation and differentiation is strongly regulated by TGF-β signaling (Rozovsky et al., 1998; Huang et al., 2010; Cekanaviciute et al., 2014; Norden et al., 2014). As HTRA1 has been found to play a role in TGF-β signaling in microglial cells, the effect of HTRA1 on microglial activation was investigated.

4.7.1. Effect of HTRA1 on classical activation of microglial (BV-2) cells via LPS treatment

To activate classical (M1) microglial activation, 50 ng/ml of LPS was used in various studies (Dirscherl et al., 2010; Karlstetter et al., 2014; Aslanidis et al., 2015). The effect of HTRA1 on LPS-activated microglia was observed by treating the BV-2 cells with 50 ng/ml of LPS in presence of increasing HTRA1 concentrations. A key microglial enzyme induced in this process is the inducible nitric oxide synthase (iNOS), which utilizes arginine to produce nitric oxide (Bagasra et al., 1995). Nitrite production was thus measured as a marker for M1 activation. BV-2 cells, serum-starved for 24 h, were treated with increasing concentrations of Strep-tagged HTRA1 (30, 60 and 90 ng/ml) in presence or absence of 50 ng/ml LPS.

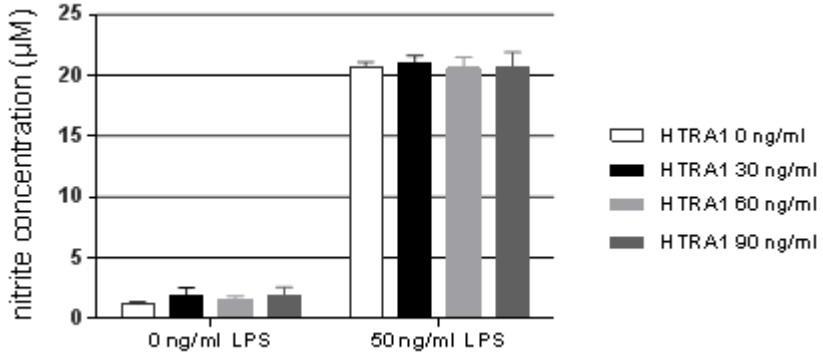

Figure 22: Effect of HTRA1 on nitrite production in BV-2 cells. BV-2 cells were serum-starved for 24 h before treatment. After 24 h, increasing concentration (30, 60, 90 ng/ml) of Strep-tagged HTRA1 was added to BV-2 cells in presence 0 or 50 ng/ml of LPS. After 24 h of treatment, nitrite production (in µM) was measured from the supernatant via NO assay. The mean +/- SD for the three independent experiments is given.

After 24 h, the NO assay revealed significant difference in nitrite production in non-activated (1.2 +/- 0.2 µM) and LPS-activated BV-2 cells (20.7 +/- 0.4 µM). However, there was no effect of HTRA1 on nitrite production by BV-2 cells in this *in vitro* assay (**Figure 22**).

In the next step, the relative mRNA expressions of M1 markers, *iNOS* and *IL6*, were analyzed by qRT-PCR. BV-2 cells were treated with LPS and HTRA1 as described above. After 24 h RNA was isolated and gene expression of *iNOS* and *IL6* was analyzed via qRT-PCR.

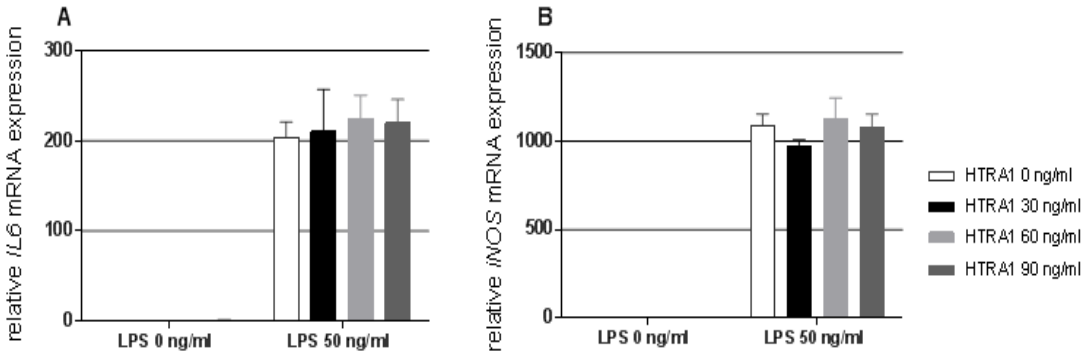

Figure 23: Effect of HTRA1 on relative mRNA expression of M1 markers of BV-2 cells induced by LPS. BV-2 cells were serum-starved for 24 h before treatment***.*** BV-2 cells were serum-starved for 24 h before treatment. After 24 h, increasing concentrations (30, 60 and 90 ng/ml) of Strep-tagged HTRA1 was added to BV-2 cells in presence of 0 or 50 ng/ml of LPS. After 24 h of treatment, the relative mRNA

expressions of M1 markers, *IL6* (**A**) and *iNOS* (**B**) were analyzed via qRT-PCR. Experiments were performed in triplicates in three independent experiments. Relative transcripts levels of *IL6* and *iNOS* in BV-2 cells treated with 0 ng/ml of LPS and 0 ng/ml of HTRA1 served as control. Results were normalized to mouse ATPase transcript levels and calibrated with the control. The mean +/- SD for the three independent experiments are given.

The addition of 50 ng/ml of LPS induced the M1 activation markers *iNOS* and *IL6* in microglial cells. With the treatment of LPS, relative mRNA expressions of *IL6* and *iNOS* show fold changes of 203.2 +/- 17.7 and 1088.5 +/- 65.3, respectively, compared to no LPS treatment. However, increasing concentrations of HTRA1 had no effect on the expression of these markers (**Figure 23 A and B**).

4.7.2. Effect of HTRA1 on alternative activation of microglial (BV-2) cells via IL4 and TGF-β1 treatment

IL4 is a well-described anti-inflammatory cytokine (Butovsky et al., 2005; Ledeboer et al., 2000; Park et al., 2005; Zhao et al., 2006), which induces alternative (M2) activation of microglia resulting in the expression of M2 markers *Arginase 1* (*Arg1*) and *Chitinase-3-Like-3* (*Chi3l3* or *Ym1*) in microglial cells (Gordon, 2003; Ponomarev et al., 2007). TGF-β1 can enhance IL4-induced M2 activation of microglia by increasing the expression of *Arg1* and *Ym1* either by a direct effect on *Ym1/Arg1* promoter activity or indirectly by upregulating the IL4Rα, a receptor of IL4 (Zhou et al., 2012).

Since HTRA1 plays a role in TGF-β signaling, role of HTRA1 in regulation of M2 microglial activation was investigated. Alternative activation was achieved via IL4 and TGF-β1 treatment as described in Zhou et al. (2012). BV-2 cells, serum-starved for 24 h, were treated separately or in combination with 1 ng/ml of TGF-β1 and 10 ng/ml of IL4 in presence of increasing Strep-tagged HTRA1 concentrations (30, 60, and 90 ng/ml).

Relative gene expression of both the M2 activation markers, *Arg1* and *Ym1* were analyzed via qRT-PCR. The results indicate that upon treatment of TGF-β1 alone there is no upregulation of the markers. In contrast, treatment of BV-2 cells with IL4 alone upregulates the M2 markers. Furthermore, when treated with IL4 and TGF-β1, enhanced upregulation was observed in comparison to treatment with IL4 alone

(**Figure 24A and B**). These findings are in full agreement with the previous study by Zhou et al. (2012).

Treatment of BV-2 cells with HTRA1 alone in increasing concentration shows no effect on gene expression of M2 markers. Increasing concentrations of HTRA1, in combination with TGF-β1, also does not show any effect on regulation of M2 markers. However, HTRA1 shows an inhibition of M2 activation markers induced by IL4 alone and a combination of IL4 and TGF-β1 (**Figure 24A and B**).

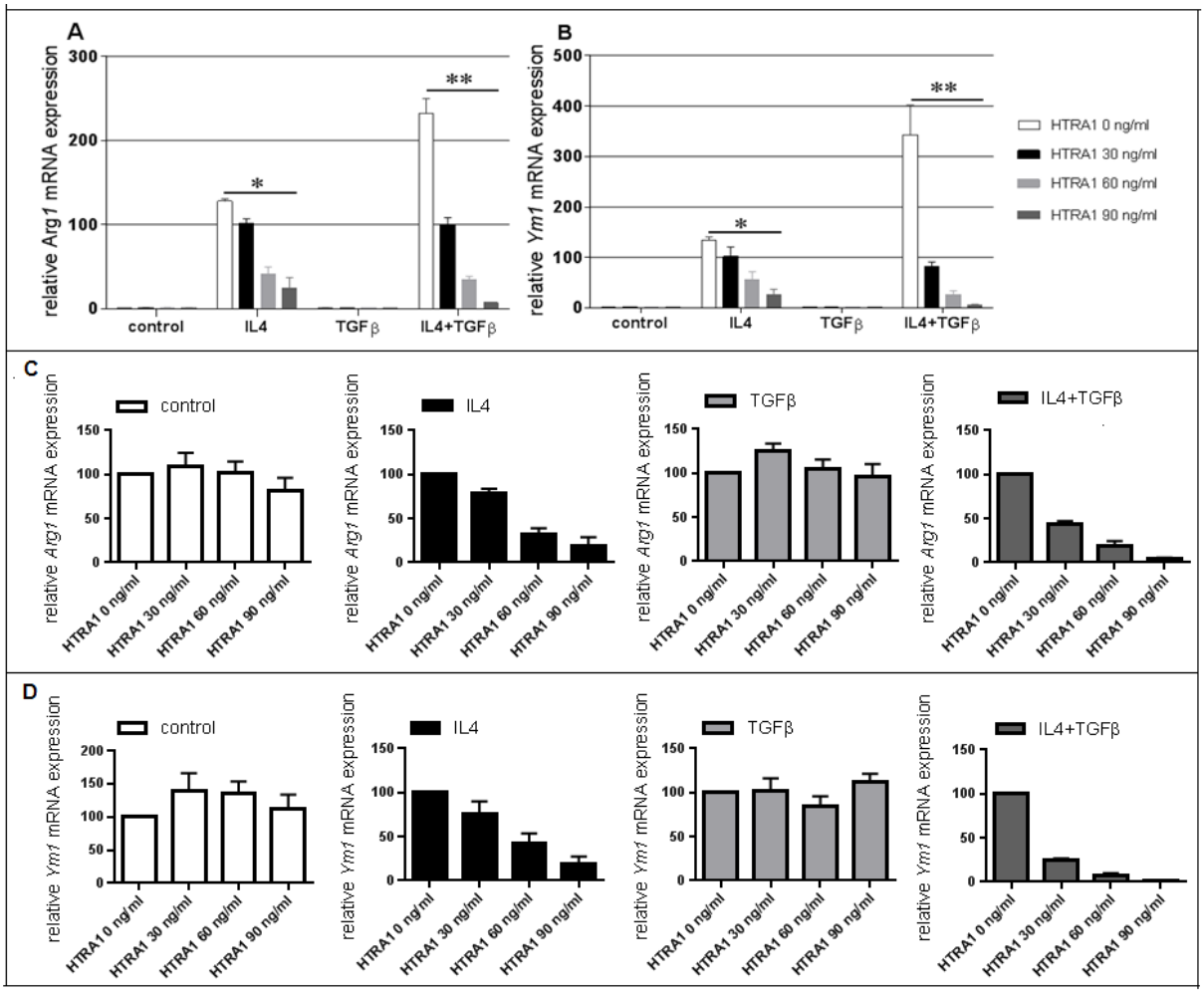

Figure 24: Effect of HTRA1 on relative mRNA expression of M2 markers of BV-2 cells induced via IL4/ TGF-β1. Relative mRNA expressions of *Arg1* (**A**) and *Ym1* (**B**) were analyzed by performing qRT-PCR of cDNA from serum-starved BV-2 cells, treated separately or in combination with 1 ng/ml of TGF-β1 and 10 ng/ml of IL4 in presence of increasing HTRA1 concentrations (30 ng/ml, 60 ng/ml, and 90 ng/ml). BV-2 cells, treated with increasing concentrations of HTRA1, in absence of IL4 and TGF-β1 were termed as "control". Experiments were performed in triplicates in three independent experiments. Firstly, results were normalized to mouse ATPase

transcript levels. Results were then calibrated against transcript levels of the M2 markers of BV-2 cells treated with 0 ng/ml of HTRA1, IL4 and TGF-β1 (**A** and **B**). Alternatively, results of each treatment (IL4 alone, TGF-β1 alone and IL4 along with TGF-β1) were separately calibrated with the respective transcript levels of the M2 markers of BV-2 cells treated with 0 ng/ml of HTRA1 (**C** and **D**). Mean +/- SD for the three independent experiments are shown. Asterisks indicate significant (*P < 0.05) and highly significant (**P < 0.01) differences.

More specifically, relative gene expression of *Arg1* shows a downregulation by 79.0 +/- 4.5%, 31.7 +/- 6.9% and 19.1 +/- 9.8% upon the treatment of BV-2 cells with IL4 in presence of 30, 60 and 90 ng/ml of HTRA1 compared to the treatment of BV-2 cells with IL4 in absence of HTRA1. (**Figure 24 C).** Similarly, relative gene expression of *Ym1* gets reduced by 75.7+/- 13.7%, 41.7 +/- 11.8% and 18.8 +/- 8.4% upon treatment of BV-2 cells with IL4 in presence of 30, 60 and 90 ng/ml of HTRA1, compared to the treatment of BV-2 cells with IL4 in absence of HTRA1(**Figure 24D**).

The relative gene expression of *Arg1* shows a downregulation by 43 +/- 3.6%, 18.8 +/- 5.4% and 4.47 +/- 1.2%, upon the treatment of BV-2 cells with IL4 and TGF-β1 in presence of 30, 60 and 90 ng/ml of HTRA1 compared to the treatment of BV-2 cells with IL4 in absence of HTRA1 (**Figure 24C**). Similarly, relative transcript levels of *Ym1* show a downregulation by 24 +/- 2.5%, 7.8 +/-2.1% and 1.7 +/- 0.3%, upon the treatment of BV-2 cells with IL4 and TGF-β1 in presence of 30, 60 and 90 ng/ml of HTRA1 compared to the treatment of BV-2 cells with IL4 and TGF-β1 in absence of HTRA1 (**Figure 24D**).

5. DISCUSSION

With around 14 million people affected worldwide, AMD is one of the most common causes of irreversible blindness (Resnikoff et al., 2004). AMD is a multifactorial disorder caused by both genetic and environmental influences. Polymorphisms in *HTRA1* and *ARMS2* on chromosome 10q26 are strongly associated with AMD. However, there are conflicting data regarding the involvement of these genes in the pathogenesis of AMD (Yang et al., 2006, Dewan et al., 2006, Kanda et al., 2007, Fritsche et al., 2008). In addition, there are speculations on an involvement of both genes in AMD development. (Yang et al., 2010).

The involvement of HTRA1 in the development of AMD, through various signaling pathways, has been investigated in several studies. It was shown that overexpression of HTRA1 in a mouse model regulates angiogenesis through TGF-β signaling (Zhang et al., 2010). Another recent study also found an involvement of HTRA1 in IGF-1 signaling. Two AMD-associated synonymous polymorphisms [(rs1049331 (c.102C>T) and rs2293870 (c.108G>T)] located in exon 1 of the *HTRA1* gene were shown to directly influence the ability of HTRA1 to regulate insulin-like growth factor 1 (IGF1) signaling (Jacobo et al., 2013). A strong association of AMD pathology with these two variants located in exon 1 of the *HTRA1* gene has been previously reported in several independent case-control association studies (Deangelis et al., 2008; Fritsche et al., 2008; Tam et al., 2008); however, the binding capacity of HTRA1 for IGF1 is contentious (Eigenbrot et al., 2012).

5.1. Effect of synonymous polymorphisms within exon 1 of *HTRA1* on its structure and secretion

In recent years, the influence of synonymous or silent mutations on protein folding and function has attracted increasing attention (Hunt et al., 2014). These alterations although not associated with changes in amino acid composition of the protein were reported to cause mRNA instability, exon skipping or alterations in co-translational protein folding (Duan and Antezana, 2003; Duan et al., 2003; Chamary and Hurst, 2005; Chamary et al., 2006; Nackley et al., 2006; Kimchi-Sarfaty et al., 2007;

Chamary and Hurst, 2009; Zhang et al., 2010; Brest et al., 2011; Lampson et al., 2013). As a consequence, synonymous alterations in protein-coding sequences may causally be involved in human pathologies. For example, synonymous changes in the multidrug resistance 1 (*MDR1*) gene were shown to cause an altered drug and inhibitor interaction leading to major changes in protein stability and transporter specificity (Kimchi-Sarfaty et al., 2007; Fung et al., 2014). A schizophrenia-associated synonymous SNP in the dopamine receptor D2 gene (*DRD2*) was also reported to alter the rate of translation (Duan et al., 2003).

The first aim of the study was focused on the impact of three synonymous SNPs (rs1049331:C>T, rs2293870:G>T and rs2293870:G>C) on conformation of HTRA1. While rs1049331:C>T and rs2293870:G>T have been found to be associated with AMD, rs2293870:G>C despite being on the identical nucleotide position of rs2293870:G>T has not been found to be associated with the disease (Deangelis et al., 2008; Fritsche et al., 2008; Tam et al., 2008; Jacobo et al., 2013; Friedrich et al., 2015). Hence, three expression constructs for HTRA1 were generated respectively including *HTRA1* exon 1 variants rs1049331:C and rs2293870:G (referred to as HTRA1:CG), the AMD-associated variants rs1049331:T and rs2293870:T (HTRA1:TT), and the non-AMD-associated variants rs1049331:C and rs2293870:C (HTRA1:CC). Thermophoretic movement of the three different isoforms was analyzed by MST. This technique is based on thermophoresis, the directed motion of molecules in temperature gradients. Thermophoresis is highly sensitive to all types of binding-induced changes of molecular properties, be it in size, charge, hydration shell or conformation (Seidel et al., 2013). It has recently been demonstrated that MST is well-suited to follow protein unfolding and to detect unfolding intermediates, and that it rivals more traditional approaches such as circular dichroism or tryptophan fluorescence measurements in this capacity due to its speed and low sample consumption (Alexander et al., 2013). Because of its high sensitivity to conformational change, MST qualifies as a good technique to study the conformational change caused by synonymous polymorphisms. In the present study, thermophoretic movement of HTRA1 were significantly altered for the protein isoform HTRA:TT, but not for the two other isoforms, HTRA1:CG or HTRA1:CC. MST results were confirmed by performing limited proteolysis assay, which is an established

technique for protein conformation studies (Varne et al., 2002; Huang, 2003; Fontana et al., 2004). These assays documented an altered accessability of HTRA1:TT isoform compared to HTRA1:CG isoform, clearly indicating structural differences of both isoforms. This is in full agreement with findings first reported by Jacobo et al. (Jacobo et al., 2013). In their work, the authors observed a decreased translation rate of the isoform HTRA1:TT, which they ascribed to differential codon usage (Jacobo et al., 2013). Synonymous codons are distinguished by the abundance of their corresponding tRNA, which is lower for rare codons than for the frequent codons (Cannarozzi et al., 2010; Tuller et al., 2010). Folding of nascent polypeptides occurs cotranslationally (Frydman et al., 1994; Makeyev et al., 1996) and is influenced by the rate of ribosome transit through the mRNA template. Therefore, codon frequency can influence the rate of translation. The hypothesis that the attainment of a conformationally immature protein with functional deficits is caused by the decreased protein translation owing to common-to-rare codon conversion is consistent with several publications (Zhang et al., 1998; Komar et al., 1999; Kimchi-Sarfaty et al., 2007; Bartoszewski et al., 2010).

Secreted proteins undergo stringent ER quality control (Ruggiano et al., 2014). Synonymous SNPs in Cystic Fibrosis Transmembrane Region (CFTR) causes local misfolding of the protein and retention of the protein in ER for a prolonged time (Zhang et al., 1998; Bartoszewski et al., 2010). That's why time-dependent secretion was monitored to compare the secretory property of the two conformationally different HTRA1 isoforms. The results indicated that HTRA1:TT had a decreased secretion as well as intracellular aggregation when compared to HTRA1:CG. Whether delayed secretion or intracellular aggregation of HTRA1 or both could affect the progression of AMD is yet to be clarified.

5.2. Effect of synonymous polymorphisms within exon 1 of *HTRA1* on its substrate specificity

As a conformational change in the AMD risk-associated isoform was suggested, the impact of the changes on substrate specificity of HTRA1 was the next the thing to be investigated in our study. HTRA1 is a serine protease having an array of substrates. HTRA1 digests major components of cartilage, such as aggrecan, decorin,

fibromodulin and soluble type II collagen (Tsuchiya et al., 2005). Various other substrates of HTRA1 that are associated with the complement system (clusterin, vitronectin and fibromodulin) were found in supernatants of primary RPE cells (An et al., 2010). An et al. (2010) additionally confirmed the proteolytic breakdown of clusterin by recombinant HTRA1 via *in vitro* digestion. The pro form of complement factor D (CFD) is cleaved by HTRA1 to activate CFD (Stanton et al., 2011). In addition to these complement proteins, An et al.(2010) also demonstrated proteins involved in the amyloid deposition (clusterin, alpha-2 macroglobulin and ADAM9) as interaction partners of HTRA1. Amyloid is a component of drusen and it could be shown that HTRA1 co-localized with so-called amyloid plaques in the brain of Alzheimer's disease patients (Grau et al., 2005; Cameron et al., 2007). Grau et al. (2005) identified the amyloid precursor protein C99 as substrate of HTRA1 by showing its cleavage by recombinant HTRA1 *in vitro*. Many ECM-associated substrates that are cleaved by HTRA1 such aggrecan, biglycan, decorin, fibromodulin, fibronectin, soluble type II collagen and elastin were identified (Tsuchiya et al., 2005; Chamberland et al., 2009; Jones et al., 2011). The study by Vierkotten et al. (2011) was able to demonstrate that fibronectin, fibulin 5 and nidogen 1 are digested *in vitro* by recombinant HTRA1, whereas, laminin and collagen type IV were not digested by recombinant HTRA1 *in vitro* (Vierkotten et al., 2011). Jacobo et al. (2013) also reported differential affinities of AMD-associated *HTRA1* (*HTRA1:TT*) variant towards IGF-1 interaction. However, the interaction between HTRA1 and IGF-1 is challenged by findings from Eigenbrot et al. (2012) who failed to obtain any evidence for binding of IGF-I or IGF-II, or insulin-binding activity by the N-domain of HTRA1. This is further supported by a biosensor binding study which found no appreciable Mac-25 interaction of HTRA1 with IGF-I or IGF-II (Vorwerk et al., 2002).

Among all the substrates of HTRA1, interaction with family of TGF-β proteins is the most widely studied (Oka et al., 2004; Launay et al., 2008; Shiga et al., 2011; Zhang et al., 2012; Graham et al., 2013; Karring et al., 2013). In several studies, HTRA1 has been shown to inhibit TGF-β signaling but the exact mechanism of the inhibition remains controversial. Shiga et al. (2011) describes that HTRA1 binds to pro-TGF-β and cleaves it intracellularly, more precisely in the endoplasmic reticulum (ER). The cleavage thereby inhibits TGF-β signaling. Oka and colleagues (2004), however,

showed an extracellular digestion of the secreted active TGF-β by HTRA1. In another independent study, *in vitro* digestion of TGF-β by HTRA1 was confirmed (Launay et al., 2008). In an HTRA1-deficient mouse model, increased mRNA expression of GDF6, a TGF-β family member, was observed. This mouse model showed increased TGF-β signaling and increased vascularization of the retina (Zhang et al., 2012). It has recently been reported that overexpression of HTRA1 causes reduced levels of TGF-β receptors type II and III: HTRA1 was found to digest the TGF-β receptors type II and III *in vitro*, but not the receptor type I or TGF-β (ligand) (Graham et al., 2013). All these contradictory studies show that it is still under discussion, how HTRA1 inhibits TGF-β signaling (Oka et al., 2004; Shiga et al., 2011; Graham et al., 2013). Since the TGF-β signaling is also closely linked to the VEGF-A signaling (Clifford et al., 2008), regulation of TGF-β by HTRA1 could possibly also affect angiogenesis in the eye influencing the progress of CNV.

In this work, an interaction between HTRA1 and TGF-β1 was investigated using MST and *in vitro* proteolysis assay. MST has been successfully applied to study the protein-protein interaction in a variety of studies (Arbel et al., 2012; Lin et al., 2012; Wilson et al., 2012; Keren-Kaplan et al., 2013; Xiong et al., 2013; Zillner et al., 2013). While a typical sigmoidal binding curve was observed in MST analyses of direct interaction between HTRA1:CG and TGF-β1, no stable interaction between HTRA1:TT and TGF-β1 was observed. In addition, evidence for a direct proteolytic activity of isoform HTRA1:CG towards mature TGF-β1 was obtained via *in vitro* digestion assay. In contrast, the *in vitro* digestion assay suggested a strongly decreased turnover rate of TGF-β1 by HTRA1:TT compared with HTRA1:CG. The apparent discrepancy raises the question why there is still an interaction of TGF-β1 and HTRA1 in the proteolysis assay, whereas at the same time, no interaction of the two proteins is apparent in the MST assay. It is hypothesized that a stable interaction between HTRA1 and TGF-β1 is measured by MST, resulting in a binding constant whereas the proteolytic assay measures enzyme kinetics over a longer period of time. A stable interaction between protease and substrate is not indispensible for proteolytic cleavage, as described, for example, in rhomboid proteases (Dickey et al., 2013). Although no physiological affinity of these proteases for their substrates were displayed, an approximate 10,000-fold difference in proteolytic efficiency with

substrate mutants and diverse rhomboid proteases were reflected in kcat values alone.

5.3. Effect of HTRA1 variants on TGF-β signaling

As the AMD-associated HTRA1 isoform exhibited decreased affinity for TGF-β1, the next step was to investigate whether this also affects TGF-β-mediated signaling pathways. Reporter assay using MLEC-PAI/Luc is a widely used bio-assay for quantification of TGF-β signaling (Abe et al., 1994; Shibuya et al., 2006; Zhou et al., 2012). It was observed that the differential effect of HTRA1 isoforms on proteolysis of TGF-β1 subsequently affected its regulation of TGF-β signaling, adressed in reporter assays assessing the *PAI-1* promoter, a prominent target of the TGF-β cascade. Hara et al. (2009) reported similar consequences due to CARASIL-associated *HTRA1* variants. Specifically, two nonsense and one missense mutation in *HTRA1* resulted in protein products that failed to repress signaling by the TGF-β family (Hara et al., 2009). As increased TGF-β levels were observed in cerebral arteries of CARASIL patients, the authors concluded that HTRA1 contributes to the pathogenic processes of CARASIL *via* its control of TGF-β signaling. In this context, it is interesting to note that increased TGF-β levels are also observed in AMD patients (Guymer et al., 2011; Bai et al., 2014) and aberrant TGF-β signaling was connected to AMD-related phenotypes in mice (Lyzogubov et al., 2011; Promsote et al., 2014) and RPE cells (Yu et al., 2009a; Yu et al., 2009b; Vidro-Kotchan et al., 2011; Promsote et al., 2014). This and our findings could imply a role for HTRA1 in AMD pathogenesis via its regulation of the TGF-β pathway.

Our results also demonstrated control of HTRA1 over TGF-β regulation in cultured microglial cells. Microglia are the major resident inflammatory cells of the central nervous system and obtain key functions of immune surveillance and tissue repair (Kreutzberg, 1996; Tambuyzer et al., 2009; Hughes, 2012). Thus, this cell type is deeply involved in the pathogenic processes of various neurodegenerative diseases like Parkinson’s disease (Schapansky et al., 2015), Alzheimer’s disease (Bamberger and Landreth, 2002; D'Andrea et al., 2004; Streit et al., 2008; Latta et al., 2015; Lue et al., 2015), Amyotrophic lateral sclerosis (ALS) (Boillee et al., 2006; Henkel et al., 2009; Brites and Vaz, 2014), inherited retinopathies (Langmann, 2007; Karlstetter et

al., 2010) or AMD (Ma et al., 2009; Damani et al., 2011; Ma et al., 2013; Wong, 2013; Karlstetter and Langmann, 2014).

Aging is associated with increased numbers of retinal microglia in mice, and along with tissue stress or injury, aging causes retinal microglia to undergo phenotypical changes whereby they become larger and less dendritic, which are typical morphological signs of activation (Xu et al., 2009). While microglia are generally believed to return to their ramified phenotype and leave the subretinal space once the injury has subsided, the response of aging microglia to injury is slower and less reversible (Langmann, 2007). Moreover, during an insult or injury, microglia migrate from the inner retina to the subretinal space, which is normally devoid of microglia. The importance of subretinal accumulation of activated microglia in AMD is not clear, but could be both a symptom of inflammatory damage and a beneficial response to injury, since infiltration of microglia/macrophages to sites of retinal injury may promote neovascularization, while impairment of this accumulation in the subretinal space exacerbates retinal degeneration (Sakurai et al., 2003; Ma et al., 2009; Ambati et al., 2013). Another study reported the role of microglia in the local control of complement activation in the retina and presented the age-related accumulation of ocular lipofuscin in subretinal microglia as a cellular mechanism capable of driving outer retinal immune dysregulation in AMD pathogenesis (Ma et al., 2013). Microglial cells express VEGF receptors and eyes treated with anti-VEGF showed a significantly decreased number of activated microglia in the retina and the choroid. This suggests that the beneficial effects of anti-VEGF therapy in wet AMD may exceed its vascular effects (Couturier et al., 2014).

Activation and differentiation of microglia is strongly regulated by TGF-β signaling (Rozovsky et al., 1998; Huang et al., 2010; Cekanaviciute et al., 2014; Norden et al., 2014). TGF-β is a pleiotropic cytokine that has inflammatory and anti-inflammatory activities depending on the cellular environment of the innate immune cells [reviewed in (Letterio and Roberts, 1998; Wan and Flavell, 2007)]. The maintenance of the normal retinal immune regulation seems to actively involve TGF-β from the RPE. TGF-β contributes to the immune privilege by predisposing microglia to the preferential production of IL10, which in turn downregulates antigen-presenting

molecules including MHC-II, CD80 and CD86 (D'Orazio and Niederkorn, 1998). TGF-β also directs TNF/IFN-γ-stimulated microglia cells to an anti-inflammatory phenotype by broadly blocking inflammatory gene expression (Paglinawan et al., 2003). Therefore, our next aim was to compare the effect of *HTRA1* variants on regulation of TGF-β signaling in BV-2 microglial cells. The results showed that phosphorylation of SMAD2 and *Pai-1* expression, both markers for activated TGF-β signaling (Cao et al., 1995; Kutz et al., 2001; Dong et al., 2002; Javelaud and Mauviel, 2004a, b, 2005), were significantly lower in microglial (BV-2) cells treated with HTRA1. Thus, our data further provide evidence for a role of HTRA1 in the differentiation and activation of microglia, and therefore likely in the pathogenesis of neurodegenerative diseases. Notably, the inhibitory effect of HTRA1:TT on microglial TGF-β signaling was weaker compared to the reference HTRA1 isoform, HTRA1:CG. In a mouse model of another adult-onset neurodegenerative disease, ALS, TGF-β1 was found to inhibit the neuroprotective response by microglia and T cells. A TGF-β signaling inhibitor slowed the disease progression and extended survival of the mice (Endo et al., 2015). In a mouse model of Alzheimer's disease, blockade of TGF-β–SMAD2/3 signaling in innate immune cells is shown to reduce senile plaque formation in the brain parenchyma (Town et al., 2008). So, it can be speculated that the altered regulation of TGF-β signaling in AMD might enhance the pathogenesis of AMD.

5.4. Effect of HTRA1 on classical and alternative microglial activation

To give first insights into a possible involvement of HTRA1 in microglial activation, the effect of HTRA1 on classical (M1) and alternative (M2) activation of microglial cells was included in this study. Microglia can be activated by the cytokines interferon-γ (IFN-γ), interleukin-17 (IL17) or LPS into a proinflammatory phenotype (M1), whereas IL4 or IL13 induce a state of anti-inflammatory phenotype (M2), which is associated with neuroprotective functions that promote repair (Butovsky et al., 2006b; Ponomarev et al., 2007; Kawanokuchi et al., 2008). IL4 and IL13 suppress the production of pro-inflammatory cytokines such as IL8, IL6 and tumor necrosis factor-α (TNF-α), and reduce nitrite release, which collectively protect against LPS/IFN-γ-induced M1 microglial activation *in vitro* and *in vivo* (Ledeboer et al., 2000; Butovsky

et al., 2005; Park et al., 2005; Zhao et al., 2006). Counteracting pro-inflammatory cytokines is accompanied by the induction of typical M2 markers, such as Arginase 1 (*Arg1*), Chitinase-3-Like-3 (*Chi3l3* or *Ym1*), Mannose receptor (*CD206*) and Found in inflammatory zone 1 (*FIZZ1*) (Gordon, 2003; Ponomarev et al., 2007). Anti-inflammatory factors are also released by M2 microglia when apoptotic cells or myelin debris are removed (Liu et al., 2006). Neurotrophic factors, such as insulin-like growth factor 1 (IGF-I) are also released by M2 microglia to assist inflammation resolution and promote neuron survival (Suh et al., 2013). It is postulated by many studies that acquired deactivation by anti-inflammatory cytokines such as IL10 and TGF-β is another state of M2 activation to alleviate acute inflammation and is induced primarily by uptake of apoptotic cells or exposure to insult or injury (Qin et al., 2006; Colton, 2009; Colton and Wilcock, 2010). Notably, the neuroprotective signals of alternative activation and acquired deactivation orchestrate each other in a coordinated way against the proinflammation responses. For example, TGF-β can enhance IL4-induced M2 microglia by increasing the expression of *Arg1* and *Ym1.* Exogenous TGF-β1 enhances IL4-induced *Ym1* and *Arg1* expression either by a direct effect on *Ym1/Arg1* promoter activity or indirectly by upregulating the IL4Rα, receptor of IL4, through activation of the MAP kinase pathway. Furthermore, treatment with IL4 shows increase in the expression and secretion of endogenous TGF-β2. Autocrine TGF-β2 in turn might be able to enhance IL4-induced *Arg1* expression similar to exogenous TGF-β1 (Zhou et al., 2012).

No effect of HTRA1 on 50 ng/ml LPS-induced M1 microglial cells was detected in our study. However, the possibility of any effect of HTRA1 on M1 activation cannot be ruled out. 50 ng/ml LPS is a very high stimulus for classical activation, giving almost maximal activation. Weak effects by HTRA1 could simply be superimposed by the strong stimulus. Therefore, it is needed to be confirmed whether HTRA1 has an effect on M1 markers induced by a lower dose of LPS. Furthermore, it has been proposed that LPS interferes with key components in the TGF-β1 signaling pathway in primary microglia. The study showed that the ability of TGF-β1 to exert anti-inflammatory effects is significantly reduced by LPS leading to prolonged survival of M1 microglia, although the exact mechanism remains to be clarified (Mitchell et al., 2014). As HTRA1 has been shown to have an interaction with TGF-β1 and plays a role in TGF-

β1 signaling, to investigate an effect of HTRA1 in regulation of TGF-β1 signaling in LPS-stimulated microglia would be interesting.

Next, the effect of HTRA1 on M2 microglial activation was investigated. HTRA1 has been shown to downregulate induced alternative activation (M2) markers of BV-2 cells, *Arg1* and *Ym1* induced by IL4 alone and IL4 in combination with TGF-β1. The downregulation of M2 microglial activation induced by a combination of IL4 and TGF-β1 can be explained by the capacity of HTRA1 to cleave TGF-β1 (as shown earlier). Interestingly, HTRA1 also downregulates expression of *Arg1* and *Ym1* induced by IL4 alone. As mentioned before Zhou et al. (2012) demonstrated that IL4-induced *Arg1* is also dependent on autocrine TGF-β2 signaling. Our results could therefore be explained by HTRA1 cleaving the endogenously produced and secreted TGF-β or TGF-β receptors type II and III, as suggested by Graham et al. (2013).

Even though this study is a preliminary study, it is first of its kind to show a novel role of HTRA1 in regulation of M2 microglial activation. Nevertheless, further read-outs like Arginase assay or studies on microglial morphology are needed to confirm these first results. It also requires more precise understanding of the exact mechanism of action of HTRA1 in downregulating IL4-induced alternative activation. It is to be noted that here only non-AMD-associated HTRA1 (HTRA1:CG) isoform was used for treating the BV-2 microglial cells. To connect this study with reference to AMD pathogenesis, the foremost requirement would be to include AMD-associated HTRA1 isoform (HTRA1:TT) to compare the effects of both HTRA1 isoforms on the activation markers. Till date, two independently studied HTRA1 transgenic mice models showed AMD-like phenotypes (Jones et al., 2011; Vierkotten et al., 2011). More detailed studies of the microglia of the HTRA1 transgenic mice may unravel a novel role of HTRA1 in AMD pathogenesis from an immunological point of view.

6. CONCLUSION

Taken together, our data show that HTRA1 is an important regulator of TGF-β signaling by direct interaction and cleavage of TGF-β. AMD-associated polymorphisms in HTRA1 [rs1049331 (c.102C>T) and rs2293870 (c.108G>T)] result in delayed protein secretion, reduced TGF-β1 affinity, and decreased capacity to control TGF-β signaling and autocrine TGF-β regulation in microglia. One might be tempted to speculate a functional contribution of AMD-associated polymorphisms in HTRA1 to AMD pathogenesis, *via* their effect on the affinity of HTRA1 for TGF-β. Nevertheless, other so-far-unknown sites of interaction at which HTRA1 antagonizes the TGF-β pathway (or might influence cellular processes involved in AMD pathogenesis) cannot be excluded. Moreover, it has also been shown that gene expression of *HTRA1* is highly heterogeneous among different individuals, independent of their *HTRA1* genotype (Friedrich et al., 2011), with expression levels of HTRA1 varying up to 20-fold. In principle, this questions an involvement of reduced HTRA1 activity on AMD development. In addition, due to high LD within the chromosomal *HTRA1* gene locus, a number of additional polymorphisms reveal an equally strong association with AMD extending to and encompassing variants at the neighboring *ARMS2* gene. The final decision about which gene, *HTRA1* or *ARMS2*, is causally involved in AMD pathogenesis requires further scrutiny and specifically needs the understanding of functional aspects of the as-of-yet unknown ARMS2 protein.

LIST OF FIGURES

LIST OF FIGURES

LIST OF TABLES

ABBREVIATIONS

Short Form	Long Form
µ	Micro
µl	Microliter
µm	Micrometer
µM	Micromolar
AMD	Age-related Macular Degeneration
Amp^r	Ampicillin resistant
APS	Ammonium Per Sulphate
ATP	Adenosine Triphosphate
BrM	Bruch's Membrane
cDNA	Complementary DNA
CFH	Complement Factor H
CNV	Choroidal Neovascularization
DMEM	Dulbecco's Modified Eagle Medium
DMSO	Dimethyl sulfoxide
DNA	Deoxyribonucleic Acid
dNTP	Deoxy nucleotide Triphosphate
E.coli	*Escherichia coli*
ECL	Enhanced Chemiluminescence
ECM	Extracellular Matrix
EDTA	Ethylendiamintetraacetate
ER	Endoplasmic Reticulum
Et al.	Et aliter (and others)
FBS	Fetal Bovine Serum
GA	Geographic Atrophy
h	Hour/s

ABBREVIATIONS

H_2O	Water
H_2O_2	Hydrogen peroxide
IB	Immunoblot
Kb	Kilobasepair
L	Liter
KDa	Kilo Dalton
LB	Liquid broth
LD	Linkage Disequilibrium
LPS	Lipopolysaccharide
Min	Minute/s
ml	Milliliter
MLEC	Mink Lung Endothelial Cells
MM	Master mix
mM	Millimolar
nM	Nano molar
OD	Optical Density
ON	Overnight
PBS	Phosphate buffered saline
PCR	Polymerase Chain Reaction
Pen/Strep	Penicillin/Streptomycin
PVDF	Polyvinylidenfluoride
qRT-PCR	Quantitative Real-Time PCR
RNA	Ribonucleic Acid
RPE	Retinal Pigment Epithelium
RPM	Rotations Per Minute
RPMI	Roswell Park Memorial Institute
RT	Room temperature
S	Second/s
SDS-PAGE	Sodium Dodecyl Sulphate-Polyacrylamide Gel Electrophoresis

ABBREVIATIONS

SNP	Single Nucleotide Polymorphism
TBE	Tris Borate EDTA
TC	Tetra-cysteine
TEMED	Tetramethylethylendiamine
TE	Tris-EDTA
V	Volt

REFERENCES

Abe, M., Harpel, J.G., Metz, C.N., Nunes, I., Loskutoff, D.J., and Rifkin, D.B. (1994). An assay for transforming growth factor-beta using cells transfected with a plasminogen activator inhibitor-1 promoter-luciferase construct. Anal Biochem *216*, 276-284.

Adamis, A.P., and Shima, D.T. (2005). The role of vascular endothelial growth factor in ocular health and disease. Retina *25*, 111-118.

Adams, S.R., Campbell, R.E., Gross, L.A., Martin, B.R., Walkup, G.K., Yao, Y., Llopis, J., and Tsien, R.Y. (2002). New biarsenical ligands and tetracysteine motifs for protein labeling in vitro and in vivo: synthesis and biological applications. J Am Chem Soc *124*, 6063-6076.

Adams, S.R., and Tsien, R.Y. (2008). Preparation of the membrane-permeant biarsenicals FlAsH-EDT2 and ReAsH-EDT2 for fluorescent labeling of tetracysteine-tagged proteins. Nat Protoc *3*, 1527-1534.

Age-Related Eye Disease Study 2 Research, G. (2013). Lutein + zeaxanthin and omega-3 fatty acids for age-related macular degeneration: the Age-Related Eye Disease Study 2 (AREDS2) randomized clinical trial. JAMA *309*, 2005-2015.

Age-Related Eye Disease Study Research, G. (2000). Risk factors associated with age-related macular degeneration. A case-control study in the age-related eye disease study: Age-Related Eye Disease Study Report Number 3. Ophthalmology *107*, 2224-2232.

Age-Related Eye Disease Study Research, G. (2001). A randomized, placebo-controlled, clinical trial of high-dose supplementation with vitamins C and E, beta carotene, and zinc for age-related macular degeneration and vision loss: AREDS report no. 8. Arch Ophthalmol *119*, 1417-1436.

Ajayi, F., Kongoasa, N., Gaffey, T., Asmann, Y.W., Watson, W.J., Baldi, A., Lala, P., Shridhar, V., Brost, B., and Chien, J. (2008). Elevated expression of serine protease HtrA1 in preeclampsia and its role in trophoblast cell migration and invasion. American journal of obstetrics and gynecology *199*, 557 e551-510.

Alexander, C.G., Jurgens, M.C., Shepherd, D.A., Freund, S.M., Ashcroft, A.E., and Ferguson, N. (2013). Thermodynamic origins of protein folding, allostery, and capsid formation in the human hepatitis B virus core protein. Proc Natl Acad Sci U S A *110*, E2782-2791.

Alliot, F., Godin, I., and Pessac, B. (1999). Microglia derive from progenitors, originating from the yolk sac, and which proliferate in the brain. Brain Res Dev Brain Res *117*, 145-152.

Ambati, J., Atkinson, J.P., and Gelfand, B.D. (2013). Immunology of age-related macular degeneration. Nat Rev Immunol *13*, 438-451.

An, E., Sen, S., Park, S.K., Gordish-Dressman, H., and Hathout, Y. (2010). Identification of novel substrates for the serine protease HTRA1 in the human RPE secretome. Invest Ophthalmol Vis Sci *51*, 3379-3386.

Anderson, D.H., Radeke, M.J., Gallo, N.B., Chapin, E.A., Johnson, P.T., Curletti, C.R., Hancox, L.S., Hu, J., Ebright, J.N., Malek, G.*, et al.* (2010). The pivotal role of the complement system in aging and age-related macular degeneration: hypothesis re-visited. Prog Retin Eye Res *29*, 95-112.

Arbel, N., Ben-Hail, D., and Shoshan-Barmatz, V. (2012). Mediation of the antiapoptotic activity of Bcl-xL protein upon interaction with VDAC1 protein. J Biol Chem *287*, 23152-23161.

Arnhold, I.J., Osorio, M.G., Oliveira, S.B., Estefan, V., Kamijo, T., Krishnamani, M.R., Cogan, J.D., Phillips, J.A., 3rd, and Mendonca, B.B. (1998). Clinical and molecular characterization of Brazilian patients with growth hormone gene deletions. Braz J Med Biol Res *31*, 491-497.

Aslanidis, A., Karlstetter, M., Scholz, R., Fauser, S., Neumann, H., Fried, C., Pietsch, M., and Langmann, T. (2015). Activated microglia/macrophage whey acidic protein (AMWAP) inhibits NFkappaB signaling and induces a neuroprotective phenotype in microglia. J Neuroinflammation *12*, 77.

Baaske, P., Wienken, C.J., Reineck, P., Duhr, S., and Braun, D. (2010). Optical thermophoresis for quantifying the buffer dependence of aptamer binding. Angew Chem Int Ed Engl *49*, 2238-2241.

Bagasra, O., Michaels, F.H., Zheng, Y.M., Bobroski, L.E., Spitsin, S.V., Fu, Z.F., Tawadros, R., and Koprowski, H. (1995). Activation of the inducible form of nitric oxide synthase in the brains of patients with multiple sclerosis. Proc Natl Acad Sci U S A *92*, 12041-12045.

Bai, Y., Liang, S., Yu, W., Zhao, M., Huang, L., Zhao, M., and Li, X. (2014). Semaphorin 3A blocks the formation of pathologic choroidal neovascularization induced by transforming growth factor beta. Molecular vision *20*, 1258-1270.

Baird, P.N., Robman, L.D., Richardson, A.J., Dimitrov, P.N., Tikellis, G., McCarty, C.A., and Guymer, R.H. (2008). Gene-environment interaction in progression of AMD: the CFH gene, smoking and exposure to chronic infection. Hum Mol Genet *17*, 1299-1305.

Baldi, A., De Luca, A., Morini, M., Battista, T., Felsani, A., Baldi, F., Catricala, C., Amantea, A., Noonan, D.M., Albini, A.*, et al.* (2002). The HtrA1 serine protease is down-regulated during human melanoma progression and represses growth of metastatic melanoma cells. Oncogene *21*, 6684-6688.

Bamberger, M.E., and Landreth, G.E. (2002). Inflammation, apoptosis, and Alzheimer's disease. The Neuroscientist : a review journal bringing neurobiology, neurology and psychiatry *8*, 276-283.

Barouch, F.C., and Miller, J.W. (2004). Anti-vascular endothelial growth factor strategies for the treatment of choroidal neovascularization from age-related macular degeneration. Int Ophthalmol Clin *44*, 23-32.

Bartoszewski, R.A., Jablonsky, M., Bartoszewska, S., Stevenson, L., Dai, Q., Kappes, J., Collawn, J.F., and Bebok, Z. (2010). A synonymous single nucleotide polymorphism in DeltaF508 CFTR alters the secondary structure of the mRNA and the expression of the mutant protein. J Biol Chem *285*, 28741-28748.

Berman, K., and Brodaty, H. (2006). Psychosocial effects of age-related macular degeneration. Int Psychogeriatr *18*, 415-428.

Bernstein, M.H., and Hollenberg, M.J. (1965). Fine structure of the choriocappillaris and retinal capillaries. Invest Ophthalmol *4*, 1016-1025.

Block, M.L., Zecca, L., and Hong, J.S. (2007). Microglia-mediated neurotoxicity: uncovering the molecular mechanisms. Nat Rev Neurosci *8*, 57-69.

Boillee, S., Yamanaka, K., Lobsiger, C.S., Copeland, N.G., Jenkins, N.A., Kassiotis, G., Kollias, G., and Cleveland, D.W. (2006). Onset and progression in inherited ALS determined by motor neurons and microglia. Science *312*, 1389-1392.

Booij, J.C., Baas, D.C., Beisekeeva, J., Gorgels, T.G., and Bergen, A.A. (2010). The dynamic nature of Bruch's membrane. Prog Retin Eye Res *29*, 1-18.

Bowden, M.A., Di Nezza-Cossens, L.A., Jobling, T., Salamonsen, L.A., and Nie, G. (2006). Serine proteases HTRA1 and HTRA3 are down-regulated with increasing grades of human endometrial cancer. Gynecologic oncology *103*, 253-260.

Brandl, C., Grassmann, F., Riolfi, J., and Weber, B.H. (2015). Tapping Stem Cells to Target AMD: Challenges and Prospects. J Clin Med *4*, 282-303.

Brest, P., Lapaquette, P., Souidi, M., Lebrigand, K., Cesaro, A., Vouret-Craviari, V., Mari, B., Barbry, P., Mosnier, J.F., Hebuterne, X.*, et al.* (2011). A synonymous variant in IRGM alters a binding site for miR-196 and causes deregulation of IRGM-dependent xenophagy in Crohn's disease. Nature genetics *43*, 242-245.

Brites, D., and Vaz, A.R. (2014). Microglia centered pathogenesis in ALS: insights in cell interconnectivity. Front Cell Neurosci *8*, 117.

Buschini, E., Fea, A.M., Lavia, C.A., Nassisi, M., Pignata, G., Zola, M., and Grignolo, F.M. (2015). Recent developments in the management of dry age-related macular degeneration. Clin Ophthalmol *9*, 563-574.

Butovsky, O., Jedrychowski, M.P., Moore, C.S., Cialic, R., Lanser, A.J., Gabriely, G., Koeglsperger, T., Dake, B., Wu, P.M., Doykan, C.E.*, et al.* (2014). Identification of a unique TGF-beta-dependent molecular and functional signature in microglia. Nature neuroscience *17*, 131-143.

Butovsky, O., Koronyo-Hamaoui, M., Kunis, G., Ophir, E., Landa, G., Cohen, H., and Schwartz, M. (2006a). Glatiramer acetate fights against Alzheimer's disease by inducing dendritic-like microglia expressing insulin-like growth factor 1. Proc Natl Acad Sci U S A *103*, 11784-11789.

Butovsky, O., Talpalar, A.E., Ben-Yaakov, K., and Schwartz, M. (2005). Activation of microglia by aggregated beta-amyloid or lipopolysaccharide impairs MHC-II expression and renders them cytotoxic whereas IFN-gamma and IL-4 render them protective. Mol Cell Neurosci *29*, 381-393.

Butovsky, O., Ziv, Y., Schwartz, A., Landa, G., Talpalar, A.E., Pluchino, S., Martino, G., and Schwartz, M. (2006b). Microglia activated by IL-4 or IFN-gamma differentially induce neurogenesis and oligodendrogenesis from adult stem/progenitor cells. Mol Cell Neurosci *31*, 149-160.

Cameron, D.J., Yang, Z., Gibbs, D., Chen, H., Kaminoh, Y., Jorgensen, A., Zeng, J., Luo, L., Brinton, E., Brinton, G.*, et al.* (2007). HTRA1 variant confers similar risks to geographic atrophy and neovascular age-related macular degeneration. Cell Cycle *6*, 1122-1125.

Campioni, M., Severino, A., Manente, L., Tuduce, I.L., Toldo, S., Caraglia, M., Crispi, S., Ehrmann, M., He, X., Maguire, J.*, et al.* (2010). The serine protease HtrA1 specifically interacts and degrades the tuberous sclerosis complex 2 protein. Mol Cancer Res *8*, 1248-1260.

Cannarozzi, G., Schraudolph, N.N., Faty, M., von Rohr, P., Friberg, M.T., Roth, A.C., Gonnet, P., Gonnet, G., and Barral, Y. (2010). A role for codon order in translation dynamics. Cell *141*, 355-367.

Cao, H.J., Hogg, M.G., Martino, L.J., and Smith, T.J. (1995). Transforming growth factor-beta induces plasminogen activator inhibitor type-1 in cultured human orbital fibroblasts. Investigative ophthalmology & visual science *36*, 1411-1419.

Carr, A.J., Smart, M.J., Ramsden, C.M., Powner, M.B., da Cruz, L., and Coffey, P.J. (2013). Development of human embryonic stem cell therapies for age-related macular degeneration. Trends Neurosci *36*, 385-395.

Cekanaviciute, E., Fathali, N., Doyle, K.P., Williams, A.M., Han, J., and Buckwalter, M.S. (2014). Astrocytic transforming growth factor-beta signaling reduces subacute neuroinflammation after stroke in mice. Glia *62*, 1227-1240.

Chamary, J.V., and Hurst, L.D. (2005). Evidence for selection on synonymous mutations affecting stability of mRNA secondary structure in mammals. Genome biology *6*, R75.

Chamary, J.V., and Hurst, L.D. (2009). The price of silent mutations. Scientific American *300*, 46-53.

Chamary, J.V., Parmley, J.L., and Hurst, L.D. (2006). Hearing silence: non-neutral evolution at synonymous sites in mammals. Nature reviews Genetics *7*, 98-108.

Chamberland, A., Wang, E., Jones, A.R., Collins-Racie, L.A., LaVallie, E.R., Huang, Y., Liu, L., Morris, E.A., Flannery, C.R., and Yang, Z. (2009). Identification of a novel HtrA1-susceptible cleavage site in human aggrecan: evidence for the involvement of HtrA1 in aggrecan proteolysis in vivo. The Journal of biological chemistry *284*, 27352-27359.

Chan, C.C., Shen, D., Zhou, M., Ross, R.J., Ding, X., Zhang, K., Green, W.R., and Tuo, J. (2007). Human HtrA1 in the archived eyes with age-related macular degeneration. Trans Am Ophthalmol Soc *105*, 92-97; discussion 97-98.

Chang, Y.C., Chang, W.C., Hung, K.H., Yang, D.M., Cheng, Y.H., Liao, Y.W., Woung, L.C., Tsai, C.Y., Hsu, C.C., Lin, T.C.*, et al.* (2014). The generation of induced pluripotent stem cells for macular degeneration as a drug screening platform: identification of curcumin as a protective agent for retinal pigment epithelial cells against oxidative stress. Front Aging Neurosci *6*, 191.

Chen, Y., Wiesmann, C., Fuh, G., Li, B., Christinger, H.W., McKay, P., de Vos, A.M., and Lowman, H.B. (1999). Selection and analysis of an optimized anti-VEGF antibody: crystal structure of an affinity-matured Fab in complex with antigen. J Mol Biol *293*, 865-881.

Chien, J., He, X., and Shridhar, V. (2009). Identification of tubulins as substrates of serine protease HtrA1 by mixture-based oriented peptide library screening. J Cell Biochem *107*, 253-263.

Chien, J., Staub, J., Hu, S.I., Erickson-Johnson, M.R., Couch, F.J., Smith, D.I., Crowl, R.M., Kaufmann, S.H., and Shridhar, V. (2004). A candidate tumor suppressor HtrA1 is downregulated in ovarian cancer. Oncogene *23*, 1636-1644.

Cho, E., Hankinson, S.E., Willett, W.C., Stampfer, M.J., Spiegelman, D., Speizer, F.E., Rimm, E.B., and Seddon, J.M. (2000). Prospective study of alcohol consumption and the risk of age-related macular degeneration. Arch Ophthalmol *118*, 681-688.

Cho, E., Hung, S., Willett, W.C., Spiegelman, D., Rimm, E.B., Seddon, J.M., Colditz, G.A., and Hankinson, S.E. (2001). Prospective study of dietary fat and the risk of age-related macular degeneration. Am J Clin Nutr *73*, 209-218.

Chong, E.W., Kreis, A.J., Wong, T.Y., Simpson, J.A., and Guymer, R.H. (2008). Alcohol consumption and the risk of age-related macular degeneration: a systematic review and meta-analysis. Am J Ophthalmol *145*, 707-715.

Chong, N.H., Keonin, J., Luthert, P.J., Frennesson, C.I., Weingeist, D.M., Wolf, R.L., Mullins, R.F., and Hageman, G.S. (2005). Decreased thickness and integrity of the macular elastic layer of Bruch's membrane correspond to the distribution of lesions associated with age-related macular degeneration. Am J Pathol *166*, 241-251.

Chowers, I., Meir, T., Lederman, M., Goldenberg-Cohen, N., Cohen, Y., Banin, E., Averbukh, E., Hemo, I., Pollack, A., Axer-Siegel, R.*, et al.* (2008). Sequence variants in HTRA1 and LOC387715/ARMS2 and phenotype and response to photodynamic

therapy in neovascular age-related macular degeneration in populations from Israel. Mol Vis *14*, 2263-2271.

Christen, W.G., Glynn, R.J., Chew, E.Y., Albert, C.M., and Manson, J.E. (2009). Folic acid, pyridoxine, and cyanocobalamin combination treatment and age-related macular degeneration in women: the Women's Antioxidant and Folic Acid Cardiovascular Study. Arch Intern Med *169*, 335-341.

Clausen, T., Southan, C., and Ehrmann, M. (2002). The HtrA family of proteases: implications for protein composition and cell fate. Mol Cell *10*, 443-455.

Clifford, R.L., Deacon, K., and Knox, A.J. (2008). Novel regulation of vascular endothelial growth factor-A (VEGF-A) by transforming growth factor (beta)1: requirement for Smads, (beta)-CATENIN, AND GSK3(beta). J Biol Chem *283*, 35337-35353.

Colton, C., and Wilcock, D.M. (2010). Assessing activation states in microglia. CNS Neurol Disord Drug Targets *9*, 174-191.

Colton, C.A. (2009). Heterogeneity of microglial activation in the innate immune response in the brain. J Neuroimmune Pharmacol *4*, 399-418.

Combadiere, C., Feumi, C., Raoul, W., Keller, N., Rodero, M., Pezard, A., Lavalette, S., Houssier, M., Jonet, L., Picard, E.*, et al.* (2007). CX3CR1-dependent subretinal microglia cell accumulation is associated with cardinal features of age-related macular degeneration. J Clin Invest *117*, 2920-2928.

Conley, Y.P., Jakobsdottir, J., Mah, T., Weeks, D.E., Klein, R., Kuller, L., Ferrell, R.E., and Gorin, M.B. (2006). CFH, ELOVL4, PLEKHA1 and LOC387715 genes and susceptibility to age-related maculopathy: AREDS and CHS cohorts and meta-analyses. Hum Mol Genet *15*, 3206-3218.

Couturier, A., Bousquet, E., Zhao, M., Naud, M.C., Klein, C., Jonet, L., Tadayoni, R., de Kozak, Y., and Behar-Cohen, F. (2014). Anti-vascular endothelial growth factor acts on retinal microglia/macrophage activation in a rat model of ocular inflammation. Mol Vis *20*, 908-920.

Crabb, J.W., Miyagi, M., Gu, X., Shadrach, K., West, K.A., Sakaguchi, H., Kamei, M., Hasan, A., Yan, L., Rayborn, M.E.*, et al.* (2002). Drusen proteome analysis: an approach to the etiology of age-related macular degeneration. Proc Natl Acad Sci U S A *99*, 14682-14687.

Cruickshanks, K.J., Klein, R., Klein, B.E., and Nondahl, D.M. (2001). Sunlight and the 5-year incidence of early age-related maculopathy: the beaver dam eye study. Arch Ophthalmol *119*, 246-250.

Curcio, C.A., Messinger, J.D., Sloan, K.R., McGwin, G., Medeiros, N.E., and Spaide, R.F. (2013). Subretinal drusenoid deposits in non-neovascular age-related macular degeneration: morphology, prevalence, topography, and biogenesis model. Retina *33*, 265-276.

Curcio, C.A., Millican, C.L., Bailey, T., and Kruth, H.S. (2001). Accumulation of cholesterol with age in human Bruch's membrane. Invest Ophthalmol Vis Sci *42*, 265-274.

Curcio, C.A., Owsley, C., and Jackson, G.R. (2000). Spare the rods, save the cones in aging and age-related maculopathy. Invest Ophthalmol Vis Sci *41*, 2015-2018.

Curcio, C.A., Sloan, K.R., Kalina, R.E., and Hendrickson, A.E. (1990). Human photoreceptor topography. J Comp Neurol *292*, 497-523.

D'Andrea, M.R., Cole, G.M., and Ard, M.D. (2004). The microglial phagocytic role with specific plaque types in the Alzheimer disease brain. Neurobiology of aging *25*, 675-683.

D'Orazio, T.J., and Niederkorn, J.Y. (1998). A novel role for TGF-beta and IL-10 in the induction of immune privilege. J Immunol *160*, 2089-2098.

Damani, M.R., Zhao, L., Fontainhas, A.M., Amaral, J., Fariss, R.N., and Wong, W.T. (2011). Age-related alterations in the dynamic behavior of microglia. Aging cell *10*, 263-276.

De Luca, A., De Falco, M., De Luca, L., Penta, R., Shridhar, V., Baldi, F., Campioni, M., Paggi, M.G., and Baldi, A. (2004). Pattern of expression of HtrA1 during mouse development. J Histochem Cytochem *52*, 1609-1617.

De Luca, A., De Falco, M., Severino, A., Campioni, M., Santini, D., Baldi, F., Paggi, M.G., and Baldi, A. (2003). Distribution of the serine protease HtrA1 in normal human tissues. The journal of histochemistry and cytochemistry : official journal of the Histochemistry Society *51*, 1279-1284.

Deangelis, M.M., Ji, F., Adams, S., Morrison, M.A., Harring, A.J., Sweeney, M.O., Capone, A., Jr., Miller, J.W., Dryja, T.P., Ott, J.*, et al.* (2008). Alleles in the HtrA serine peptidase 1 gene alter the risk of neovascular age-related macular degeneration. Ophthalmology *115*, 1209-1215 e1207.

Delcourt, C., Carriere, I., Ponton-Sanchez, A., Fourrey, S., Lacroux, A., Papoz, L., and Group, P.S. (2001). Light exposure and the risk of age-related macular degeneration: the Pathologies Oculaires Liees a l'Age (POLA) study. Arch Ophthalmol *119*, 1463-1468.

Delori, F.C., Goger, D.G., and Dorey, C.K. (2001). Age-related accumulation and spatial distribution of lipofuscin in RPE of normal subjects. Invest Ophthalmol Vis Sci *42*, 1855-1866.

Dickey, S.W., Baker, R.P., Cho, S., and Urban, S. (2013). Proteolysis inside the membrane is a rate-governed reaction not driven by substrate affinity. Cell *155*, 1270-1281.

Ding, J.D., Johnson, L.V., Herrmann, R., Farsiu, S., Smith, S.G., Groelle, M., Mace, B.E., Sullivan, P., Jamison, J.A., Kelly, U.*, et al.* (2011). Anti-amyloid therapy protects against retinal pigmented epithelium damage and vision loss in a model of age-related macular degeneration. Proc Natl Acad Sci U S A *108*, E279-287.

Ding, J.D., Lin, J., Mace, B.E., Herrmann, R., Sullivan, P., and Bowes Rickman, C. (2008). Targeting age-related macular degeneration with Alzheimer's disease based immunotherapies: anti-amyloid-beta antibody attenuates pathologies in an age-related macular degeneration mouse model. Vision Res *48*, 339-345.

Dirscherl, K., Karlstetter, M., Ebert, S., Kraus, D., Hlawatsch, J., Walczak, Y., Moehle, C., Fuchshofer, R., and Langmann, T. (2010). Luteolin triggers global changes in the microglial transcriptome leading to a unique anti-inflammatory and neuroprotective phenotype. J Neuroinflammation *7*, 3.

Dong, C., Zhu, S., Wang, T., Yoon, W., and Goldschmidt-Clermont, P.J. (2002). Upregulation of PAI-1 is mediated through TGF-beta/Smad pathway in transplant arteriopathy. The Journal of heart and lung transplantation : the official publication of the International Society for Heart Transplantation *21*, 999-1008.

Duan, J., and Antezana, M.A. (2003). Mammalian mutation pressure, synonymous codon choice, and mRNA degradation. Journal of molecular evolution *57*, 694-701.

Duan, J., Wainwright, M.S., Comeron, J.M., Saitou, N., Sanders, A.R., Gelernter, J., and Gejman, P.V. (2003). Synonymous mutations in the human dopamine receptor D2 (DRD2) affect mRNA stability and synthesis of the receptor. Human molecular genetics *12*, 205-216.

Duhr, S., and Braun, D. (2006). Why molecules move along a temperature gradient. Proceedings of the National Academy of Sciences of the United States of America *103*, 19678-19682.

Eigenbrot, C., Ultsch, M., Lipari, M.T., Moran, P., Lin, S.J., Ganesan, R., Quan, C., Tom, J., Sandoval, W., van Lookeren Campagne, M.*, et al.* (2012). Structural and functional analysis of HtrA1 and its subdomains. Structure *20*, 1040-1050.

Endo, F., Komine, O., Fujimori-Tonou, N., Katsuno, M., Jin, S., Watanabe, S., Sobue, G., Dezawa, M., Wyss-Coray, T., and Yamanaka, K. (2015). Astrocyte-derived TGF-beta1 accelerates disease progression in ALS mice by interfering with the neuroprotective functions of microglia and T cells. Cell Rep *11*, 592-604.

Espinosa-Heidmann, D.G., Suner, I.J., Catanuto, P., Hernandez, E.P., Marin-Castano, M.E., and Cousins, S.W. (2006). Cigarette smoke-related oxidants and the development of sub-RPE deposits in an experimental animal model of dry AMD. Invest Ophthalmol Vis Sci *47*, 729-737.

Fagerness, J.A., Maller, J.B., Neale, B.M., Reynolds, R.C., Daly, M.J., and Seddon, J.M. (2009). Variation near complement factor I is associated with risk of advanced AMD. Eur J Hum Genet *17*, 100-104.

Fariss, R.N., Apte, S.S., Olsen, B.R., Iwata, K., and Milam, A.H. (1997). Tissue inhibitor of metalloproteinases-3 is a component of Bruch's membrane of the eye. Am J Pathol *150*, 323-328.

Feeney-Burns, L., and Ellersieck, M.R. (1985). Age-related changes in the ultrastructure of Bruch's membrane. Am J Ophthalmol *100*, 686-697.

Ferrara, N., Hillan, K.J., Gerber, H.P., and Novotny, W. (2004). Discovery and development of bevacizumab, an anti-VEGF antibody for treating cancer. Nat Rev Drug Discov *3*, 391-400.

Ferris, F.L., 3rd (2004). A new treatment for ocular neovascularization. N Engl J Med *351*, 2863-2865.

Ferris, F.L., 3rd, Fine, S.L., and Hyman, L. (1984). Age-related macular degeneration and blindness due to neovascular maculopathy. Arch Ophthalmol *102*, 1640-1642.

Ferris, F.L., Davis, M.D., Clemons, T.E., Lee, L.Y., Chew, E.Y., Lindblad, A.S., Milton, R.C., Bressler, S.B., Klein, R., and Age-Related Eye Disease Study Research, G. (2005). A simplified severity scale for age-related macular degeneration: AREDS Report No. 18. Arch Ophthalmol *123*, 1570-1574.

Fisher, S.A., Abecasis, G.R., Yashar, B.M., Zareparsi, S., Swaroop, A., Iyengar, S.K., Klein, B.E., Klein, R., Lee, K.E., Majewski, J.*, et al.* (2005). Meta-analysis of genome scans of age-related macular degeneration. Hum Mol Genet *14*, 2257-2264.

Flood, V., Smith, W., Wang, J.J., Manzi, F., Webb, K., and Mitchell, P. (2002). Dietary antioxidant intake and incidence of early age-related maculopathy: the Blue Mountains Eye Study. Ophthalmology *109*, 2272-2278.

Fontana, A., de Laureto, P.P., Spolaore, B., Frare, E., Picotti, P., and Zambonin, M. (2004). Probing protein structure by limited proteolysis. Acta Biochim Pol *51*, 299-321.

Forrester, J.V., and Xu, H. (2012). Good news-bad news: the Yin and Yang of immune privilege in the eye. Front Immunol *3*, 338.

Friedrich, U., Datta, S., Schubert, T., Plossl, K., Schneider, M., Grassmann, F., Fuchshofer, R., Tiefenbach, K.J., Langst, G., and Weber, B.H. (2015). Synonymous variants in HTRA1 implicated in AMD susceptibility impair its capacity to regulate TGF-beta signaling. Hum Mol Genet *24*, 6361-6373.

Friedrich, U., Myers, C.A., Fritsche, L.G., Milenkovich, A., Wolf, A., Corbo, J.C., and Weber, B.H. (2011). Risk- and non-risk-associated variants at the 10q26 AMD locus influence ARMS2 mRNA expression but exclude pathogenic effects due to protein deficiency. Human molecular genetics *20*, 1387-1399.

Fritsche, L.G., Chen, W., Schu, M., Yaspan, B.L., Yu, Y., Thorleifsson, G., Zack, D.J., Arakawa, S., Cipriani, V., Ripke, S.*, et al.* (2013). Seven new loci associated with age-related macular degeneration. Nat Genet *45*, 433-439, 439e431-432.

Fritsche, L.G., Fariss, R.N., Stambolian, D., Abecasis, G.R., Curcio, C.A., and Swaroop, A. (2014). Age-related macular degeneration: genetics and biology coming together. Annu Rev Genomics Hum Genet *15*, 151-171.

Fritsche, L.G., Loenhardt, T., Janssen, A., Fisher, S.A., Rivera, A., Keilhauer, C.N., and Weber, B.H. (2008). Age-related macular degeneration is associated with an unstable ARMS2 (LOC387715) mRNA. Nat Genet *40*, 892-896.

Frydman, J., Nimmesgern, E., Ohtsuka, K., and Hartl, F.U. (1994). Folding of nascent polypeptide chains in a high molecular mass assembly with molecular chaperones. Nature *370*, 111-117.

Fung, K.L., Pan, J., Ohnuma, S., Lund, P.E., Pixley, J.N., Kimchi-Sarfaty, C., Ambudkar, S.V., and Gottesman, M.M. (2014). MDR1 synonymous polymorphisms alter transporter specificity and protein stability in a stable epithelial monolayer. Cancer research *74*, 598-608.

Gehrmann, J., Matsumoto, Y., and Kreutzberg, G.W. (1995). Microglia: intrinsic immuneffector cell of the brain. Brain Res Brain Res Rev *20*, 269-287.

Gold, B., Merriam, J.E., Zernant, J., Hancox, L.S., Taiber, A.J., Gehrs, K., Cramer, K., Neel, J., Bergeron, J., Barile, G.R.*, et al.* (2006). Variation in factor B (BF) and complement component 2 (C2) genes is associated with age-related macular degeneration. Nat Genet *38*, 458-462.

Gopinath, B., Flood, V.M., Kifley, A., Liew, G., and Mitchell, P. (2015). Smoking, antioxidant supplementation and dietary intakes among older adults with age-related macular degeneration over 10 years. PLoS One *10*, e0122548.

Gordon, S. (2003). Alternative activation of macrophages. Nat Rev Immunol *3*, 23-35.

Gragoudas, E.S., Adamis, A.P., Cunningham, E.T., Jr., Feinsod, M., Guyer, D.R., and Group, V.I.S.i.O.N.C.T. (2004). Pegaptanib for neovascular age-related macular degeneration. N Engl J Med *351*, 2805-2816.

Graham, J.R., Chamberland, A., Lin, Q., Li, X.J., Dai, D., Zeng, W., Ryan, M.S., Rivera-Bermudez, M.A., Flannery, C.R., and Yang, Z. (2013). Serine protease HTRA1 antagonizes transforming growth factor-beta signaling by cleaving its receptors and loss of HTRA1 in vivo enhances bone formation. PLoS One *8*, e74094.

Grau, S., Baldi, A., Bussani, R., Tian, X., Stefanescu, R., Przybylski, M., Richards, P., Jones, S.A., Shridhar, V., Clausen, T.*, et al.* (2005). Implications of the serine protease HtrA1 in amyloid precursor protein processing. Proc Natl Acad Sci U S A *102*, 6021-6026.

Grau, S., Richards, P.J., Kerr, B., Hughes, C., Caterson, B., Williams, A.S., Junker, U., Jones, S.A., Clausen, T., and Ehrmann, M. (2006). The role of human HtrA1 in arthritic disease. The Journal of biological chemistry *281*, 6124-6129.

Grisanti, S., Lüke, J., Peters, S., (2013) Anti-VEGF therapy: basics and substances. In: Holz FG, Pauleikhoff D, Spaide RF, Bird AC, eds.*Age-Related Macular Degeneration*. Heidelberg, Germany: Springer: 225–232

Gupta, N., Brown, K.E., and Milam, A.H. (2003). Activated microglia in human retinitis pigmentosa, late-onset retinal degeneration, and age-related macular degeneration. Exp Eye Res *76*, 463-471.

Guymer, R.H., Tao, L.W., Goh, J.K., Liew, D., Ischenko, O., Robman, L.D., Aung, K., Cipriani, T., Cain, M., Richardson, A.J.*, et al.* (2011). Identification of urinary

biomarkers for age-related macular degeneration. Investigative ophthalmology & visual science *52*, 4639-4644.

Hadfield, K.D., Rock, C.F., Inkson, C.A., Dallas, S.L., Sudre, L., Wallis, G.A., Boot-Handford, R.P., and Canfield, A.E. (2008). HtrA1 inhibits mineral deposition by osteoblasts: requirement for the protease and PDZ domains. The Journal of biological chemistry *283*, 5928-5938.

Hageman, G.S., Anderson, D.H., Johnson, L.V., Hancox, L.S., Taiber, A.J., Hardisty, L.I., Hageman, J.L., Stockman, H.A., Borchardt, J.D., Gehrs, K.M.*, et al.* (2005). A common haplotype in the complement regulatory gene factor H (HF1/CFH) predisposes individuals to age-related macular degeneration. Proc Natl Acad Sci U S A *102*, 7227-7232.

Haines, J.L., Hauser, M.A., Schmidt, S., Scott, W.K., Olson, L.M., Gallins, P., Spencer, K.L., Kwan, S.Y., Noureddine, M., Gilbert, J.R.*, et al.* (2005). Complement factor H variant increases the risk of age-related macular degeneration. Science *308*, 419-421.

Hara, K., Shiga, A., Fukutake, T., Nozaki, H., Miyashita, A., Yokoseki, A., Kawata, H., Koyama, A., Arima, K., Takahashi, T.*, et al.* (2009). Association of HTRA1 mutations and familial ischemic cerebral small-vessel disease. The New England journal of medicine *360*, 1729-1739.

Hawkins, B.S., Bird, A., Klein, R., and West, S.K. (1999). Epidemiology of age-related macular degeneration. Mol Vis *5*, 26.

Heiba, I.M., Elston, R.C., Klein, B.E., and Klein, R. (1994). Sibling correlations and segregation analysis of age-related maculopathy: the Beaver Dam Eye Study. Genet Epidemiol *11*, 51-67.

Henkel, J.S., Beers, D.R., Zhao, W., and Appel, S.H. (2009). Microglia in ALS: the good, the bad, and the resting. J Neuroimmune Pharmacol *4*, 389-398.

Holz, F.G., Strauss, E.C., Schmitz-Valckenberg, S., and van Lookeren Campagne, M. (2014). Geographic atrophy: clinical features and potential therapeutic approaches. Ophthalmology *121*, 1079-1091.

Huang, S.G. (2003). Limited proteolysis reveals conformational changes in uncoupling protein-1 from brown adipose tissue mitochondria. Arch Biochem Biophys *420*, 40-45.

Huang, W.C., Yen, F.C., Shie, F.S., Pan, C.M., Shiao, Y.J., Yang, C.N., Huang, F.L., Sung, Y.J., and Tsay, H.J. (2010). TGF-beta1 blockade of microglial chemotaxis toward Abeta aggregates involves SMAD signaling and down-regulation of CCL5. J Neuroinflammation *7*, 28.

Hughes, A.E., Orr, N., Esfandiary, H., Diaz-Torres, M., Goodship, T., and Chakravarthy, U. (2006). A common CFH haplotype, with deletion of CFHR1 and CFHR3, is associated with lower risk of age-related macular degeneration. Nat Genet *38*, 1173-1177.

Hughes, V. (2012). Microglia: The constant gardeners. Nature *485*, 570-572.

Hunt, R.C., Simhadri, V.L., Iandoli, M., Sauna, Z.E., and Kimchi-Sarfaty, C. (2014). Exposing synonymous mutations. Trends in genetics : TIG *30*, 308-321.

Iejima, D., Itabashi, T., Kawamura, Y., Noda, T., Yuasa, S., Fukuda, K., Oka, C., and Iwata, T. (2015). HTRA1 (high temperature requirement A serine peptidase 1) gene is transcriptionally regulated by insertion/deletion nucleotides located at the 3' end of the ARMS2 (age-related maculopathy susceptibility 2) gene in patients with age-related macular degeneration. J Biol Chem *290*, 2784-2797.

Jacobo, S.M., Deangelis, M.M., Kim, I.K., and Kazlauskas, A. (2013). Age-related macular degeneration-associated silent polymorphisms in HtrA1 impair its ability to antagonize insulin-like growth factor 1. Mol Cell Biol *33*, 1976-1990.

Jakobsdottir, J., Conley, Y.P., Weeks, D.E., Mah, T.S., Ferrell, R.E., and Gorin, M.B. (2005). Susceptibility genes for age-related maculopathy on chromosome 10q26. Am J Hum Genet *77*, 389-407.

Javelaud, D., and Mauviel, A. (2004a). Mammalian transforming growth factor-betas: Smad signaling and physio-pathological roles. The international journal of biochemistry & cell biology *36*, 1161-1165.

Javelaud, D., and Mauviel, A. (2004b). [Transforming growth factor-betas: smad signaling and roles in physiopathology]. Pathologie-biologie *52*, 50-54.

Javelaud, D., and Mauviel, A. (2005). Crosstalk mechanisms between the mitogen-activated protein kinase pathways and Smad signaling downstream of TGF-beta: implications for carcinogenesis. Oncogene *24*, 5742-5750.

Johnson, L.V., Leitner, W.P., Rivest, A.J., Staples, M.K., Radeke, M.J., and Anderson, D.H. (2002). The Alzheimer's A beta -peptide is deposited at sites of complement activation in pathologic deposits associated with aging and age-related macular degeneration. Proc Natl Acad Sci U S A *99*, 11830-11835.

Johnson, L.V., Ozaki, S., Staples, M.K., Erickson, P.A., and Anderson, D.H. (2000). A potential role for immune complex pathogenesis in drusen formation. Exp Eye Res *70*, 441-449.

Jones, A., Kumar, S., Zhang, N., Tong, Z., Yang, J.H., Watt, C., Anderson, J., Amrita, Fillerup, H., McCloskey, M.*, et al.* (2011). Increased expression of multifunctional serine protease, HTRA1, in retinal pigment epithelium induces polypoidal choroidal vasculopathy in mice. Proc Natl Acad Sci U S A *108*, 14578-14583.

Kalayoglu, M.V., Galvan, C., Mahdi, O.S., Byrne, G.I., and Mansour, S. (2003). Serological association between Chlamydia pneumoniae infection and age-related macular degeneration. Arch Ophthalmol *121*, 478-482.

Kamei, M., and Hollyfield, J.G. (1999). TIMP-3 in Bruch's membrane: changes during aging and in age-related macular degeneration. Invest Ophthalmol Vis Sci *40*, 2367-2375.

Kanda, A., Chen, W., Othman, M., Branham, K.E., Brooks, M., Khanna, R., He, S., Lyons, R., Abecasis, G.R., and Swaroop, A. (2007). A variant of mitochondrial protein LOC387715/ARMS2, not HTRA1, is strongly associated with age-related macular degeneration. Proc Natl Acad Sci U S A *104*, 16227-16232.

Kanda, A., Stambolian, D., Chen, W., Curcio, C.A., Abecasis, G.R., and Swaroop, A. (2010). Age-related macular degeneration-associated variants at chromosome 10q26 do not significantly alter ARMS2 and HTRA1 transcript levels in the human retina. Mol Vis *16*, 1317-1323.

Karlstetter, M., Ebert, S., and Langmann, T. (2010). Microglia in the healthy and degenerating retina: insights from novel mouse models. Immunobiology *215*, 685-691.

Karlstetter, M., and Langmann, T. (2014). Microglia in the aging retina. Advances in experimental medicine and biology *801*, 207-212.

Karlstetter, M., Nothdurfter, C., Aslanidis, A., Moeller, K., Horn, F., Scholz, R., Neumann, H., Weber, B.H., Rupprecht, R., and Langmann, T. (2014). Translocator protein (18 kDa) (TSPO) is expressed in reactive retinal microglia and modulates microglial inflammation and phagocytosis. J Neuroinflammation *11*, 3.

Karring, H., Poulsen, E.T., Runager, K., Thogersen, I.B., Klintworth, G.K., Hojrup, P., and Enghild, J.J. (2013). Serine protease HtrA1 accumulates in corneal transforming growth factor beta induced protein (TGFBIp) amyloid deposits. Molecular vision *19*, 861-876.

Katta, S., Kaur, I., and Chakrabarti, S. (2009). The molecular genetic basis of age-related macular degeneration: an overview. J Genet *88*, 425-449.

Kawanokuchi, J., Shimizu, K., Nitta, A., Yamada, K., Mizuno, T., Takeuchi, H., and Suzumura, A. (2008). Production and functions of IL-17 in microglia. J Neuroimmunol *194*, 54-61.

Keren-Kaplan, T., Attali, I., Estrin, M., Kuo, L.S., Farkash, E., Jerabek-Willemsen, M., Blutraich, N., Artzi, S., Peri, A., Freed, E.O.*, et al.* (2013). Structure-based in silico identification of ubiquitin-binding domains provides insights into the ALIX-V:ubiquitin complex and retrovirus budding. EMBO J *32*, 538-551.

Kettenmann, H., Hanisch, U.K., Noda, M., and Verkhratsky, A. (2011). Physiology of microglia. Physiol Rev *91*, 461-553.

Khan, J.C., Shahid, H., Thurlby, D.A., Bradley, M., Clayton, D.G., Moore, A.T., Bird, A.C., Yates, J.R., and Genetic Factors in, A.M.D.S. (2006). Age related macular degeneration and sun exposure, iris colour, and skin sensitivity to sunlight. Br J Ophthalmol *90*, 29-32.

Kim, M.S., Song, J., and Park, C. (2009). Determining protein stability in cell lysates by pulse proteolysis and Western blotting. Protein science : a publication of the Protein Society *18*, 1051-1059.

Kimchi-Sarfaty, C., Oh, J.M., Kim, I.W., Sauna, Z.E., Calcagno, A.M., Ambudkar, S.V., and Gottesman, M.M. (2007). A "silent" polymorphism in the MDR1 gene changes substrate specificity. Science *315*, 525-528.

King, R.E., Kent, K.D., and Bomser, J.A. (2005). Resveratrol reduces oxidation and proliferation of human retinal pigment epithelial cells via extracellular signal-regulated kinase inhibition. Chem Biol Interact *151*, 143-149.

Klaver, C.C., Assink, J.J., van Leeuwen, R., Wolfs, R.C., Vingerling, J.R., Stijnen, T., Hofman, A., and de Jong, P.T. (2001). Incidence and progression rates of age-related maculopathy: the Rotterdam Study. Invest Ophthalmol Vis Sci *42*, 2237-2241.

Klaver, C.C., Wolfs, R.C., Assink, J.J., van Duijn, C.M., Hofman, A., and de Jong, P.T. (1998). Genetic risk of age-related maculopathy. Population-based familial aggregation study. Arch Ophthalmol *116*, 1646-1651.

Klein, M.L., Mauldin, W.M., and Stoumbos, V.D. (1994). Heredity and age-related macular degeneration. Observations in monozygotic twins. Arch Ophthalmol *112*, 932-937.

Klein, R., Cruickshanks, K.J., Nash, S.D., Krantz, E.M., Nieto, F.J., Huang, G.H., Pankow, J.S., and Klein, B.E. (2010). The prevalence of age-related macular degeneration and associated risk factors. Arch Ophthalmol *128*, 750-758.

Klein, R., Klein, B.E., and Cruickshanks, K.J. (1999a). The prevalence of age-related maculopathy by geographic region and ethnicity. Prog Retin Eye Res *18*, 371-389.

Klein, R., Klein, B.E., Jensen, S.C., Mares-Perlman, J.A., Cruickshanks, K.J., and Palta, M. (1999b). Age-related maculopathy in a multiracial United States population: the National Health and Nutrition Examination Survey III. Ophthalmology *106*, 1056-1065.

Klein, R., Klein, B.E., Knudtson, M.D., Wong, T.Y., Cotch, M.F., Liu, K., Burke, G., Saad, M.F., and Jacobs, D.R., Jr. (2006). Prevalence of age-related macular degeneration in 4 racial/ethnic groups in the multi-ethnic study of atherosclerosis. Ophthalmology *113*, 373-380.

Klein, R., Li, X., Kuo, J.Z., Klein, B.E., Cotch, M.F., Wong, T.Y., Taylor, K.D., and Rotter, J.I. (2013). Associations of candidate genes to age-related macular degeneration among racial/ethnic groups in the multi-ethnic study of atherosclerosis. Am J Ophthalmol *156*, 1010-1020 e1011.

Klein, R.J., Zeiss, C., Chew, E.Y., Tsai, J.Y., Sackler, R.S., Haynes, C., Henning, A.K., SanGiovanni, J.P., Mane, S.M., Mayne, S.T.*, et al.* (2005). Complement factor H polymorphism in age-related macular degeneration. Science *308*, 385-389.

Komar, A.A., Lesnik, T., and Reiss, C. (1999). Synonymous codon substitutions affect ribosome traffic and protein folding during in vitro translation. FEBS Lett *462*, 387-391.

Kreutzberg, G.W. (1996). Microglia: a sensor for pathological events in the CNS. Trends in neurosciences *19*, 312-318.

Kutz, S.M., Hordines, J., McKeown-Longo, P.J., and Higgins, P.J. (2001). TGF-beta1-induced PAI-1 gene expression requires MEK activity and cell-to-substrate adhesion. Journal of cell science *114*, 3905-3914.

Kvanta, A., Algvere, P.V., Berglin, L., and Seregard, S. (1996). Subfoveal fibrovascular membranes in age-related macular degeneration express vascular endothelial growth factor. Invest Ophthalmol Vis Sci *37*, 1929-1934.

Lampson, B.L., Pershing, N.L., Prinz, J.A., Lacsina, J.R., Marzluff, W.F., Nicchitta, C.V., MacAlpine, D.M., and Counter, C.M. (2013). Rare codons regulate KRas oncogenesis. Current biology : CB *23*, 70-75.

Landa, G., Butovsky, O., Shoshani, J., Schwartz, M., and Pollack, A. (2008). Weekly vaccination with Copaxone (glatiramer acetate) as a potential therapy for dry age-related macular degeneration. Curr Eye Res *33*, 1011-1013.

Langmann, T. (2007). Microglia activation in retinal degeneration. Journal of leukocyte biology *81*, 1345-1351.

Latta, C.H., Brothers, H.M., and Wilcock, D.M. (2015). Neuroinflammation in Alzheimer's disease; a source of heterogeneity and target for personalized therapy. Neuroscience *302*, 103-111.

Launay, S., Maubert, E., Lebeurrier, N., Tennstaedt, A., Campioni, M., Docagne, F., Gabriel, C., Dauphinot, L., Potier, M.C., Ehrmann, M*., et al.* (2008). HtrA1-dependent proteolysis of TGF-beta controls both neuronal maturation and developmental survival. Cell Death Differ *15*, 1408-1416.

LaVail, M.M. (1983). Outer segment disc shedding and phagocytosis in the outer retina. Trans Ophthalmol Soc U K *103 (Pt 4)*, 397-404.

Le, W., Rowe, D., Xie, W., Ortiz, I., He, Y., and Appel, S.H. (2001). Microglial activation and dopaminergic cell injury: an in vitro model relevant to Parkinson's disease. J Neurosci *21*, 8447-8455.

Ledeboer, A., Breve, J.J., Poole, S., Tilders, F.J., and Van Dam, A.M. (2000). Interleukin-10, interleukin-4, and transforming growth factor-beta differentially regulate lipopolysaccharide-induced production of pro-inflammatory cytokines and nitric oxide in co-cultures of rat astroglial and microglial cells. Glia *30*, 134-142.

Lee, J.E., Liang, K.J., Fariss, R.N., and Wong, W.T. (2008). Ex vivo dynamic imaging of retinal microglia using time-lapse confocal microscopy. Invest Ophthalmol Vis Sci *49*, 4169-4176.

Letterio, J.J., and Roberts, A.B. (1998). Regulation of immune responses by TGF-beta. Annu Rev Immunol *16*, 137-161.

Leveziel, N., Tilleul, J., Puche, N., Zerbib, J., Laloum, F., Querques, G., and Souied, E.H. (2011). Genetic factors associated with age-related macular degeneration. Ophthalmologica *226*, 87-102.

Levy, O., Calippe, B., Lavalette, S., Hu, S.J., Raoul, W., Dominguez, E., Housset, M., Paques, M., Sahel, J.A., Bemelmans, A.P.*, et al.* (2015). Apolipoprotein E promotes subretinal mononuclear phagocyte survival and chronic inflammation in age-related macular degeneration. EMBO Mol Med *7*, 211-226.

Li, J.J., Lu, J., Kaur, C., Sivakumar, V., Wu, C.Y., and Ling, E.A. (2008). Effects of hypoxia on expression of transforming growth factor-beta1 and its receptors I and II in the amoeboid microglial cells and murine BV-2 cells. Neuroscience *156*, 662-672.

Li, M., Atmaca-Sonmez, P., Othman, M., Branham, K.E., Khanna, R., Wade, M.S., Li, Y., Liang, L., Zareparsi, S., Swaroop, A.*, et al.* (2006). CFH haplotypes without the Y402H coding variant show strong association with susceptibility to age-related macular degeneration. Nat Genet *38*, 1049-1054.

Li, R., Huang, Y.G., Fang, D., and Le, W.D. (2004). (-)-Epigallocatechin gallate inhibits lipopolysaccharide-induced microglial activation and protects against inflammation-mediated dopaminergic neuronal injury. J Neurosci Res *78*, 723-731.

Lin, C.C., Melo, F.A., Ghosh, R., Suen, K.M., Stagg, L.J., Kirkpatrick, J., Arold, S.T., Ahmed, Z., and Ladbury, J.E. (2012). Inhibition of basal FGF receptor signaling by dimeric Grb2. Cell *149*, 1514-1524.

Lin, M.T., and Beal, M.F. (2006). Mitochondrial dysfunction and oxidative stress in neurodegenerative diseases. Nature *443*, 787-795.

Lipinska, B., Fayet, O., Baird, L., and Georgopoulos, C. (1989). Identification, characterization, and mapping of the Escherichia coli htrA gene, whose product is essential for bacterial growth only at elevated temperatures. J Bacteriol *171*, 1574-1584.

Lipinska, B., Sharma, S., and Georgopoulos, C. (1988). Sequence analysis and regulation of the htrA gene of Escherichia coli: a sigma 32-independent mechanism of heat-inducible transcription. Nucleic Acids Res *16*, 10053-10067.

Liu, Y., Hao, W., Letiembre, M., Walter, S., Kulanga, M., Neumann, H., and Fassbender, K. (2006). Suppression of microglial inflammatory activity by myelin phagocytosis: role of p47-PHOX-mediated generation of reactive oxygen species. J Neurosci *26*, 12904-12913.

Lue, L.F., Schmitz, C., and Walker, D.G. (2015). What happens to microglial TREM2 in Alzheimer's disease: Immunoregulatory turned into immunopathogenic? Neuroscience *302*, 138-150.

Luo, D.G., Xue, T., and Yau, K.W. (2008). How vision begins: an odyssey. Proc Natl Acad Sci U S A *105*, 9855-9862.

Lyzogubov, V.V., Tytarenko, R.G., Liu, J., Bora, N.S., and Bora, P.S. (2011). Polyethylene glycol (PEG)-induced mouse model of choroidal neovascularization. The Journal of biological chemistry *286*, 16229-16237.

Ma, W., Coon, S., Zhao, L., Fariss, R.N., and Wong, W.T. (2013). A2E accumulation influences retinal microglial activation and complement regulation. Neurobiol Aging *34*, 943-960.

Ma, W., Zhao, L., Fontainhas, A.M., Fariss, R.N., and Wong, W.T. (2009). Microglia in the mouse retina alter the structure and function of retinal pigmented epithelial cells: a potential cellular interaction relevant to AMD. PloS one *4*, e7945.

Maccarone, R., Di Marco, S., and Bisti, S. (2008). Saffron supplement maintains morphology and function after exposure to damaging light in mammalian retina. Invest Ophthalmol Vis Sci *49*, 1254-1261.

Madani, F., Lind, J., Damberg, P., Adams, S.R., Tsien, R.Y., and Graslund, A.O. (2009). Hairpin structure of a biarsenical-tetracysteine motif determined by NMR spectroscopy. Journal of the American Chemical Society *131*, 4613-4615.

Makeyev, E.V., Kolb, V.A., and Spirin, A.S. (1996). Enzymatic activity of the ribosome-bound nascent polypeptide. FEBS Lett *378*, 166-170.

Malet, H., Canellas, F., Sawa, J., Yan, J., Thalassinos, K., Ehrmann, M., Clausen, T., and Saibil, H.R. (2012). Newly folded substrates inside the molecular cage of the HtrA chaperone DegQ. Nature structural & molecular biology *19*, 152-157.

Maller, J., George, S., Purcell, S., Fagerness, J., Altshuler, D., Daly, M.J., and Seddon, J.M. (2006). Common variation in three genes, including a noncoding variant in CFH, strongly influences risk of age-related macular degeneration. Nat Genet *38*, 1055-1059.

Mandal, M.N., Patlolla, J.M., Zheng, L., Agbaga, M.P., Tran, J.T., Wicker, L., Kasus-Jacobi, A., Elliott, M.H., Rao, C.V., and Anderson, R.E. (2009). Curcumin protects retinal cells from light-and oxidant stress-induced cell death. Free Radic Biol Med *46*, 672-679.

Mata, N.L., Lichter, J.B., Vogel, R., Han, Y., Bui, T.V., and Singerman, L.J. (2013). Investigation of oral fenretinide for treatment of geographic atrophy in age-related macular degeneration. Retina *33*, 498-507.

Mauney, J., Olsen, B.R., and Volloch, V. (2010). Matrix remodeling as stem cell recruitment event: a novel in vitro model for homing of human bone marrow stromal cells to the site of injury shows crucial role of extracellular collagen matrix. Matrix biology : journal of the International Society for Matrix Biology *29*, 657-663.

McCarty, C.A., Mukesh, B.N., Fu, C.L., Mitchell, P., Wang, J.J., and Taylor, H.R. (2001). Risk factors for age-related maculopathy: the Visual Impairment Project. Arch Ophthalmol *119*, 1455-1462.

Mitchell, K., Shah, J.P., Tsytsikova, L.V., Campbell, A.M., Affram, K., and Symes, A.J. (2014). LPS antagonism of TGF-beta signaling results in prolonged survival and activation of rat primary microglia. J Neurochem *129*, 155-168.

Mitchell, P., Smith, W., Attebo, K., and Wang, J.J. (1995). Prevalence of age-related maculopathy in Australia. The Blue Mountains Eye Study. Ophthalmology *102*, 1450-1460.

Morimoto, R.I. (2008). Proteotoxic stress and inducible chaperone networks in neurodegenerative disease and aging. Genes Dev *22*, 1427-1438.

Moss, S.E., Klein, R., Klein, B.E., Jensen, S.C., and Meuer, S.M. (1998). Alcohol consumption and the 5-year incidence of age-related maculopathy: the Beaver Dam eye study. Ophthalmology *105*, 789-794.

Mullany, S.A., Moslemi-Kebria, M., Rattan, R., Khurana, A., Clayton, A., Ota, T., Mariani, A., Podratz, K.C., Chien, J., and Shridhar, V. (2011). Expression and functional significance of HtrA1 loss in endometrial cancer. Clinical cancer research : an official journal of the American Association for Cancer Research *17*, 427-436.

Mullins, R.F., Russell, S.R., Anderson, D.H., and Hageman, G.S. (2000). Drusen associated with aging and age-related macular degeneration contain proteins common to extracellular deposits associated with atherosclerosis, elastosis, amyloidosis, and dense deposit disease. FASEB J *14*, 835-846.

Murwantoko, Yano, M., Ueta, Y., Murasaki, A., Kanda, H., Oka, C., and Kawaichi, M. (2004). Binding of proteins to the PDZ domain regulates proteolytic activity of HtrA1 serine protease. Biochem J *381*, 895-904.

Na, Y.R., and Park, C. (2009). Investigating protein unfolding kinetics by pulse proteolysis. Protein science : a publication of the Protein Society *18*, 268-276.

Nackley, A.G., Shabalina, S.A., Tchivileva, I.E., Satterfield, K., Korchynskyi, O., Makarov, S.S., Maixner, W., and Diatchenko, L. (2006). Human catechol-O-methyltransferase haplotypes modulate protein expression by altering mRNA secondary structure. Science *314*, 1930-1933.

Nagineni, C.N., Raju, R., Nagineni, K.K., Kommineni, V.K., Cherukuri, A., Kutty, R.K., Hooks, J.J., and Detrick, B. (2014). Resveratrol Suppresses Expression of VEGF by Human Retinal Pigment Epithelial Cells: Potential Nutraceutical for Age-related Macular Degeneration. Aging Dis *5*, 88-100.

Nakayama, M., Iejima, D., Akahori, M., Kamei, J., Goto, A., and Iwata, T. (2014). Overexpression of HtrA1 and exposure to mainstream cigarette smoke leads to choroidal neovascularization and subretinal deposits in aged mice. Invest Ophthalmol Vis Sci *55*, 6514-6523.

Norden, D.M., Fenn, A.M., Dugan, A., and Godbout, J.P. (2014). TGFbeta produced by IL-10 redirected astrocytes attenuates microglial activation. Glia *62*, 881-895.

Ohno-Matsui, K. (2011). Parallel findings in age-related macular degeneration and Alzheimer's disease. Prog Retin Eye Res *30*, 217-238.

Ohr, M., and Kaiser, P.K. (2012). Aflibercept in wet age-related macular degeneration: a perspective review. Ther Adv Chronic Dis *3*, 153-161.

Oka, C., Tsujimoto, R., Kajikawa, M., Koshiba-Takeuchi, K., Ina, J., Yano, M., Tsuchiya, A., Ueta, Y., Soma, A., Kanda, H.*, et al.* (2004). HtrA1 serine protease inhibits signaling mediated by Tgfbeta family proteins. Development *131*, 1041-1053.

Paglinawan, R., Malipiero, U., Schlapbach, R., Frei, K., Reith, W., and Fontana, A. (2003). TGFbeta directs gene expression of activated microglia to an anti-inflammatory phenotype strongly focusing on chemokine genes and cell migratory genes. Glia *44*, 219-231.

Park, C., and Marqusee, S. (2005). Pulse proteolysis: a simple method for quantitative determination of protein stability and ligand binding. Nature methods *2*, 207-212.

Park, K.W., Lee, D.Y., Joe, E.H., Kim, S.U., and Jin, B.K. (2005). Neuroprotective role of microglia expressing interleukin-4. J Neurosci Res *81*, 397-402.

Polur, I., Lee, P.L., Servais, J.M., Xu, L., and Li, Y. (2010). Role of HTRA1, a serine protease, in the progression of articular cartilage degeneration. Histology and histopathology *25*, 599-608.

Ponomarev, E.D., Maresz, K., Tan, Y., and Dittel, B.N. (2007). CNS-derived interleukin-4 is essential for the regulation of autoimmune inflammation and induces a state of alternative activation in microglial cells. J Neurosci *27*, 10714-10721.

Presta, L.G., Chen, H., O'Connor, S.J., Chisholm, V., Meng, Y.G., Krummen, L., Winkler, M., and Ferrara, N. (1997). Humanization of an anti-vascular endothelial growth factor monoclonal antibody for the therapy of solid tumors and other disorders. Cancer Res *57*, 4593-4599.

Promsote, W., Veeranan-Karmegam, R., Ananth, S., Shen, D., Chan, C.C., Lambert, N.A., Ganapathy, V., and Martin, P.M. (2014). L-2-oxothiazolidine-4-carboxylic acid attenuates oxidative stress and inflammation in retinal pigment epithelium. Molecular vision *20*, 73-88.

Qin, H., Wilson, C.A., Roberts, K.L., Baker, B.J., Zhao, X., and Benveniste, E.N. (2006). IL-10 inhibits lipopolysaccharide-induced CD40 gene expression through induction of suppressor of cytokine signaling-3. J Immunol *177*, 7761-7771.

Ratnapriya, R., and Chew, E.Y. (2013). Age-related macular degeneration-clinical review and genetics update. Clin Genet *84*, 160-166.

Rawlings, N.D., Tolle, D.P., and Barrett, A.J. (2004). Evolutionary families of peptidase inhibitors. Biochem J *378*, 705-716.

Raychaudhuri, S., Iartchouk, O., Chin, K., Tan, P.L., Tai, A.K., Ripke, S., Gowrisankar, S., Vemuri, S., Montgomery, K., Yu, Y.*, et al.* (2011). A rare penetrant mutation in CFH confers high risk of age-related macular degeneration. Nat Genet *43*, 1232-1236.

Resnikoff, S., Pascolini, D., Etya'ale, D., Kocur, I., Pararajasegaram, R., Pokharel, G.P., and Mariotti, S.P. (2004). Global data on visual impairment in the year 2002. Bull World Health Organ *82*, 844-851.

Rivera, A., Fisher, S.A., Fritsche, L.G., Keilhauer, C.N., Lichtner, P., Meitinger, T., and Weber, B.H. (2005). Hypothetical LOC387715 is a second major susceptibility gene for age-related macular degeneration, contributing independently of complement factor H to disease risk. Hum Mol Genet *14*, 3227-3236.

Rosenfeld, P.J., Shapiro, H., Tuomi, L., Webster, M., Elledge, J., Blodi, B., Marina, and Groups, A.S. (2011). Characteristics of patients losing vision after 2 years of monthly dosing in the phase III ranibizumab clinical trials. Ophthalmology *118*, 523-530.

Rozovsky, I., Finch, C.E., and Morgan, T.E. (1998). Age-related activation of microglia and astrocytes: in vitro studies show persistent phenotypes of aging, increased proliferation, and resistance to down-regulation. Neurobiol Aging *19*, 97-103.

Rubinsztein, D.C. (2006). The roles of intracellular protein-degradation pathways in neurodegeneration. Nature *443*, 780-786.

Ruggiano, A., Foresti, O., and Carvalho, P. (2014). Quality control: ER-associated degradation: protein quality control and beyond. The Journal of cell biology *204*, 869-879.

Sakurai, E., Anand, A., Ambati, B.K., van Rooijen, N., and Ambati, J. (2003). Macrophage depletion inhibits experimental choroidal neovascularization. Invest Ophthalmol Vis Sci *44*, 3578-3585.

Schapansky, J., Nardozzi, J.D., and LaVoie, M.J. (2015). The complex relationships between microglia, alpha-synuclein, and LRRK2 in Parkinson's disease. Neuroscience *302*, 74-88.

Schmidt, S., Hauser, M.A., Scott, W.K., Postel, E.A., Agarwal, A., Gallins, P., Wong, F., Chen, Y.S., Spencer, K., Schnetz-Boutaud, N.*, et al.* (2006). Cigarette smoking strongly modifies the association of LOC387715 and age-related macular degeneration. Am J Hum Genet *78*, 852-864.

Scholl, H.P., Fleckenstein, M., Fritsche, L.G., Schmitz-Valckenberg, S., Gobel, A., Adrion, C., Herold, C., Keilhauer, C.N., Mackensen, F., Mossner, A.*, et al.* (2009). CFH, C3 and ARMS2 are significant risk loci for susceptibility but not for disease progression of geographic atrophy due to AMD. PLoS One *4*, e7418.

Seddon, J.M., Cote, J., Page, W.F., Aggen, S.H., and Neale, M.C. (2005). The US twin study of age-related macular degeneration: relative roles of genetic and environmental influences. Arch Ophthalmol *123*, 321-327.

Seddon, J.M., Cote, J., and Rosner, B. (2003). Progression of age-related macular degeneration: association with dietary fat, transunsaturated fat, nuts, and fish intake. Arch Ophthalmol *121*, 1728-1737.

Seidel, S.A., Dijkman, P.M., Lea, W.A., van den Bogaart, G., Jerabek-Willemsen, M., Lazic, A., Joseph, J.S., Srinivasan, P., Baaske, P., Simeonov, A.*, et al.* (2013).

Microscale thermophoresis quantifies biomolecular interactions under previously challenging conditions. Methods *59*, 301-315.

Sennlaub, F., Auvynet, C., Calippe, B., Lavalette, S., Poupel, L., Hu, S.J., Dominguez, E., Camelo, S., Levy, O., Guyon, E.*, et al.* (2013). CCR2(+) monocytes infiltrate atrophic lesions in age-related macular disease and mediate photoreceptor degeneration in experimental subretinal inflammation in Cx3cr1 deficient mice. EMBO Mol Med *5*, 1775-1793.

Shibuya, H., Okamoto, O., and Fujiwara, S. (2006). The bioactivity of transforming growth factor-beta1 can be regulated via binding to dermal collagens in mink lung epithelial cells. J Dermatol Sci *41*, 187-195.

Shiga, A., Nozaki, H., Yokoseki, A., Nihonmatsu, M., Kawata, H., Kato, T., Koyama, A., Arima, K., Ikeda, M., Katada, S.*, et al.* (2011). Cerebral small-vessel disease protein HTRA1 controls the amount of TGF-beta1 via cleavage of proTGF-beta1. Hum Mol Genet *20*, 1800-1810.

Shridhar, V., Sen, A., Chien, J., Staub, J., Avula, R., Kovats, S., Lee, J., Lillie, J., and Smith, D.I. (2002). Identification of underexpressed genes in early- and late-stage primary ovarian tumors by suppression subtraction hybridization. Cancer research *62*, 262-270.

Singh, N., Kuppili, R.R., and Bose, K. (2011). The structural basis of mode of activation and functional diversity: a case study with HtrA family of serine proteases. Archives of biochemistry and biophysics *516*, 85-96.

Smith, W., Assink, J., Klein, R., Mitchell, P., Klaver, C.C., Klein, B.E., Hofman, A., Jensen, S., Wang, J.J., and de Jong, P.T. (2001). Risk factors for age-related macular degeneration: Pooled findings from three continents. Ophthalmology *108*, 697-704.

Sparrow, J.R., and Boulton, M. (2005). RPE lipofuscin and its role in retinal pathobiology. Exp Eye Res *80*, 595-606.

Spencer, K.L., Hauser, M.A., Olson, L.M., Schmidt, S., Scott, W.K., Gallins, P., Agarwal, A., Postel, E.A., Pericak-Vance, M.A., and Haines, J.L. (2008). Deletion of CFHR3 and CFHR1 genes in age-related macular degeneration. Hum Mol Genet *17*, 971-977.

Spiess, C., Beil, A., and Ehrmann, M. (1999). A temperature-dependent switch from chaperone to protease in a widely conserved heat shock protein. Cell *97*, 339-347.

Spittau, B., Wullkopf, L., Zhou, X., Rilka, J., Pfeifer, D., and Krieglstein, K. (2013). Endogenous transforming growth factor-beta promotes quiescence of primary microglia in vitro. Glia *61*, 287-300.

Spraul, C.W., Lang, G.E., and Grossniklaus, H.E. (1996). Morphometric analysis of the choroid, Bruch's membrane, and retinal pigment epithelium in eyes with age-related macular degeneration. Invest Ophthalmol Vis Sci *37*, 2724-2735.

Strauss, O. (2005). The retinal pigment epithelium in visual function. Physiol Rev *85*, 845-881.

Streit, W.J., Miller, K.R., Lopes, K.O., and Njie, E. (2008). Microglial degeneration in the aging brain--bad news for neurons? Frontiers in bioscience : a journal and virtual library *13*, 3423-3438.

Suh, H.S., Zhao, M.L., Derico, L., Choi, N., and Lee, S.C. (2013). Insulin-like growth factor 1 and 2 (IGF1, IGF2) expression in human microglia: differential regulation by inflammatory mediators. J Neuroinflammation *10*, 37.

Supanji, Shimomachi, M., Hasan, M.Z., Kawaichi, M., and Oka, C. (2013). HtrA1 is induced by oxidative stress and enhances cell senescence through p38 MAPK pathway. Experimental eye research *112*, 79-92.

Suzumura, A., Sawada, M., Yamamoto, H., and Marunouchi, T. (1993). Transforming growth factor-beta suppresses activation and proliferation of microglia in vitro. J Immunol *151*, 2150-2158.

Tam, P.O., Ng, T.K., Liu, D.T., Chan, W.M., Chiang, S.W., Chen, L.J., DeWan, A., Hoh, J., Lam, D.S., and Pang, C.P. (2008). HTRA1 variants in exudative age-related macular degeneration and interactions with smoking and CFH. Invest Ophthalmol Vis Sci *49*, 2357-2365.

Tambuyzer, B.R., Ponsaerts, P., and Nouwen, E.J. (2009). Microglia: gatekeepers of central nervous system immunology. Journal of leukocyte biology *85*, 352-370.

Thompson, R.B., Reffatto, V., Bundy, J.G., Kortvely, E., Flinn, J.M., Lanzirotti, A., Jones, E.A., McPhail, D.S., Fearn, S., Boldt, K.*, et al.* (2015). Identification of hydroxyapatite spherules provides new insight into subretinal pigment epithelial deposit formation in the aging eye. Proc Natl Acad Sci U S A *112*, 1565-1570.

Town, T., Laouar, Y., Pittenger, C., Mori, T., Szekely, C.A., Tan, J., Duman, R.S., and Flavell, R.A. (2008). Blocking TGF-beta-Smad2/3 innate immune signaling mitigates Alzheimer-like pathology. Nat Med *14*, 681-687.

Truebestein, L., Tennstaedt, A., Monig, T., Krojer, T., Canellas, F., Kaiser, M., Clausen, T., and Ehrmann, M. (2011). Substrate-induced remodeling of the active site regulates human HTRA1 activity. Nat Struct Mol Biol *18*, 386-388.

Tserentsoodol, N., Gordiyenko, N.V., Pascual, I., Lee, J.W., Fliesler, S.J., and Rodriguez, I.R. (2006a). Intraretinal lipid transport is dependent on high density lipoprotein-like particles and class B scavenger receptors. Mol Vis *12*, 1319-1333.

Tserentsoodol, N., Sztein, J., Campos, M., Gordiyenko, N.V., Fariss, R.N., Lee, J.W., Fliesler, S.J., and Rodriguez, I.R. (2006b). Uptake of cholesterol by the retina occurs primarily via a low density lipoprotein receptor-mediated process. Mol Vis *12*, 1306-1318.

Tsuchiya, A., Yano, M., Tocharus, J., Kojima, H., Fukumoto, M., Kawaichi, M., and Oka, C. (2005). Expression of mouse HtrA1 serine protease in normal bone and

cartilage and its upregulation in joint cartilage damaged by experimental arthritis. Bone *37*, 323-336.

Tuller, T., Carmi, A., Vestsigian, K., Navon, S., Dorfan, Y., Zaborske, J., Pan, T., Dahan, O., Furman, I., and Pilpel, Y. (2010). An evolutionarily conserved mechanism for controlling the efficiency of protein translation. Cell *141*, 344-354.

Varne, A., Muthukumaraswamy, K., Jatiani, S.S., and Mittal, R. (2002). Conformational analysis of the GTP-binding protein MxA using limited proteolysis. FEBS Lett *516*, 129-132.

Vidro-Kotchan, E., Yendluri, B.B., Le-Thai, T., and Tsin, A. (2011). NBHA reduces acrolein-induced changes in ARPE-19 cells: possible involvement of TGFbeta. Current eye research *36*, 370-378.

Vierkotten, S., Muether, P.S., and Fauser, S. (2011). Overexpression of HTRA1 leads to ultrastructural changes in the elastic layer of Bruch's membrane via cleavage of extracellular matrix components. PLoS One *6*, e22959.

Vingerling, J.R., Hofman, A., Grobbee, D.E., and de Jong, P.T. (1996). Age-related macular degeneration and smoking. The Rotterdam Study. Arch Ophthalmol *114*, 1193-1196.

Vorwerk, P., Hohmann, B., Oh, Y., Rosenfeld, R.G., and Shymko, R.M. (2002). Binding properties of insulin-like growth factor binding protein-3 (IGFBP-3), IGFBP-3 N- and C-terminal fragments, and structurally related proteins mac25 and connective tissue growth factor measured using a biosensor. Endocrinology *143*, 1677-1685.

Wan, Y.Y., and Flavell, R.A. (2007). 'Yin-Yang' functions of transforming growth factor-beta and T regulatory cells in immune regulation. Immunol Rev *220*, 199-213.

Wang, G., Dubovy, S.R., Kovach, J.L., Schwartz, S.G., Agarwal, A., Scott, W.K., Haines, J.L., and Pericak-Vance, M.A. (2013). Variants at chromosome 10q26 locus and the expression of HTRA1 in the retina. Exp Eye Res *112*, 102-105.

Wang, G., Scott, W.K., Haines, J.L., and Pericak-Vance, M.A. (2010a). Genotype at polymorphism rs11200638 and HTRA1 expression level. Arch Ophthalmol *128*, 1491-1493.

Wang, G., Spencer, K.L., Court, B.L., Olson, L.M., Scott, W.K., Haines, J.L., and Pericak-Vance, M.A. (2009). Localization of age-related macular degeneration-associated ARMS2 in cytosol, not mitochondria. Invest Ophthalmol Vis Sci *50*, 3084-3090.

Wang, G., Spencer, K.L., Scott, W.K., Whitehead, P., Court, B.L., Ayala-Haedo, J., Mayo, P., Schwartz, S.G., Kovach, J.L., Gallins, P.*, et al.* (2010b). Analysis of the indel at the ARMS2 3'UTR in age-related macular degeneration. Hum Genet *127*, 595-602.

Wang, X.L., Li, C.F., Guo, H.W., and Cao, B.Z. (2012). A novel mutation in the HTRA1 gene identified in Chinese CARASIL pedigree. CNS neuroscience & therapeutics *18*, 867-869.

Weeks, D.E., Conley, Y.P., Mah, T.S., Paul, T.O., Morse, L., Ngo-Chang, J., Dailey, J.P., Ferrell, R.E., and Gorin, M.B. (2000). A full genome scan for age-related maculopathy. Hum Mol Genet *9*, 1329-1349.

Weikel, K.A., Chiu, C.J., and Taylor, A. (2012). Nutritional modulation of age-related macular degeneration. Mol Aspects Med *33*, 318-375.

Weiter, J.J., Delori, F.C., Wing, G.L., and Fitch, K.A. (1986). Retinal pigment epithelial lipofuscin and melanin and choroidal melanin in human eyes. Invest Ophthalmol Vis Sci *27*, 145-152.

Wilson, S.M., Schmutzler, B.S., Brittain, J.M., Dustrude, E.T., Ripsch, M.S., Pellman, J.J., Yeum, T.S., Hurley, J.H., Hingtgen, C.M., White, F.A.*, et al.* (2012). Inhibition of transmitter release and attenuation of anti-retroviral-associated and tibial nerve injury-related painful peripheral neuropathy by novel synthetic Ca2+ channel peptides. J Biol Chem *287*, 35065-35077.

Wong-Riley, M.T. (2010). Energy metabolism of the visual system. Eye Brain *2*, 99-116.

Wong, T.Y., Chakravarthy, U., Klein, R., Mitchell, P., Zlateva, G., Buggage, R., Fahrbach, K., Probst, C., and Sledge, I. (2008). The natural history and prognosis of neovascular age-related macular degeneration: a systematic review of the literature and meta-analysis. Ophthalmology *115*, 116-126.

Wong, W.L., Su, X., Li, X., Cheung, C.M., Klein, R., Cheng, C.Y., and Wong, T.Y. (2014). Global prevalence of age-related macular degeneration and disease burden projection for 2020 and 2040: a systematic review and meta-analysis. Lancet Glob Health *2*, e106-116.

Wong, W.T. (2013). Microglial aging in the healthy CNS: phenotypes, drivers, and rejuvenation. Frontiers in cellular neuroscience *7*, 22.

Wright, A.F., Jacobson, S.G., Cideciyan, A.V., Roman, A.J., Shu, X., Vlachantoni, D., McInnes, R.R., and Riemersma, R.A. (2004). Lifespan and mitochondrial control of neurodegeneration. Nat Genet *36*, 1153-1158.

Wu, Y., Tian, L., and Huang, Y. (2015). Correlation between the interactions of ABCA4 polymorphisms and smoking with the susceptibility to age-related macular degeneration. Int J Clin Exp Pathol *8*, 7403-7408.

Xiong, X., Coombs, P.J., Martin, S.R., Liu, J., Xiao, H., McCauley, J.W., Locher, K., Walker, P.A., Collins, P.J., Kawaoka, Y.*, et al.* (2013). Receptor binding by a ferret-transmissible H5 avian influenza virus. Nature *497*, 392-396.

Xu, H., Chen, M., and Forrester, J.V. (2009). Para-inflammation in the aging retina. Prog Retin Eye Res *28*, 348-368.

Yang, Z., Camp, N.J., Sun, H., Tong, Z., Gibbs, D., Cameron, D.J., Chen, H., Zhao, Y., Pearson, E., Li, X.*, et al.* (2006). A variant of the HTRA1 gene increases susceptibility to age-related macular degeneration. Science *314*, 992-993.

Yang, Z., Tong, Z., Chen, Y., Zeng, J., Lu, F., Sun, X., Zhao, C., Wang, K., Davey, L., Chen, H.*, et al.* (2010). Genetic and functional dissection of HTRA1 and LOC387715 in age-related macular degeneration. PLoS Genet *6*, e1000836.

Yanoff, M. and Duker, Y. (2009) Ophthalmology 4th edition. Elsevier (Textbook)

Yates, J.R., Sepp, T., Matharu, B.K., Khan, J.C., Thurlby, D.A., Shahid, H., Clayton, D.G., Hayward, C., Morgan, J., Wright, A.F.*, et al.* (2007). Complement C3 variant and the risk of age-related macular degeneration. N Engl J Med *357*, 553-561.

Yoshida, S., Yashar, B.M., Hiriyanna, S., and Swaroop, A. (2002). Microarray analysis of gene expression in the aging human retina. Invest Ophthalmol Vis Sci *43*, 2554-2560.

Young, R.W. (1969). The organization of vertebrate photoreceptor cells. UCLA Forum Med Sci *8*, 177-210.

Yu, A.L., Fuchshofer, R., Kook, D., Kampik, A., Bloemendal, H., and Welge-Lussen, U. (2009a). Subtoxic oxidative stress induces senescence in retinal pigment epithelial cells via TGF-beta release. Investigative ophthalmology & visual science *50*, 926-935.

Yu, A.L., Lorenz, R.L., Haritoglou, C., Kampik, A., and Welge-Lussen, U. (2009b). Biological effects of native and oxidized low-density lipoproteins in cultured human retinal pigment epithelial cells. Experimental eye research *88*, 495-503.

Zahn, J.M., Poosala, S., Owen, A.B., Ingram, D.K., Lustig, A., Carter, A., Weeraratna, A.T., Taub, D.D., Gorospe, M., Mazan-Mamczarz, K.*, et al.* (2007). AGEMAP: a gene expression database for aging in mice. PLoS Genet *3*, e201.

Zareparsi, S., Branham, K.E., Li, M., Shah, S., Klein, R.J., Ott, J., Hoh, J., Abecasis, G.R., and Swaroop, A. (2005). Strong association of the Y402H variant in complement factor H at 1q32 with susceptibility to age-related macular degeneration. Am J Hum Genet *77*, 149-153.

Zhan, X., Larson, D.E., Wang, C., Koboldt, D.C., Sergeev, Y.V., Fulton, R.S., Fulton, L.L., Fronick, C.C., Branham, K.E., Bragg-Gresham, J.*, et al.* (2013). Identification of a rare coding variant in complement 3 associated with age-related macular degeneration. Nat Genet *45*, 1375-1379.

Zhang, F., Kartner, N., and Lukacs, G.L. (1998). Limited proteolysis as a probe for arrested conformational maturation of delta F508 CFTR. Nat Struct Biol *5*, 180-183.

Zhang, F., Saha, S., Shabalina, S.A., and Kashina, A. (2010). Differential arginylation of actin isoforms is regulated by coding sequence-dependent degradation. Science *329*, 1534-1537.

Zhang, L., Lim, S.L., Du, H., Zhang, M., Kozak, I., Hannum, G., Wang, X., Ouyang, H., Hughes, G., Zhao, L.*, et al.* (2012). High temperature requirement factor A1 (HTRA1) gene regulates angiogenesis through transforming growth factor-beta family member growth differentiation factor 6. The Journal of biological chemistry *287*, 1520-1526.

Zhao, W., Xie, W., Xiao, Q., Beers, D.R., and Appel, S.H. (2006). Protective effects of an anti-inflammatory cytokine, interleukin-4, on motoneuron toxicity induced by activated microglia. J Neurochem *99*, 1176-1187.

Zhou, J., Jang, Y.P., Kim, S.R., and Sparrow, J.R. (2006). Complement activation by photooxidation products of A2E, a lipofuscin constituent of the retinal pigment epithelium. Proc Natl Acad Sci U S A *103*, 16182-16187.

Zhou, J., Kim, S.R., Westlund, B.S., and Sparrow, J.R. (2009). Complement activation by bisretinoid constituents of RPE lipofuscin. Invest Ophthalmol Vis Sci *50*, 1392-1399.

Zhou, X., Spittau, B., and Krieglstein, K. (2012). TGFbeta signalling plays an important role in IL4-induced alternative activation of microglia. J Neuroinflammation *9*, 210.

Zillner, K., Filarsky, M., Rachow, K., Weinberger, M., Langst, G., and Nemeth, A. (2013). Large-scale organization of ribosomal DNA chromatin is regulated by Tip5. Nucleic Acids Res *41*, 5251-5262.

Zumbrunn, J., and Trueb, B. (1997). Localization of the gene for a serine protease with IGF-binding domain (PRSS11) to human chromosome 10q25.3-q26.2. Genomics *45*, 461-462.

ACKNOWLEDGMENT

Firstly, I would like to express my sincere gratitude to my advisor Prof. Dr. Bernhard Weber for the continuous support in my Ph.D. study and related research, for his patience, motivation, and immense knowledge. His guidance helped me throughout my Ph.D. and writing of this thesis. I could not have imagined having a better advisor and mentor for my Ph.D. study.

I cannot thank Dr. Ulrike Friedrich enough for her support and love throughout the period of my Ph.D. Her relentless support and suggestions on a regular basis were indispensable.

Besides my advisor, I would like to thank the rest of my mentors: Prof. Dr. Gunter Meister and Dr. Sascha Fauser not only for their insightful comments and encouragement, but also for the critical questions which helped me to widen my research from various perspectives. I would like to thank Dr. Heidi Stoehr, Dr. Helmut Roth, Dr. Diana Pauly, Prof. Dr. Thomas Langmann and Prof. Dr. Antje Grosche for their valuable inputs about my research during the lab meetings.

My sincere thanks also go to Prof. Gernot Laengst and Dr. Rudolf Fuchshofer for a successful collaboration. Without their precious support it would not be possible to conduct this research. I would specially want to thank Dr. Thomas Schubert and Magdalena Schneider for their co-operation.

I thank my fellow labmates and interns for the stimulating discussions when we were working together, before deadlines, and for all the fun we have had in the last four years. I specially want to thank Dr. Felix Grassman, Karolina Ploessl, Kerstin Rueckl, Kerstin Meier, Andrea Milenkovic for their valuable suggestions and assistance. I also want to thank my colleagues in Diagnostics: Katja, Julia, Yvone, Chris, Merve.

Last but not the least, I would like to thank my family: my parents and my wife for supporting me throughout the writing of my thesis.